CHANGING NUTRIENT AND PRODUCTIVITY REGIMES IN LAKE SUPERIOR: CAUSES AND TIME COURSE

A THESIS SUBMITTED TO THE FACULTY OF THE GRADUATE SCHOOL OF THE UNIVERSITY OF MINNESOTA
BY

LADISLAUS J. STRZOK

IN PARTIAL FULFILLMENT OF THE REQUIREMENTS
FOR THE DEGREE OF MASTER OF SCIENCE

JOSEF P. WERNE

AUGUST 2011

Acknowledgements

This research would not have been possible without the support of many wonderful and selfless individuals. I thank my advisor Josef Werne, his flexibility and capacity to put things in perspective was essential to ultimately finishing this writing. Thanks to Robert Hecky, both the trust of this project and encouragement along the way was invaluable. I acknowledge Sarah Grosshuesch, who sets a benchmark to which every laboratory should aspire. Thank you Tom Johnson, you opened my eyes to reading a book and figuring it out. Revisions by Elizabeth Minor improved the clarity and quality of this writing, thank you. I thank Melissa Berke and Martijn Woltering who together combined to form the peanut butter and jelly of my research experience and the glue of the Werne Lab. Thank you Paul Siders, for the encouragement to pursue further education. Thanks to John Evans for asking difficult questions that promote critical thinking. Additionally, I would like to express thanks to Koushik Dutta, Brittany Krueger, Prosper Zigah, XiJiu Liu, Sergei Katsev, Carla Steinbring, Yvonne Chan, Kathy Oliver, JoAnn Ellis, Steven Berry, Steve Colman, Large Lakes Observatory Faculty and Staff, UMD Department of Chemistry Faculty and Staff, Crew of the Blue Heron, U of M LacCore/LRC Staff, U of Manitoba Staff, friends and fellow students for their instruction, involvement, trust, incite and advice. I would also like to recognize the Strzok, Beresford, Moen, Miner and Colvin families, all have provided encouragement, wisdom and peace of mind during my time at UMD. Lastly, this would not have been possible without funding from Minnesota Sea Grant and University of Minnesota Duluth in the form of grants, scholarships and work assistantships.

To my parents, Lad and Jenny.

Abstract

Understanding nutrient and productivity trends in Lake Superior is necessary to better manage the largest freshwater lake in the world. Investigations of six sediment cores, from the western basin of Lake Superior, were used to characterize the greater lake basin. Sedimentary geochemical trends were measured as indicators of historic change due to effects associated with increasing population and land use changes in Lake Superior's watershed. Measurements were concentrated within the last two centuries, providing historic context to evidence of observations of the mid to late 1800s and into the present.

Bulk and stable isotopic composition of C and N indicate that the lake has undergone productivity changes in response to nutrient availability within the strongly P-limited system. Interpretable response by the $\delta^{13}C$ productivity proxy was significant despite the highly oligotrophic condition and low sedimentation rates of the lake. Primary production of the lake has shown a marked increase starting in the early 1900s reaching a maximum in the 1960s, heavier by 1.7‰ on average ($\delta^{13}C_{Bulk}$), observed most strongly in proximity to the populated western end of the lake. Subsequent recovery from nutrient enrichment is observed as decreased productivity by 1980, in agreement with P reduction mandated by the United States and Canada. Measurements of n-alkane biomarkers were used as an additional method of determining changes in aquatic production. Carbon isotopic analysis of algal-derived biomarkers support bulk measurement indicating changes in aquatic primary production drive the sedimentary organic geochemical record. N cycling within the lake appears to be driven by different

environmental factors in individual regions. $\delta^{15}N$ in the most western samples appears to be dominated by aquatic primary productivity chances, but in other regions of the lake productivity has much less influence of $\delta^{15}N$. Sedimentary nitrogen isotopes provide little indication to the source or timeline of the lake wide increase in nitrate concentration.

Changing Nutrient and Productivity Regimes in Lake Superior: Causes and time course

Table of Contents

Changing Nutrient and Productivity Regimes in Lake Superior: Causes and time course

List of Figures:

List of Figures (continued):

Changing Nutrient and Productivity Regimes in Lake Superior: Causes and time course

List of Tables:

1. Introduction

Lake Superior has yet to be studied addressing historic nutrient and productivity changes concurrent with early development of the lake basin. Similar to the lower Great Lakes, Lake Superior has experienced an increase in anthropogenic impacts corresponding to increased population including increased land use, urbanization and industrialization. Over the last century, anthropogenic nutrient inputs have influenced the rate of production within the lake, which is ultra-oligotrophic and therefore sensitive to slight nutrient increases. Primary production estimates of 65 g C m^{-2} y^{-1} in the 1970s (Vollenweider *et al*., 1973) decreased to a recent estimate of 25 g C m^{-2} y^{-1} (Urban *et al*., 2005), suggesting significant decline during the late 1900s. The lake is intensely P-limited (Ivanikova et al., 2007) and such an event would likely be driven by P availability. This corresponds with historical simulation modeling for the period from 1800 to 1970 (Chapra 1977) which suggests a significant increase starting in the late 1800s.

Indicators of historic primary productivity are important tools for understanding nutrient and productivity trends in aquatic systems with limited records, and are invaluable in Lake Superior for which direct measurement is largely absent prior to the 1970s. The chemical composition of sediment cores, largely the sedimented organic matter (OM), allow for a historical reconstruction of prior conditions in the water column (Meyers, 1997). Although the organic material that survives recycling within the water column represents a small fraction of the original mass, factors controlling preferential

preservation are fairly well understood and allow for informed proxy selection (Burdige, 2007).

Due to the oligotrophic nature and generally low sedimentation rates found within Lake Superior, the effectiveness of recognized productivity indictors has been called into question. Far from exhaustive, the current study sought to examine several generally accepted and measured sedimentary geochemical trends to provide the means to interpret historical changes within the lake. Six cores from the western basin were selected to best characterize regional environments representative of the larger basin. Analysis of sediment cores included measurement of the concentration and stable isotope composition of bulk organic C and N, as well as the abundance and isotopic composition of individual n-alkane, which are biomarker for algae (shorter chain lengths) and terrestrial plants (longer chain lengths). The measurement of the bulk isotope composition ($\delta^{13}C$), has been used with great success in other lakes, notably in Lakes Erie and recently Ontario to study P-influenced paleoproductivity in the mid-1900s (Hodell and Schelske, 1998). The present study specifically examined the following hypotheses, using and evaluating the listed proxies with the intent that understanding the role of current and historic impacts will help to better manage the biology and water quality of the lake for the future.

Also of interest is the source and fate of anthropogenic nitrogen within the environment, as measured nitrate within Lake Superior has increased nearly 5 fold since the first measurement in 1906 (Finlay et al., 2007). We hypothesize that nitrification may have begun at the turn of the last century, initially driven by increased nitrogen loading

from the catchment by deforestation and subsequently by atmospheric loading due to combustion sources. If so, nitrification would likely have grown concurrently with population, industrialization, and intensity of fertilizer use in agriculture. Indication of nitrification would be evident by changing $\delta^{15}N$ and an increase in long-chain terrigenous n-alkane biomarkers (Collister *et al*., 1994; Talbot, 2001). If nitrogen sources are in balance between inputs and losses we would not expect recent change in nitrogen cycling, evident primarily by changing $\delta^{15}N$ values (Talbot, 2001).

We also hypothesize that primary productivity in Lake Superior has always been phosphorus limited, (co-limited by Fe, Ivanikova et al., 2007) and it did not respond to early nitrogen enrichment. This hypothesis will be explored using initial trends of $\delta^{15}N$, which began increasing before $\delta^{13}C$, similar to Lake Ontario results (Hodell and Schelske, 1998). Increased urbanization, volumes of sewage and domestic use of P peaked in the 1960s followed by decline, and likely influenced primary productivity driven by P loading. Recent declines in primary productivity will indicate long term oligotrophication of the lake, since 1980. Indication of continued decline in productivity will be evident in low $\delta^{13}C_{org}$ and lower abundance of short-chain n-alkanes (Meyers, 2003).

2. Background

2.1 General Information

Known for its deep, clear, cold waters, Lake Superior is the quintessential ultra-oligotrophic freshwater lake. The largest freshwater lake in the world by surface area, 82,100 km^2, it is 563 km long and 237 km wide containing 12,100 km^3 of water. The lake surface is 183 m above sea level, highest of the Laurentian Great Lakes, with its deepest point found in the eastern basin at a depth of 406 m (MN Sea Grant, 2010).

The primary source of water to the lake is in the form of precipitation, on average 56% of total input falls directly to the lake surface. The largest sources of water from the catchment are the St. Louis (MN/WI) and Nipigon (ON) Rivers, which account for roughly one quarter of the watershed input (MN Sea Grant, 2010). Water loss due to evaporation accounts for approximately one third of the outflow, the remainder empties into Lake Huron through the St Marys River, a flow 28 times greater than the St Louis River. Water in the lake has an average residence time of 191 years (MN Sea Grant, 2010).

2.2 Lake Superior Basin

Bordered by Canada and the United States, the local governments of the province of Ontario and the states of Michigan, Minnesota, and Wisconsin share rights and provide regulation over Lake Superior. Currently the most significant cities by population are Marquette, MI; Thunder Bay, ON; Duluth, MN; Superior, WI; and Sault Saint Marie, ON/MI. The lake basin is home to approximately 607,000 people who are primarily

focused in cities and small towns which occupy roughly 10% of the region, the remaining 90% is currently undeveloped and forested (MN Sea Grant, 2010). Much of this forested land has re-grown since initial logging starting in the late 1800s.

Logging of the basin is one of the largest of anthropogenic impacts experienced by the watershed ecosystem (White and Mladenoff, 1994). Significant impacts prior to logging include infrequent natural fires and vegetation disturbance by weather events (Freidman and Reich, 2005; White and Host, 2008; White and Mladenoff, 1994). Logging of the basin moved from east to west starting in Michigan and Wisconsin. The real commercial boom, possibly posing significant impact to the watershed, started in the 1880s with demand for white pine before moving to hardwoods and hemlock then onto more remote lumber. This logging effort for white pine peaked during the early 1890s along the south shore of the lake and later in the decade in Ontario. Minnesota did not experience the extent of logging found in other portions of the basin due to quality and access as pine production peaked in 1902 (Larson, 2007). Following logging, fires were commonplace and left the land scorched and barren, exacerbating the impacts of prior logging. Fires ravaged the basin until 'fire suppression' policy was enacted in the 1910s. Conservation policy in both Ontario and the United States was accompanied by reforestation efforts to restore white pine as hardwood logging declined moving into the 1920s (White and Mladenoff, 1994).

2.3 Context

Previous investigations studying nutrients and productivity in Lake Superior suggest that further study is needed. To a lesser degree than the other Great Lakes, due primarily to its larger volume, Lake Superior has experienced an increase in anthropogenic input as a result of increasing population of the region. This input has likely changed available nutrient concentrations within the lake, giving rise to measureable changes in primary production. Unfortunately, historical measurements are limited in resolution, both in space and time. The timing of measured changes is important for a historical understanding of the underlying sources of nutrients that may have altered lake production. The interval of interest, the last two centuries, encompasses both pre-industrialized conditions and the modestly developed populated region currently found. Without knowledge of historical changes, measurements in recent studies remain subjective, showing variation between methodology and sample sites unable to adequately address aspects of the larger region. Improved understanding of nutrient and productivity events will help to better manage Lake Superior in the future as conditions continue to change.

2.4 Nutrient Concentrations

Primary production in Lake Superior is controlled by the availability of nutrients, specifically P and Fe (Sterner *et al*., 2004). A study by Weiler (1978) based on measurements made from the 1880s through 1977 concluded that the major ions found in

Lake Superior (calcium, manganese, sulfate, and chloride) had not changed significantly over time, although measurements were taken infrequently and varied in methodology.

The measure of nitrate concentration is the longest available record for a nutrient essential to phytoplankton production in Lake Superior. Weiler (1978) suggested that the concentration of nitrate in Lake Superior has maintained a logarithmic increase since the first measurement in 1906. The substantial increasing trend suggested by Weiler (1978) conflicts with the observation of recent measurements, as recent data fit from the 1950s through the 1980s result in trends giving a positive linear increase, not logarithmic (Sterner *et al*. 2004). Sterner *et al.* (2004) suggests the use of nitrate data from the 1940s, often disregarded, which contributes an additional quadratic term to equations fit to the trend. Such a fit could be interpreted to predict a future decline in nitrate concentrations in the lake. Samples taken since the 1980s demonstrate that current nitrate concentrations are statistically unchanging in the lake, after having a significant increase previously (Urban *et al*., 2007). Isotopic studies suggest that the production of nitrate is dominated by in-lake fixation (Sterner *et al.,* 2007). Previously, the observed increase in nitrate concentration was presumed to be a response from an increase in atmospheric concentrations associated with the burning of fossil fuels (Bennett, 1986), which is likely significant in nitrogen mass balance. Current nitrate concentrations have increased to approximately 300 μg/L and are now over 5 times greater than when measurements were first taken in 1906 (Weiler, 1978; Bennett, 1986; McManus et al., 2003).

In contrast to nitrate measurements, total phosphorus (TP) levels in Lake Superior showed significant decline from the earliest measurements made in the 1950s to that

measured in the 1970s (Weiler, 1978). The cause of the decline could simply be difference in methodological technique between studies. Weiler (1978) was skeptical of large changes in such a large lake, citing seasonal variability as a plausible cause of the difference. Urban *et al*. (2007) suggests that reduced phosphorus (P) discharge from waste water plants combined with removal from detergents would predict subsequent decline in TP input from anthropogenic sources. These suggested changes correspond to measureable continued decline, nearly 50% in concentration of TP and chlorophyll in the lake from the 1970s to the most recent measurements (Urban et al., 2007).

Studies in Lakes Erie and Ontario have correlated increased phosphorus availability with increased eutrophication as examined by investigation of sediment cores (Schelske and Hodell, 1991; Hodell and Schelske, 1995, 1998, 2004). Phosphorus has been highlighted as the primary limiting nutrient for production in the great lakes (Guildford *et al*., 1994), though Lake Superior seems to be co-limited with P and Fe (Sterner *et. al*., 2004; Ivanikova *et al*., 2007). Lake Superior has been shown to deviate from the traditional Redfield stoichiometric ratio commonly observed in typical lacustrine and oceanic environments.

Modeling proposed by Chapra (1977) to investigate the nutrient loading in the great lakes does not predict significant TP enrichment for Lake Superior; however it correlates TP well with measurement of population and nutrient concentrations in the lower great lakes over time. Potential decline in P, predicted as the result of management of Lake Superior is without a period of prior significant enrichment, necessary for subsequent decline in current observations (Urban *et al*., 2007; Weiler, 1978). The fact

that nitrate has increased over time suggests that the availability of nitrogen has not been limiting growth; the ratio of nitrate to TP in Lake Superior is rising, while already high for such a large body of water (Guildford and Hecky, 2000; Sterner *et al*., 2007). Estimated rates of P recycling in Lake Superior range from single core values as high as 38% and as low as 6% (Heinen, 2002), to lake wide estimates of 13% (Callender and Granini, 1997). With recycling of P playing a large role in production within the lake and high rates of remineralization in the sediments, measurement from within the sedimentary record may not properly indicate the prior production environment of the water column.

2.5 Primary Production

The limited measurements of primary productivity in Lake Superior provide estimates of production within the lake; dependent upon spatial and temporal resolution. Cotner *et al*. (2004) suggest that the respiration of organic matter and the inability of studies to balance the carbon budget in the lake have led to productivity estimates that may be low. Isotopic measurements of organic matter have concluded that autochthonous production is the dominant driving force in the lake (Cotner *et al*., 2004; Urban *et al*., 2005). Vollenweider *et al*. (1973) estimated an annual production of 65 g C m^{-2} y^{-1} based on cruises from the early 1970s, these values described the production rate for a depth integrated profile. A rate of 50-60 g C m^{-2} y^{-1} was determined by Fee *et al*. (1994) from seasonal measurements of ^{14}C experiments near Isle Royal from 1991-92. Significantly lower values of 16-18 g C m^{-2} y^{-1} for a 7 month period, extrapolated to 25 g C m^{-2} y^{-1} as a 'true' estimate of annual production, are among the most current estimates

by Urban *et al.* (2005). If TP and chlorophyll decline since the 1970s is accurate, estimates of production, since the early measurements of Vollenweider *et al*. (1973), represent production constrained by nutrient availability. However these productivity estimates present a myriad of differences among studies that are ultimately estimating a single value. Interpretation and comparison among studies is therefore difficult but appear to represent significant decline in the last 40 years. Urban *et al.* (2005) concluded that production has shown a decline from a prior event, most likely lake wide loading of P. These studies taken together suggest that Lake Superior, directly influenced by human impact on the region, has primary production limited by P availability with changes linked accordingly.

2.6 Age of Sediments

Significant to the study of (paleo) productivity is the accurate dating of sediment age with depth; age can be determined using a wide variety of methods. In this study we chose to use concentration changes of ^{210}Pb, with a half life of 22.26 years, an ideal element for radiometric dating of materials younger then 150 years (Oldfield and Appleby, 1984). In numerous studies ^{210}Pb has been shown to be a good fit for dating recent lacustrine sediments and is widely used (Oldfield and Appleby, 1984; Noller, 2004; Tylmann, 2004; Evans, 1981). ^{210}Pb is a natural occurring radionuclide found in the ^{238}U decay series, following ^{222}Rn and prior to ^{210}Po. ^{222}Rn with a half life of 3.82 days decays very quickly through ^{218}Po, ^{218}At, ^{214}Pb, ^{214}Bi, ^{214}Bo, ^{210}Tl in a matter of minutes to the longer lived daughter ^{210}Pb (Noller, 2004; Evans, 1980). Many factors

give rise to the concentration of ^{222}Rn released from the Earths crust; however, these factors give rise to little variation in the atmosphere when mixed from numerous sources (Oldfield and Appleby, 1984; Van Alstine, 2006).

The short period of time ^{210}Pb spends in the atmosphere, estimated to be 5 - 10 days, plays a large role in its incorporation into lacustrine sediments (Evans, 1980). ^{210}Pb becomes easily attached to airborne dust particles, and this adsorbed ^{210}Pb enters the lacustrine environment primarily as precipitation. Once in the water body ^{210}Pb passes rapidly through the water column and becomes deposited within the sediment (Appleby, 2001). ^{210}Pb and its precursors can also become deposited within the catchment and reach the lake through erosion of soils. Alternative methods of introduction to the sediment include diffusion of ^{222}Rn and ^{226}Ra from source waters and decay within the water column, prior to sedimentation (Van Alstine, 2006). These sources of ^{210}Pb make up the 'unsupported' ^{210}Pb signal used in age calculations. The supported portion of ^{210}Pb signals is derived from the natural decay of elements such as ^{226}Ra higher in the uranium decay series.

The two most common approaches using ^{210}Pb to calculate age include the constant flux/constant sedimentation rate model (CFCS) and the constant rate of supply model (CRS). Each model has strengths and weaknesses due to the initial assumptions (Appleby 2001, Oldfield and Appleby 1984). The CRS model is commonly used to interpret sediments in which sedimentation rate may have changed over time (Oldfield and Appleby, 1984; Noller, 2004; Tylmann, 2004; Evans, 1981). Calculations may be checked with a variety of methods; most common is the matching of significant events of

known age. Radioactive ^{137}Cs is commonly used as an age marker, as maximum concentrations of the element occur in 1963 due to an intense period of nuclear atmospheric testing; however, in large lakes the signal is found to lag the actual atmospheric maximum due to slow transport (Robbins and Eadie, 1991).

2.7 Sedimentary Productivity Proxies

With the residence time of Lake Superior's catchment being longer than that of the lake, the ideal method of historical reconstruction is found in the sedimentary record. Organic matter found in the sediment of the Great Lakes is an ideal source for elemental, isotopic and molecular indicators (Meyers, 2003) with which to probe questions of changing nutrient and productivity regimes (Schelske and Hodell, 1991; Hodell and Schelske, 1995, 1998). Although the organic content found within the sediments is a mixture derived from numerous sources, the remains of aquatic photosynthetic vegetation typically makes up the majority of the organics (Wakeham, 2006). These simple non-vascular algal plants are found along with remnants of vascular land plant material. The material of land plants contributes molecules that tend to degrade slower in aquatic conditions, including cellulose and lignin (Meyers, 2003). Proximity to sources of terrestrially derived material along with higher burial rates leads to higher concentrations of terrestrially produced organic material in near shore locations.

Reconstructing the organic carbon and nitrogen cycles has been studied by measuring bulk element concentrations of carbon and nitrogen along with their stable isotope compositions (Meyers, 2003). Research investigating lacustrine productivity in

Lakes Erie and Ontario used these methods successfully (Schelske and Hodell, 1991, 1995; Hodell and Schelske, 1998) and are recreated herein.

It is important to recognize that the burial of sedimentary material is a function of environmental factors including but not limited to production rate and quantity, source of material, oxygen content of water column and sediment, selective preservation of molecular properties, oxidation duration, sorptive interaction with mineral surfaces, bioturbation, and degradation (Meyers, 1997; Burdige, 2007; Wakeham et al., 2006). Remineralization is expected of all bulk nutrients with depth, as organics slowly pass through the well-oxygenated environment at the sediment surface they are further oxidized until buried sufficiently within the anoxic portion of the sediment. Typical plots of remineralization behavior portray a sharp decline of organic content of sediments during early diagenesis at the sediment surface, followed by steady values at depth under fixed conditions (Burdige, 2007).

Total organic carbon (C_{org}) acts as a general organic material marker that qualitatively interprets energy flow through ecosystems with higher content generally indicating higher production for an otherwise steady state system. Studies indicate that shallow sample sites bury C_{org} more effectively with less mineralization than sites over 100 m in depth, particularly in Lake Superior (Heinen, 2002). A general estimate of organic matter content within the sediment is determined as twice the concentration of C_{org} (Oldfield and Appleby, 1984). Plots of C_{org} vs depth (or time) both need to be interpreted with caution and reference to additional proxies due to remineralization and metabolism (Burdige, 2007).

Total nitrogen, similar to C_{org}, is valuable to identify periods of change in nutrient cycling within the lake; however, interpretation of results is limited by factors such as remineralization. Of greater significance may be the ratio of organic carbon to total nitrogen (C/N ratio). Due to the inherent structure of cellular compounds, the C/N ratio of N-containing protein rich algae (typically 4-10) and N-poor cellulose rich vascular land plants (+20) differs; changes in C/N therefore suggest changes in source material (Meyers, 1997). These fundamental composition differences typically survive sinking and sedimentation at equivalent rates (Meyers, 2003).

Measuring the stable isotope composition of organic matter is a widely utilized method to resolve questions of productivity, source material, and changes, when used in combination with additional proxies. Isotopes, atoms of an element which contain the same number of protons but differ in the number of neutrons, can be easily distinguished as they differ in mass (Kendall and Caldwell, 1998). Due to the kinetics and thermodynamics of chemical reactions, heavier isotopes require larger energy inputs to drive reactions forward and over energy barriers. In both geological and biological chemical systems lighter isotopes are preferentially incorporated into, and removed from, compounds with lower energy states (Freeman, 2001; Kendall and Caldwell, 1998, Hayes, 1993). This preference of lighter isotopes in reaction products is known as kinetic isotopic fractionation. The degree to which the resulting compounds differ in isotope composition is a function of the pathway the chemical reaction follows and constraints due to the isotope composition of the source material. The isotope composition of a sample is reported relative to the concentration of a reference standard, and is reported in

standard 'delta notation' given by the formula is below and typically reported in parts per thousand, or per mil (‰) because changes in isotopic concentration are typically on the order of $1/1000^{th}$ of a percent, this delta notation allows for easier numerical interpretation (Hayes, 2003).

$$\delta^{13}C = [(^{13}C/^{12}C_{sample})/(^{13}C/^{12}C_{ref}) - 1] \times 10^3$$

The standard used for isotopic carbon measurements, Vienna PeeDee Belemnite (VPDB), calculates $\delta^{13}C$ values in terms of negative numbers for cellular photosynthetic products (Kendall and Caldwell, 1998), an arbitrary consequence of the standard selection.

The two most common pathways of photosynthesis involve differing numbers of carbon atoms in starting molecules, 3 or 4 carbon atoms, upon incorporation of CO_2 into the initial chemical structures formed during photosynthesis. The more common pathway, Calvin-Benson (C_3), utilizes 3 carbon atoms and is found in the majority of plants: trees and cold-season grasses. C_3 plants have typical $\delta^{13}C$ values around -36‰. C_4 plants, utilizing Hatch-Slack photosynthesis, are found in the tropics or temperate grass lands and have typical values around -21.5‰ (O'Leary, 1981; Collister et al., 1994). The difference among these pathways allows for interpretation of changing sources, in addition to changing production rates. Increasing $\delta^{13}C$ values often correlate to increased primary productivity, and decreased production is often interpreted from decreasing values.

Algae using dissolved $CO_{2(aq)}$ at equilibrium with the atmosphere ($CO_{2(atm)}$) have $\delta^{13}C$ values similar to those of C_3 plants (Meyers, 1997). As both bicarbonate and dissolved carbon dioxide are sources of inorganic carbon; preferences of carbon source

among phytoplankton species gives rise to changes in measured $\delta^{13}C$, as fractionation applies to the equilibrium of both chemical species (Mook *et al.*, 2004). Oligotrophic systems contain aqueous CO_2; often at supersaturated levels (Duarte and Prairie, 2005). Modeling inorganic carbon uptake in freshwater systems tends to assume that $CO_{2(aq)}$ is the predominant form of carbon incorporated into pelagic algae, and the resulting $\delta^{13}C$ reflects such a source with variations attributed to $CO_{2(aq)}$ availability and the lower energy of uptake by diffusion (Burkhardt *et al*., 1999).

The $\delta^{13}C$ found in atmospheric CO_2 is widely acknowledged to be influenced by historic and continued burning of fossil fuels, the Suess Effect (Gruber *et al*., 1999; Verburg, 2007). $\delta^{13}C$ analysis requires a correction factor to interpret data within a historical context (Verburg, 2007). Dissolved inorganic carbon (DIC) makes up the primary pool from which phytoplankton draw carbon, and when in equilibrium with atmospheric CO_2 has a carbon isotope composition that is ~8‰ enriched in ^{13}C compared to the atmosphere.

Studies have shown the validity of using $\delta^{13}C$ as a productivity proxy in Lakes Ontario and Erie (Schelske and Hodell, 1991; Hodell and Schelske, 1995;1998). In these studies $\delta^{13}C$ trends correlated with both predicted TP modeling and measured non-apatite inorganic phosphorus (NAIP) of the sediment. The majority of the $\delta^{13}C$ signal is undoubtedly from phytoplankton remnants in the sediment in Lakes Ontario and Erie, values measured range from -26 to -24‰ (Hodell and Schelske, 1998). Diagenetic alteration of $\delta^{13}C$ isn't a concern to interpretation. Replicate analysis of cores taken from

analogous locations 7 years apart yield matching trends, despite significant remineralization of C_{org} over time (Hodell and Schelske, 1998).

The interpretation of the stable isotope composition of sedimentary nitrogen $\delta^{15}N$ (based on the ratio of ^{15}N to ^{14}N), is generally more complicated than $\delta^{13}C$. Nevertheless, it can provide valuable insight when combined with additional proxies (Talbot, 2001). Changes in $\delta^{15}N$ may result from a variety of factors including biological and chemical fractionation, an enriched N source pool, and changes in sedimented organics or trophic level (Hodell and Schelske, 1998; Talbot, 2001). ^{15}N-riched nitrogen sources found in sediments may include eroded soils, fertilizers and urban wastewater. An increase in $\delta^{15}N$ was observed in bulk analysis of Lake Ontario sediments 40 years prior to increasing $\delta^{13}C$; likely indicating that productivity in the water column associated with P outstripped available N (Hodell and Schelske, 1998).

Biomarkers, n-alkanes in particular, are of great value as they represent stable fractions of the organic matter that resists alteration and destruction by microbial degradation keeping fundamental properties that can be used in paleoenvironmental reconstruction (Meyers, 1997). The abundance of n-alkanes, aliphatic hydrocarbons, may be attributed to production by photosynthetic organisms when observed with the following guidelines and act as a biological marker (biomarker) from specific sources within and surrounding lacustrine systems (Meyers, 2003). Biologically produced immature (i.e., not petroleum source) n-alkanes display an odd over even carbon chain-length predominance, and vary in chain length depending on the photosynthetic source. The primary assumption using the n-alkane biomarker is that short chain alkanes (15-21

carbons or C_{15-21}) are produced in larger concentrations primarily by aquatic organisms (Giger et al., 1980; Cranwell et al., 1987). Conversely, terrestrial organisms produce higher concentrations of long chain alkanes (25-35 carbons or C_{25-35}) (Eglinton and Hamilton, 1967). The odd chain predominance in biomarker n-alkanes is advantageous in the respect that contamination of samples with petroleum can be identified by the loss of this predominance. Petroleum contains a wide variety of alkanes and has lost the odd-even predominance over time, as initial biological compounds have gone through diagenesis and catagenesis (Meyers, 2003). Ratios of this odd over even predominance (called the 'Carbon Preference Index') of less than 3 for terrestrial compounds suggest petroleum hydrocarbon contamination, and should not therefore be used to make interpretations related to biological production (Bray and Evans, 1961; Castañeda *et al*., 2009b). For samples with the appropriate Carbon Preference Index, the ratio of long chain (terrestrial) to short chain (aquatic) n-alkanes (TAR_{HC}) has been applied in a variety of forms to indicate varying terrestrial/aquatic sources of organic matter (Goossens *et al*., 1989; Meyers and Ishiwatari, 1993; Castañeda *et al*., 2009b).

The photosynthetic pathway of particular plants may be determined by the isotopic composition of the individual n-alkanes, similar to that of bulk organic analysis of sediments. Extracted C_{25} to C_{29} n-alkanes of Ellesmere, England were used to determine that the source of sedimented n-alkanes appeared to be primarily from willow leaves of trees overhanging the lake (Riley *et al*., 1991). Studying the stable isotope composition of the carbon in n-alkanes may show input changes of particular sources and

act as an independent verification of changes in primary production and changes in the contribution of sources.

3. Methods

3.1 Field Methods

3.1.1 Sediment Coring

Sediment cores used in this study include BH09-2MC, BH09-3MC, BH09-4MC, BH09-5MC, BH03-1MC and BH03-3MC. All cores were recovered from the western and central basin of Lake Superior from the Research Vessel (R/V) Blue Heron (Fig. 1). The locations of the coring sites are indicated by name in Fig. 2. The sediment core naming scheme as follows: BH refers to Blue Heron, the following two digit number represents the year of the sampling (example: 03 is 2003), the last number refers to the sequential number of multicore sampling sites from a given year and which site it was in numerical order, and lastly MC refers to the core sampling type: multicore. The Ocean Instruments multi-corer is shown in on the deck of the R/V Blue Heron in Fig 1. The unit consists of four 10 cm polycarbonate tubes suspended vertically in a central location, tubes spaced approximately 0.3 m apart. The unit has 4 legs that support the central coring platform. As the multi-corer is lowered toward the lake bottom to collect core samples it is monitored acoustically, allowing for depth and location to be known. Once the multi-corer reaches the bottom, slack in cable supporting the instrument allows the weighted center sled to drive the core tubes into the sediment. The multicorer is hydraulically dampened for consistency during sampling. The cores are mechanically capped on the top and pulled from the surface of the sediment. Once the tube is free of the sediment, the core (which is held intact due to the suction of the top cap) is capped on the bottom. The multi-core is known for retrieving cores with little to no visible

disturbance of the sediment-water interface as was the case for the cores retrieved and used in this study.

Figure 1. R/V Blue Heron

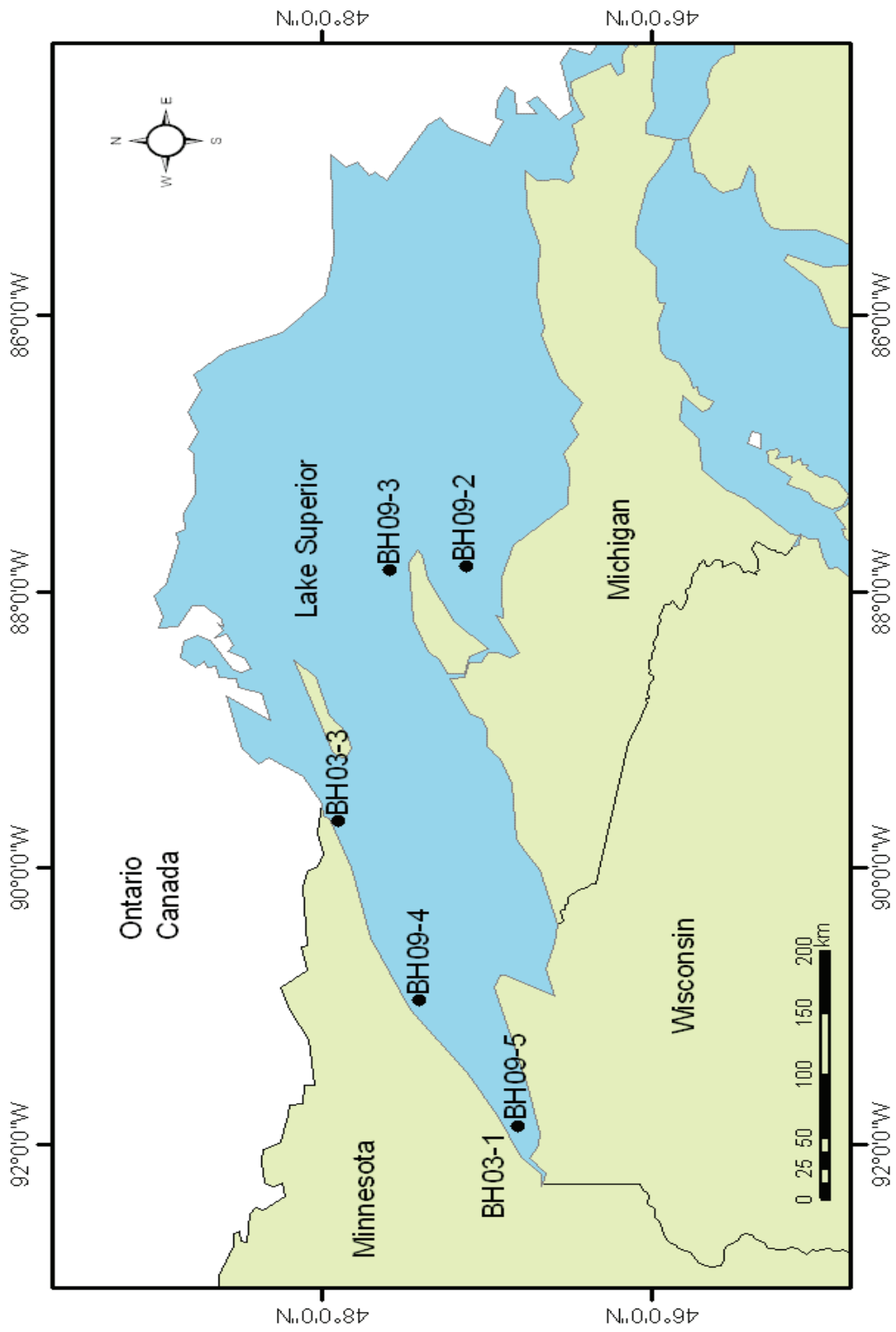

Figure 2. Map of Lake Superior Coring Sites

3.1.2 Sampling Locations and Dates

Of the 6 sediment cores used in this study, 2 were gathered during the summer of 2003 and 4 additional cores were retrieved in summer 2009. Information including the sample name, latitude, longitude, water depth, average sedimentation rate, and core length, and coring date can be found in Table 1. Coring sites are shown in Fig. 2. Core sites were identified using a Knudsen 12 kHz Hi-Res and CHIRP seismic reflection profilers onboard the R/V Blue Heron. The coring sites were chosen based on evidence of uninterrupted stratigraphy resulting from continuous sedimentation to characterize representative locations in Lake Superior. Core BH09-5MC was selected to give an indication of the reproducibility of results, acting as a sister location to core BH03-1MC. Core BH09-5MC provides a more recent profile of the region in addition to a higher average sedimentation allowing for improved temporal resolution for comparing the two cores at this location.

Core	Latitude	Longitude	Water Depth (m)	Sed. Rate (mm/yr)	Length (cm)
BH03 - 1MC	46-48.51	91-51.95	44	1.82	41.25
BH03 - 3MC	47-53.95	89-39.59	247	0.55	38
BH09 - 2MC	47-07.7	87-49.2	127	0.94	50
BH09 - 3MC	47-35.4	87-50.8	222	0.63	34
BH09 - 4MC	47-24.7	90-57.4	256	1.00	48
BH09 - 5MC	46-49.0	91-51.9	48	2.34	50

Table 1. General Core Information

3.1.3 Core processing on board the R/V Blue Heron

Cores retrieved from the sediment surface were removed from the multi-corer carefully to avoid disturbing the sediment water interface. One core from each 2009

sampling site was extruded on board the Blue Heron. Cores were extruded at 0.5 cm intervals in the upper 10 cm and at 1 cm intervals from 10 to 20 cm depth.

Extruding the cores involved placing the core in the vertical position, within the extruding device onboard. A 10 cm diameter piston mechanically operated from below shifts the core mass upward a known amount with turns of a nut on a threaded shaft. Cores are pushed upward until the sediment layer is brought above the lip of the core tube, this extruded layer is removed by the flat edge of a trowel. Each successive extruded interval was placed within glass sampling jars. Jars were pre-cleaned by ashing, caps were solvent rinsed with a regimen of 3 solvents in succession MeOH, acetone, and hexane and allowed to evaporate until dry. All sample jars were refrigerated onboard the Blue Heron post sampling. Frequently, one or more of the cores do not have the suction needed during the retrieval process; the cores are subsequently lost from the sample suite of four possible cores. The additional cores that were not extruded onboard were prepared for long term storage. This involved using an extruding piston to push the sediment to the top of the core tube. As the core was pushed upward the excess water was pushed off, the remaining water was solidified using Zorbitrol®Plus (poly (sodium acrylate) homopolymer), commonly used to absorb chemical and biological spills in laboratories. Once the top of the core was stabilized the cap was placed and taped in place. The bottom of each core tube was cut to length using a saw, in some cores green floral foam was used to fill the space left by the piston and isolate the core from the bottom cap that was placed and taped. Cores were marked by name, including core reference letter A-C with and an arrow indicating the top of the core.

3.2 Laboratory Methods

3.2.1 Initial Core Description

Initial core description was performed at LacCore (the National Lacustrine Core Repository) at the University of Minnesota Minneapolis. Whole cores were measured for density using the Geotek standard multi-sensor core logger using the gamma function program. Following density measurement cores were split using a multi-step method. Each polycarbonate core liner was cut/scored lengthwise on opposite faces of the core tube simultaneously, leaving a very thin layer of polycarbonate intact next to the sediment inside using cutting heads using vibration. Once the tube had been etched the remaining cut was finished using a razorblade and included the core caps, which were left taped in place. To split the material portion of the sediment each core was divided using a wire or core splitting blades. After being split each half of the core was smoothed by hand with a glass slide to repair and remove all disturbed material on the surface resulting from the splitting process. The more ideal half of each core was then imaged using a Geotek Geoscan-III digital linescan camera at 400 pixel/cm resolution, a reference scale was provided next to each core along with the core name. The other half was measured for magnetic susceptibility using Geotek XYZ multi-section automated split core logger. Finishing these analyses the cores were wrapped in protective plastic and placed into clean and labeled core tubes.

3.2.2 Core Sub-Sampling

Sub-sampling of sediment cores was performed in the Sedimentology Laboratory at the Large Lakes Observatory. Cores that had been split at LacCore were retrieved

from the adjacent storage. Using guides with metric dimensions, the working half of each core was unwrapped from the protective plastic and oriented with the top of the core marking zero, all depths down core given a positive number as a numeric metric interval. In preparation for sampling the surface of interest of each split core was cleaned of debris and material that was in contact with the protective plastic with a clean glass slide that was wiped clean after each pass. Cores BH03-1MC, BH03-3MC and BH09-5MC were sampled in this fashion. Sampling of each core was performed with 1 cm width spatulas or razorblades depending on the consistency of the associated sediment and the width of the sample interval. In between each sub-sample the spatula was wiped off using a paper towel and then rinsed in distilled water, excess water was wiped from the spatula. Cores were re-wrapped in protective plastic and returned to cold storage at LacCore.

3.2.3 Water Content and Porosity

Portions of the extruded core sample or the sub-sampled portions of split cores were placed into pre-weighed, ashed sample vials or glass jars depending on the intended sample size. The jars were 60 mL with Teflon caps, the vials were either 8 or 4 mL with Teflon caps, all caps were solvent rinsed and allowed to evaporate until dry prior to use. The wet weight was recorded for each sample, sub-sample weights ranged dependent on sample size, water content, and sample container. These samples were frozen and freeze dried. Dried samples were then re-weighed for a determination of the water content and porosity. Samples with measured water content were ground in preparation for further laboratory work using a mortar and pestle, between each grinding the mortar and pestle

was rinsed with deionized water (Milli-Q, MQ), wiped with paper towel, rinsed again with MQ, final rinse with MeOH, and allowed to evaporate to dryness before grinding the next sample.

3.2.4 ^{210}Pb Activity Analysis

Analyses of ^{210}Pb concentrations on two cores, BH09-1MC and BH09-3MC, obtained during 2003 were completed prior to this research project, age calculations were completed by UMD undergraduate Kimberly Smith under the advisement of Dr. Tom Johnson during 2003/2004. Smith's calculations were duplicated for confirmation and used for the age determination of these cores. The four cores obtained during the summer of 2009 were analyzed in the lab of Dr. Paul Wilkinson by Eva Slavicek at the Department of Soil Science, University of Manitoba. ^{210}Pb was measured in alternating 0.5 cm intervals to 10 cm depth and alternating 1 cm intervals from 10 to 20 cm, for a total of 15 subsamples for each core. Core BH09-5MC had additional 1 cm intervals centered at 24.5, 29.5, 34.5, 39.5, and 44.5 cm included for analysis. Dried and ground sediment samples from extruded core portions were collected for each interval, 0.5 to 1.0 grams were analyzed for ^{210}Pb by leaching in 6N HCl in the presence of a ^{209}Po tracer. Plating Po onto a silver disc, an alpha spectrometer was used to count radio decay through alpha emission (Appleby 2001). With this method ^{210}Pb concentration is determined from the concentration of its ^{210}Po daughter in the ^{238}U decay series.

3.2.5 Bulk Elemental Analysis: Carbon, Nitrogen and Stable Isotopes

Portions of each dried and ground sample of sediment were measured for stable C and N isotope composition using a Costech Elemental Analyzer coupled to a ThermoFinnigan DeltaPlusXP stable isotope ratio monitoring mass spectrophotometer located at the Large Lakes Observatory. Dry sediment samples of known weight (15 mg), were placed into Silver (Ag) foil capsules, 1 μL of nanopure filtered H_2O was dispensed into each sample capsule, trays of sediment and water treated cups were placed in a desiccater containing a 200 mL beaker of 12M HCl for 4 hours to remove inorganic carbon from the sediment. Once removed from the acid environment samples were allowed to off gas the residual HCl, then dried in a 60^{o}C oven for 4 hours. Dried samples in Ag capsules were folded and placed into Tin (Sn) foil cups and folded ready for analysis. All cups were prepared with care to avoid trapping atmospheric gases and were rounded until spherical in anticipation of possible pneumatic auto-sampling complications of the instrument. Every 4th sediment sample was run in duplicate. Isotopic standards used by the instrument included 0.0400 mg acetanilide, 0.250 mg caffeine, 20.0 mg B2153, 0.500 mg B2159 and 0.150 mg urea weighed into Sn capsules and run as every 3rd measured sample on the instrument. A total of 145 samples excluding standards were analyzed. The instrument uses a 1700^{o}C combustion chamber in which a stream of oxygen oxidizes the sample forming N_2 and CO_2 gas. An inline reduction furnace held at 650^{o}C removes O_2, through formation of CuO, prior to detection of N_2 and CO_2 by the mass spectrometer. Values are given in standard delta notation as per mil deviation from the VPDB standard.

3.2.6 n-alkane Biomarker Extraction

The total lipid extract (TLE) was obtained from sediment samples using a DIONEX Automated Solvent Extractor (ASE) 350. Dry ground sediment samples, of known weight, were mixed in a qualitative ratio of 4 to 1 by weight with diatomaceous earth (DE) which acts to break up samples and increase surface area, allowing for maximum extraction of the lipid content. The sediment/DE mixture was placed into an ASE sample cell with a cellulose filter placed at the bottom of the cell. Additional DE filled any remaining space and the top cap was placed onto the cell. Once sample cells were placed onto the instrument the TLE was collect using 'Method 1.' Method 1 included the following parameters: Temperature: 100^{o}C, Heat: 5 min, Static Time: 5 min, Cycles: 3, Rinse Volume: 30%, Purge: 80 S, Solvent A: 5 mL 9:1 DCM/MeOH, Solvent B: 1 mL MeOH, Solvent C: 4 mL 9:1 DCM/MeOH, Cell Type: SST, Method Rinse: Yes, 5 mL. The instrument extracts the lipid content with aliquots of 9:1 DCM/MeOH and MeOH under N_2 pressure of a heated sediment sample. Glass ASE collection vials were prepared by ashing at 450^{o}C for 4 hours, caps with Teflon liners were solvent rinsed (MeOH, Acetone, and Hexane) and labeled prior to extraction. Clean preparation of the ASE cell bodies is imperative for accurate results. Cells comprised of cell bodies and caps were each cleaned with separate protocols. Cell bodies were rinsed in H_20 and brushed, soaked in a tub of hot water and rinsed again, allowed to dry, rinsed in order with MeOH, Acetone, and 9:1 DCM/MeOH. Cell caps were soaked in water, dried, sonicated in MeOH for 30 min, rinsed with MeOH, Acetone, and 9:1 DCM/MeOH. Cells were assembled then wrapped in ashed foil for storage.

3.2.7 Bond Elute Column Separation

The TLE was separated into sub-fractions based on polarity using Alltech® aminopropyl bond elute columns, 6 cm in length and 1 cm wide. The flow of sample through the column was regulated by N_2 pressure gas at ~5 psi, 1 drip from the column every 2-3 seconds. The nozzle of the N_2 gas line was rinsed with MeOH and allowed to dry prior to each sample run on the column to avoid contamination. The column was suspended using a typical laboratory ring stand. The column was rinsed with 8 mL of MeOH followed by 8 mL of 9:1 DCM/MeOH. When just a meniscus of 9:1 remained on the column the sample dissolved in 9:1 was added. Only half of the TLE fraction brought back up in a known amount of 9:1 was transferred to the column, this was less than the sample size limit of the column, and allowed analysis of the second half to determine processing precision. Upon addition the sample was allowed to interact with the column surface for 2 min. prior to elution. The column was eluted with 8 mL each in the order of 9:1 DCM/MeOH, 4% glacial acetic acid in ethyl ether, and MeOH. Each solvent was added successively, the column was blown dry from the prior solvent before continuing with the next. The fractions eluted in order respective to the chemical treatment were neutral lipids, free fatty acid (FFA), and phospholipid fatty acid (PLFA), the fractions are named operationally to describe the primary constituent of interest or chemical properties of the fraction. Each eluent was collected into 30 mL vials and evaporated for transfer to preweighed and ashed 4 mL vials. The FFA and PLFA fractions were archived for future study, the neutral fraction was further separated in an additional column step, an alumina column separation.

3.2.8 Alumina Column Separation

Alumina column chromatography was used to separate the neutral lipids into apolar and polar fractions. Alumina used in the column was solvent rinsed and preactivated at 150^{o}C for 2 hours less than 24 hours prior to use. An ashed 5 ¾“ Pasteur pipette was lightly plugged with a small amount of cotton wool, the activated alumina was then added to a desired height of 2” in the pipette, about ½ full. The column was then lightly tapped twice to settle the contents. The pipette was suspended using a ring stand. Each run used 4 collection vessels: 1 for waste and three 4mL prelabeled vials to collect the apolar, polar 1, and polar 2 fractions. The column was initially cleaned using 1 column volume of 9:1 hexane/DCM. Transferring the sample of known weight in a small portion of 9:1 hexane/DCM to the wet column the apolar fraction was collected with an additional 2 pipette volumes of 9:1 hexane/DCM, the solvent first being added to the sample jar and then to the column. The 4th addition of 9:1 hexane/DCM did not contain sample and was used to flush the remaining apolar fraction from the column. The second of the 3 fractions in the mixture, operationally called polar 1 was isolated with 1:1 DCM/MeOH. When the column had just a small portion of 9:1 remaining from the previous step, 1:1 DCM/MeOH that was first added to the sample vial was added to the column. The apolar collection vial was then replaced with the polar 1 collection vial and 3 additional volumes of 1:1 DCM/MeOH were added to the column, these were not added to the sample vial prior to addition. When just a meniscus of 1:1 DCM/MeOH remained on the column, pure MeOH was added to collect the remaining compounds stuck to the column. The polar 1 collection vial was replaced by the polar 2 collection

vial and a total of 4 pipette volumes were used to flush these remaining compounds from the column. Each fraction from the process was dried and either quantified or archived. The apolar fraction contained the n-alkanes desired for analysis for both abundance quantification and carbon isotope composition.

3.2.9 Removal of Elemental Sulfur

Elemental sulfur was removed from the TLE (total lipid extract) with copper beads. Copper beads were reduced by adding a low concentration of HCl to dry beads and stirring, after being returned to a shiny luster the beads were rinsed 5 times with distilled H_2O. To remove water, beads were treated 3 times each in 3 solvents in succession: MeOH, acetone, and hexane and allowed to evaporate until dry prior to use. Beads were dispensed into containers containing the lipid extract dissolved in 9:1 DCM/MeOH, 3-5 beads added to each. If the beads turned black shortly after addition more were added. Beads reacted in vials overnight or a minimum of 10 hours. The TLE was transferred to new vials following the prescribed time and beads were recycled to be used again. In several samples multiple treatments of this method were necessary to remove all the sulfur.

3.2.10 Biomarker (n-alkane) Quantification

The apolar fraction derived from the alumina column was weighed and transferred to GC vial inserts. The external vials for each set were dosed with ~0.5 mL of hexane to limit transfer and loss of liquid sample out of the smaller inside insert from

physical processes including surface tension and vapor pressure. Vials were ashed at 450^{o}C for 4 hours prior to use, caps were solvent rinsed in MeOH, acetone, and hexane. Each sample was dried in the GC vial insert and brought to a known volume prior to analysis on the GC. The internal standard androstane was used to quantify all n-alkane samples. Androstane at concentrations of 30 ng/μL was determined to give peak areas that fell within the range of the average peaks heights of the n-alkane samples with linear detection behavior over the desired detection range. 1200 ng of androstane was added to each sample. If samples were quantified multiple times, hexane was adjusted to maintain the 30 ng/μL concentration.

Samples were quantified using an Agilent 6890 GC equipped with a 7683 auto-sampler. The injection size used for quantification was 1 μL of sample. The equipment set-up and run method used to elute n-alkanes was as follows. Instrument setup: 30 m HP-1 capillary column with 320 μm inner diameter and 0.25 μm film thickness, flow rate 2.6 ml/min He, with a splitless injector held at 250^{o}C and 80.9kPa, analysis by flame ionization detector (FID) and flame photometric detector (FPD). Temperature ramp conditions: Initial: 50^{o}C - 1min, ramp 1: 10^{o}C/min to 130^{o}C, ramp 2: 4^{o}C/min to 320^{o}C, total run time 66.60 min.

Well established predictable retention times for n-alkane elution were checked, using an Agilent 6890A Series GC System equipped with a quadrupole mass spectrometer (MS) in the Werne lab, allowing identification of specific n-alkanes in our samples. The retention time specific to this GC set-up is a function of chemical and

physical properties, as the only change among compounds is in length, the elution time is particularly predictable.

3.2.11 n-alkane Stable Isotope Composition Analysis

Stable carbon isotope composition of n-alkanes was completed using the ThermoFinnigan Delta PlusXP isotope ratio mass spectrometer, using a modified GCC III interface, commonly referred to as a GC-C-IRMS instrument. Under splitless conditions samples of 1 μL containing approximately 10^{-8} g of sample were co-injected with 0.6 μL of squalane internal isotopic standard, which eluted between the C_{26} and C_{27} n-alkanes. Instrument setup: 30 m HP-1 capillary column with 320 μm inner diameter and 0.25 μm film thickness flow of 2.6 ml/min He, with a splitless injector held at 300°C, into an oxidizer held at 950°C, the stream of He and CO_2 leaving the oxidizer was measured using ThermoFinnigan Delta PlusXP. Method and temperature ramp conditions: Initial: 50°C – 1 min, ramp 1: 10°C/min to 130°C, ramp 2: 4°C/min to 320°C. Calibration was performed using a mixture of n-alkanes C_{16} to C_{30} of known isotopic value. Peaks comprising n-alkanes from C_{31} to C_{34} were predicted using retention times from GC-FID plots and GC-MS known peaks. Isodat 3.0 software was used to interpret isotopic results. Selected samples were run in duplicate, several multiple times (3-5) to interpret instrument variability, response, and error. Values are given in standard delta notation as per mil deviations from the VPDB standard.

4. Results

4.1 Core Descriptions

Core BH03-1MC pictured in Fig. 3, 41 cm in length, was imaged after sub-sampling with a standard handheld digital camera. The core consists of a homogenous brown mud the length of the core. A darker interval, dispersed banding of precipitated metals additionally identified in other cores is apparent from 6-16 cm depth. The core lacks structured horizons corresponding to iron (Fe).

Core BH03-3MC shown in Fig. 4 is 38 cm in length, the core was sub-sampled prior to imaging. The core top consists of a dark brown mud to a depth of 4 cm followed by a light brown silty clay band from 4-6 cm. The remainder of the core consists of a gray silty loam from 6-38 cm depth. The core displays no prominent physical horizons.

Core BH09-2MC displayed in Fig. 5, 50 cm in length, has a core top that was disturbed by zorbitrol. The zorbitrol layer extends to a depth of 10 cm, this layer appears to have both displaced some sediment material and been incorporated into the rest, the displacement due to its use did not shift the layers found beneath 10 cm depth. The sub-samples from this core were sampled as extruded layers from a sister core, untreated with zorbitrol. The core consists of a homogenous brown mud to a depth of 14 cm. The 14-17 cm interval contains a darker silty clay layer, marking the boundary of the oxygenated sediment (Richardson and Nealson, 1989), this diffuse darkened layer shows no structure. The core displays no prominent horizon marking iron oxides. The remainder of the core, 17-50 cm depth, returns to the lighter brown color silty clay. This lower portion of the

core is similar to that found above the oxic/anoxic boundary, with no visible structure or prominent features shown.

Core BH09-3MC pictured in Fig. 6 is 34 cm in length, has a disrupted core top to a depth of 4 cm from zorbitrol use. As with core BH09-2MC, the solidifying agent (zorbitrol) was incorporated into a portion of the sediment but does not appear to have shifted the core mass in the core tube. The core top consists of a brown mud to a depth of 6 cm. Below this layer a black horizon formed from dispersed metal oxides, 1 cm in thickness, extend to 7 cm depth. A reddish horizon containing a diffuse Fe-oxide boundary, 2 cm thick, exists below the Mn horizon at 7-9 cm depth. Below 9 cm the brown silty clay is repeatedly highlighted by bedding features of thin (2-5 mm) light and dark bands.

Core BH09-4MC pictured in Fig. 7, 48 cm in length, contains a layer of zorbitrol to 4 cm that appears to have incorporated sediment material into its mass but not to have displaced sediment material downward. Sub-samples were taken from a sister core not dosed with zorbitrol for analysis besides imaging and MS. The core consists of a red-brown mud at the top of the core extending to 5 cm. Below, a tan silt layer occurs from 5-6.5 cm, accented by a deeper dark boundary to the reddish clay slit at 6.5-7.5 cm depth. Beneath this interval is a 4 cm horizon encompassing the oxic/anoxic boundary found from 7.5-11.5 cm. This layer is highlighted by several very thin darker bedding features. From 11.5 cm to the end of the core is a silty clay grayish brown in color.

Core BH09-5MC, pictured in Fig. 8, is 50 cm in length. The core top had limited zorbitrol dosing and very minor cracking damage due to handling, the uppermost

sediment layers are a red brown mud to depth of 3 cm. Below this mud lies reddish silty clay, lightening in the 33-39 cm depth interval, for the remainder of the core to a depth of 50 cm with repeated thin banding. A slightly darker feature highlights the core at 14-22 cm depth but doesn't contain an apparent oxic/anoxic horizon found in other cores.

Figure 3. Core BH03-1MC

Figure 4. Core BH03-3MC

4.2 Magnetic Susceptibility

Changes in the concentration of magnetic materials down the length of a sediment core are the consequence of various physical and chemical processes within sediments including erosion, deposition, and mixing of surface sediments as well as solubility properties associated with the availability of oxygen at depth (Ngobi 1998, Nowaczyk 2001). Magnetic susceptibility (MS) profiles, given in SI units are plotted vs depth in the following figures of the 2009 cores. MS data for the cores retrieved during 2003 was unavailable. Each MS profile is shown to the left of the image of the measured core.

The MS profile of Core BH09-2MC (Fig. 5) starts below the zorbitrol layer at 10 cm depth, decreasing from a maximum at 12 cm depth of 23.5, likely due to increased magnetic properties of Mn and Fe corresponding to the oxic/anoxic boundary layer with little visible presence noted initially, in an undulating fashion to a local minimum at 34 cm depth corresponding to a value of 4.75. From 25 to 43 cm depth the profile remains steady near 10, likely a period of constant sedimentary processes. The profile dips to a core minimum of 2 at 45 cm depth, an event estimated from extrapolated age calculations to be between 400-500 years old, measurement increases to 13 by 46 cm depth. The remaining profile to 50 cm drops off with proximity to the end of the core.

Core BH09-3MC in Fig. 6 displays a maximum of 29 units at 6 cm depth corresponding to the oxic/anoxic boundary and the associated precipitated metals concentrated in these layered horizons. The profile from 10-25 cm shows minor fluctuation around 10 SI units. The profile displays a local maximum of 18 at 28 cm depth before decreasing at the end of the core.

In core BH09-4MC (Fig. 7), the MS profile reaches a maximum of 200 SI units appearing to exceed the limit of the MS measurement scale of the Geotek core logger. These are likely to be iron rich tailings, providing a means of physically capping the sediments below. The remainder of the core's MS profile is rather constant hovering near 20 for the remainder of the core.

Core BH09-5MC, profile displayed in Fig. 8, is the only core collected in 2009 not having Zorbitrol use effect the core top and associated MS values. The profile increases steadily through the top 2 cm to a value of 60, likely an effect of both the edge of the core and mixing of uppermost sediments. The profile reaches a maximum of 83 at 10 cm depth before falling to a nearly constant value of 50 through a long interval 15-40 cm depth. At 44.5 cm depth we see a slight increase to 63 followed by a return to 50 before tailing off at the end of the core at 50 cm.

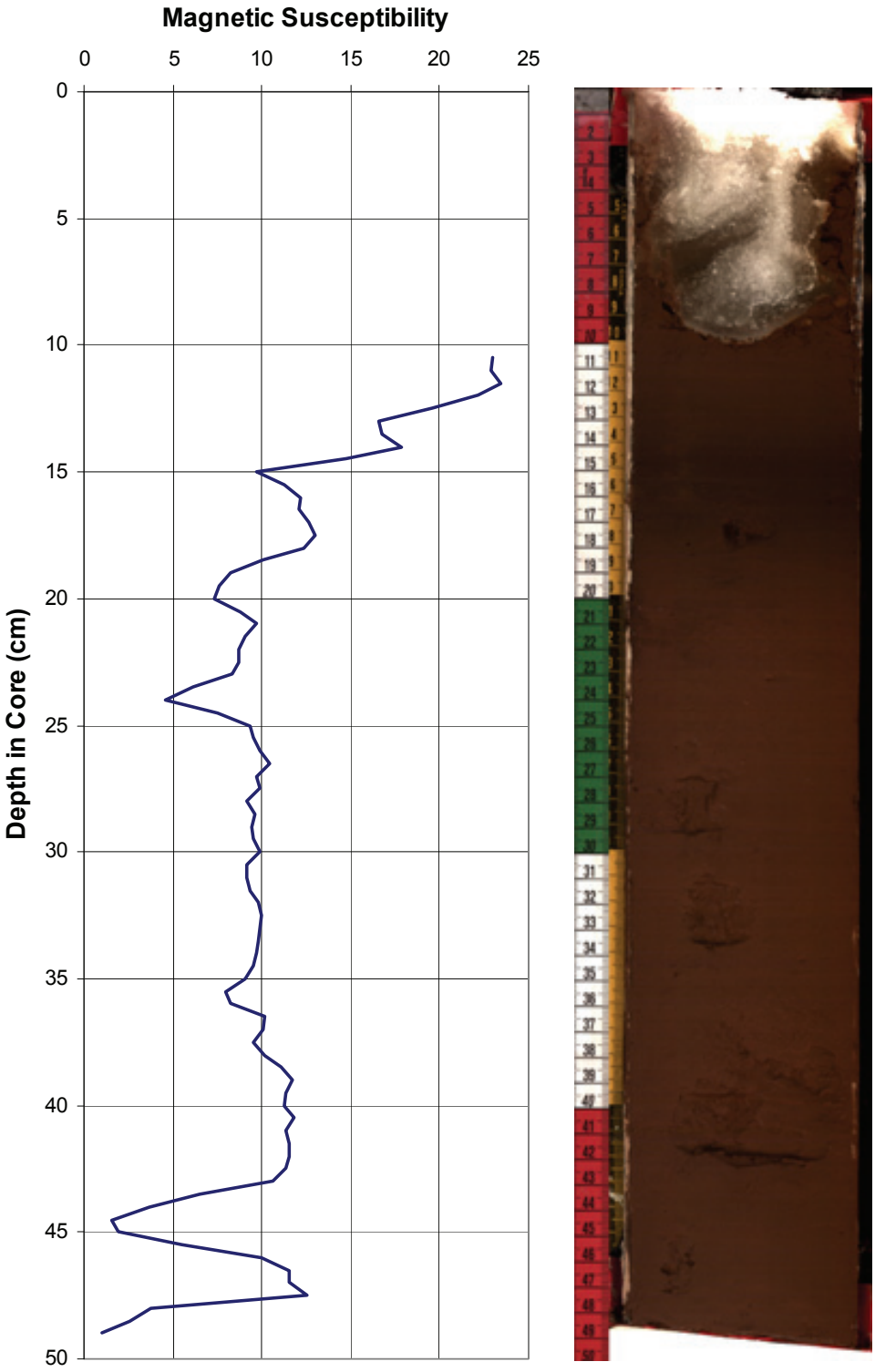

Figure 5. Magnetic Susceptibility Profile, Core BH09-2MC

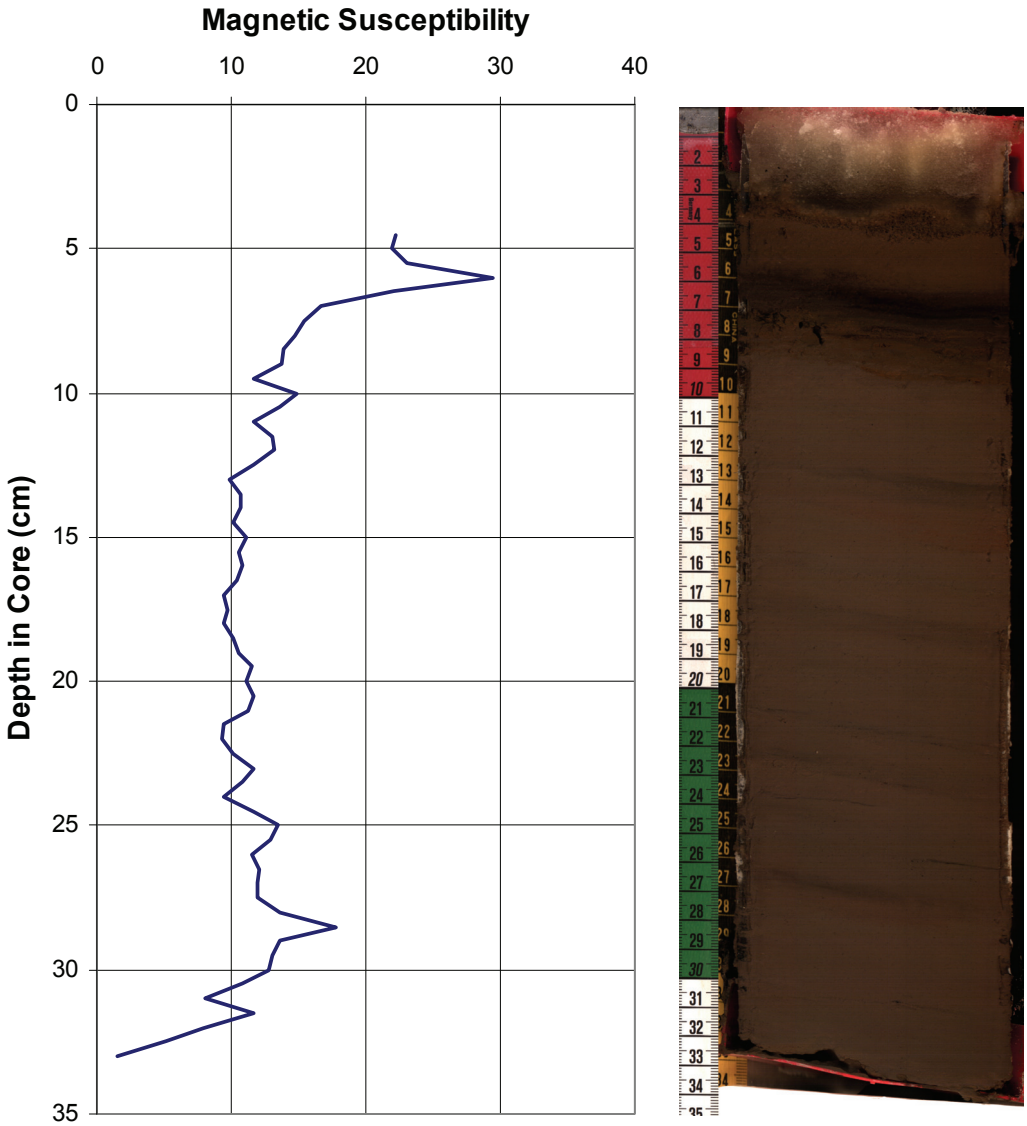

Figure 6. Magnetic Susceptibility Profile, Core BH09-3MC

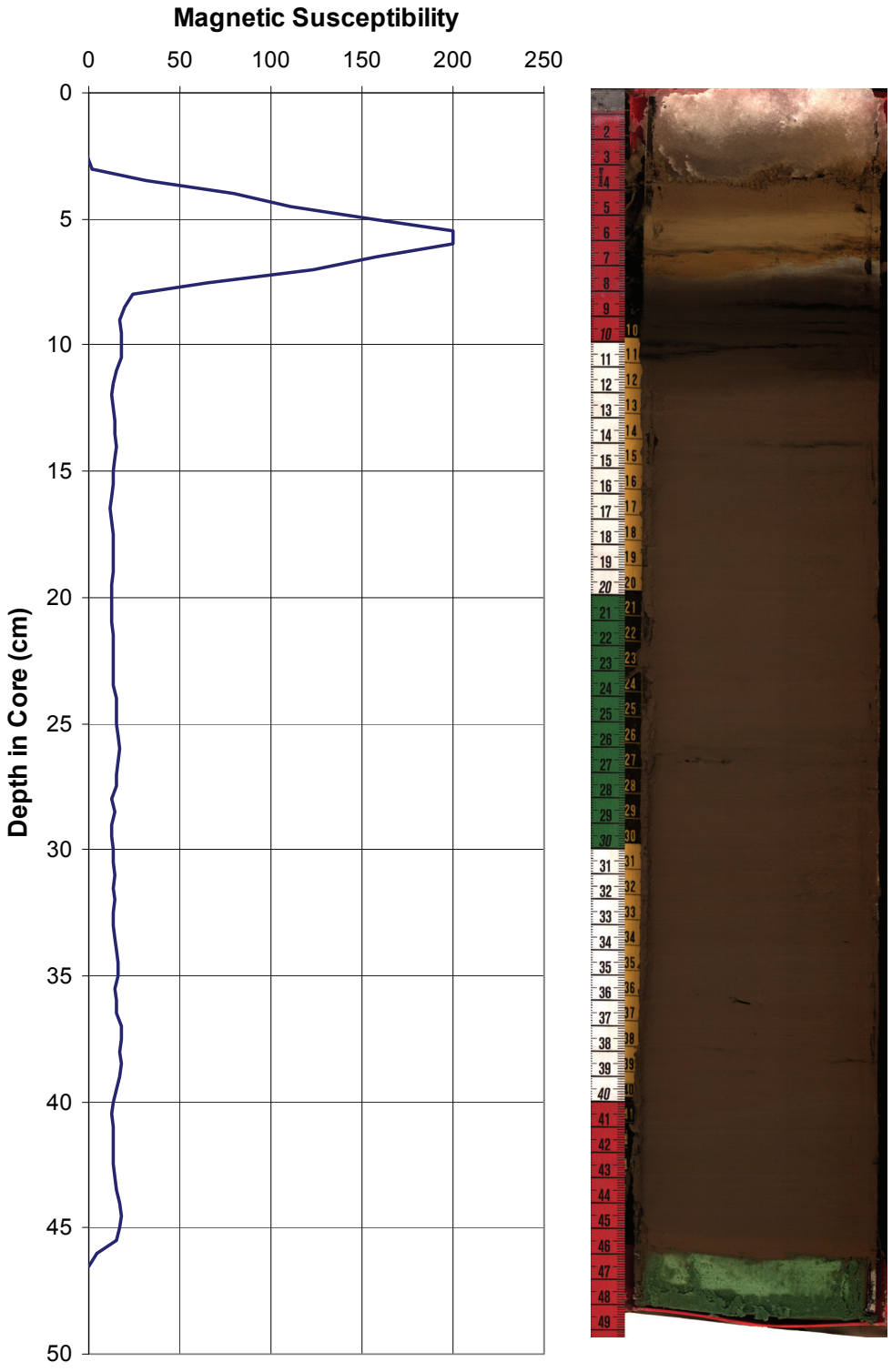

Figure 7. Magnetic Susceptibility Profile, Core BH09-4MC

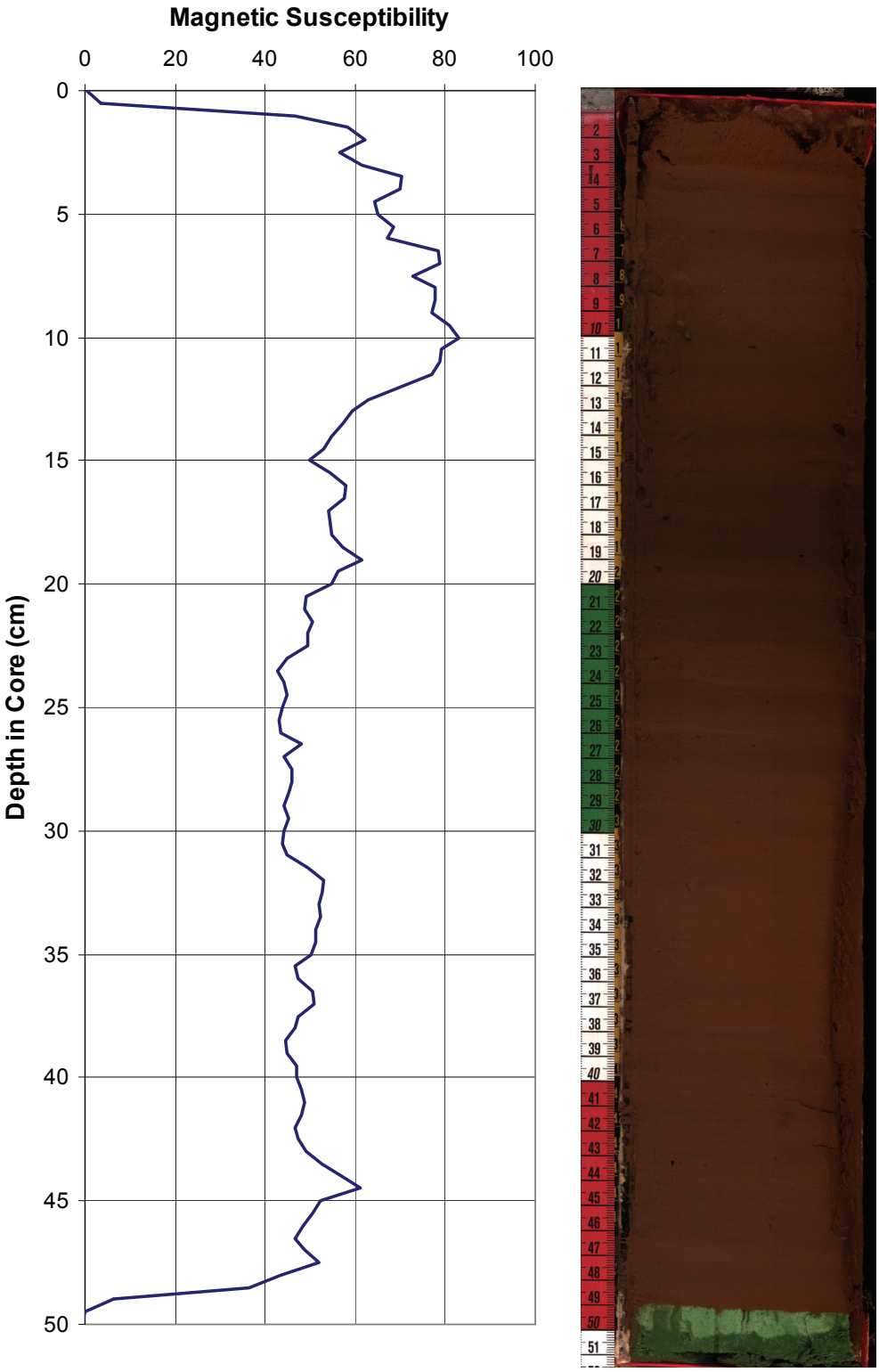

Figure 8. Magnetic Susceptibility Profile, Core BH09-5MC

4.3 Water content

Water content of cores retrieved in 2009 is plotted in Fig. 9; data is not available for cores retrieved in 2003. Due to the long term horizontal storage of these (2003) cores; interpretation of water mass from current measurements would be unrepresentative (as water has drained and filled prior sample sites within the core). Water content is not necessary for age calculations as they were completed in a previous study (see Sec 3.2.4); cores are thought to follow similar trends to those sampled/measured in 2009. Sample size ranged from 0.5-15 g wet sediment; small sample sizes may have led to unexpected water mass values. In several samples solid sediment portions expelled water during unintentional freezing prior to secondary subsampling, giving uncharacteristically low water content values. Samples suspected of such behavior include intervals centered at 4.25 and 9.5 cm (in BH09-3MC), 5.25, 6.25, and 7.25 cm (in BH09-4MC). All cores display compaction (lower porosity) of sediment down core, the largest change with the top 5 cm, a smaller rate of loss after 10 cm depth. Core BH09-2MCs profile displays general loss of porosity/water until ~10 cm depth, the following 10 cm depth show little change. Deviation of water content in BH09-3MC is likely caused by complications between repeated measurements, without these data the profile appears very similar to core BH09-2MC, smaller particle size may have led to lower porosity and less water content overall. Core BH09-4MC displays dramatic reduction in water content initially to ~3.5 cm, this includes points we believe may show atypical behavior, followed by a marked increase in water content after ~7.5 cm depth. The outlier at 19.5 cm depth interval is likely the result of sub-sampling a large piece of hard mineral debris. Core

BH09-5MC displays general loss of porosity with depth until ~12 cm at which point deeper measurements profiles constant water content.

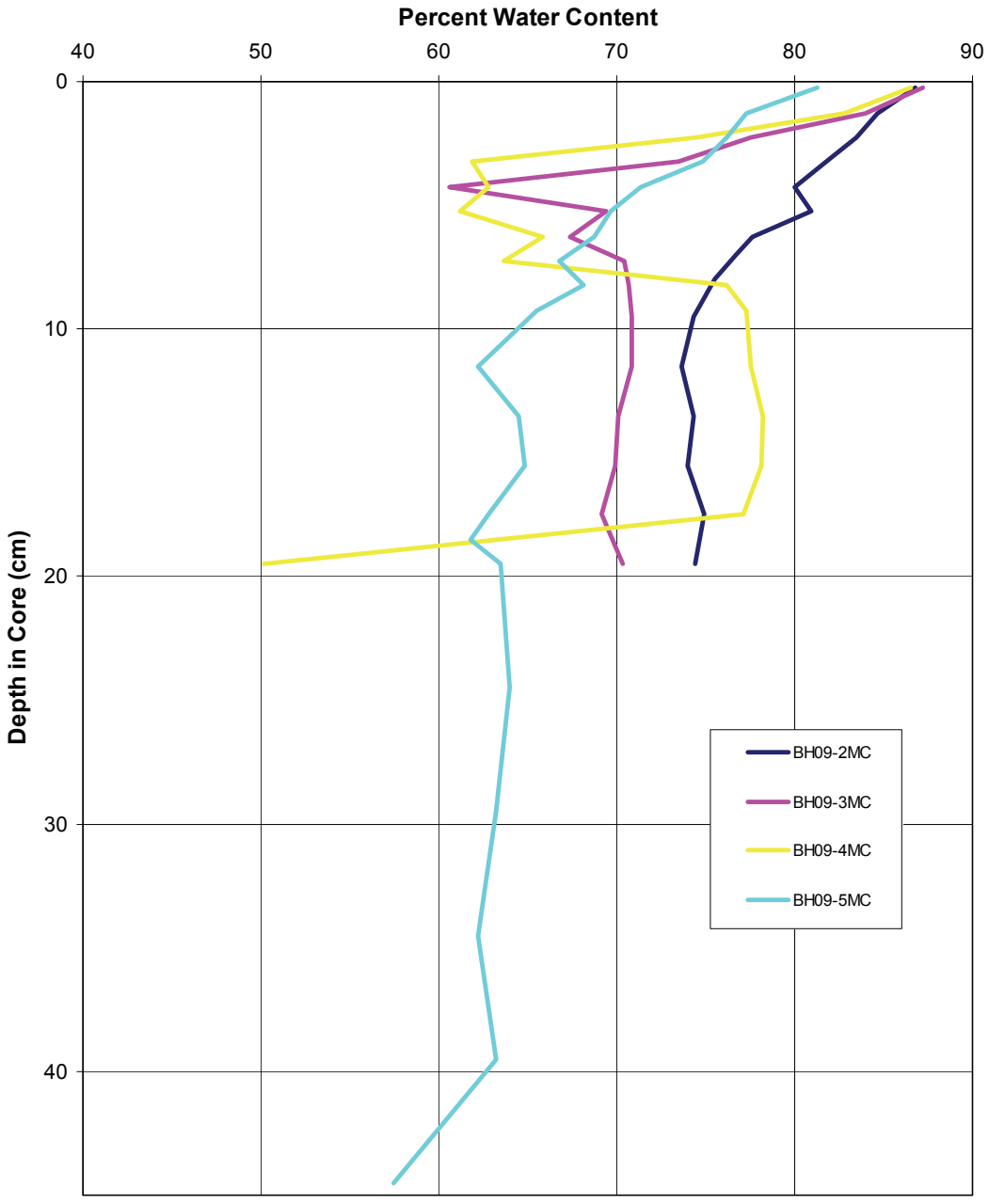

Figure 9. Percentage Water Content (2009 Cores)

4.4 Geochronology

4.4.1 ^{210}Pb Dating

^{210}Pb which has a half life of 22.26 years is ideal for radiometric dating of materials that are younger then 150 years, in samples containing sufficient nuclide for measurement (Oldfield and Appleby, 1984), and is widely used (Oldfield and Appleby, 1984; Noller, 2004; Tylmann, 2004; Evans, 1981).

The 'supported' portion of ^{210}Pb within lake sediments is derived from precursors such as ^{226}Ra and elements higher up the ^{238}U decay series, incorporated into the sediment, prior to decay resulting in ^{210}Pb. These radionuclides are transported to the sediments primarily through erosional processes in the drainage basin, without the aid of a gas phase as with ^{222}Rn the atmosphere plays a much smaller role in its eventual sedimentation (Appleby, 2001). The supported portion of ^{210}Pb within the sediments is effectively in equilibrium with the deposited ^{226}Ra. With a half life of 1602 years ^{226}Ra undergoes subsequent in-situ decay to ^{210}Pb, ^{226}Ra gives rise to persistent ^{210}Pb long after that which arrived primarily through atmospheric processes has decayed away (Oldfield and Appleby, 1984). An overview of the processes producing and moving ^{210}Pb into sediments is shown in Fig. 10.

The assumption that the 'unsupported' component of the ^{210}Pb signal is much larger than the 'supported' portion is a necessary for age calculations. To determine the excess ^{210}Pb portion of the signal, the ^{226}Ra activity is subtracted from the total ^{210}Pb activity (Appleby, 2001). The ^{226}Ra activity is estimated from the mean ^{210}Pb activity at a depth down core when ^{210}Pb activities show asymptotic behavior approaching constant

values, assuming at these depths the unsupported component was effectively zero, the difference in these activities were less then the uncertainty of the measurement the ^{210}Pb signal and effectively all from the 'supported' lead component (Appleby, 2001; Oldfield and Appleby, 1984). In several of the cores the 'supported' activities were averaged values of several data points, all having lost the "unsupported' portion of the ^{210}Pb signal to decay. All 'supporting' ^{210}Pb activities selected agreed with the suggestions by Oldfield and Appleby; having decayed more then 6-7 half-lives.

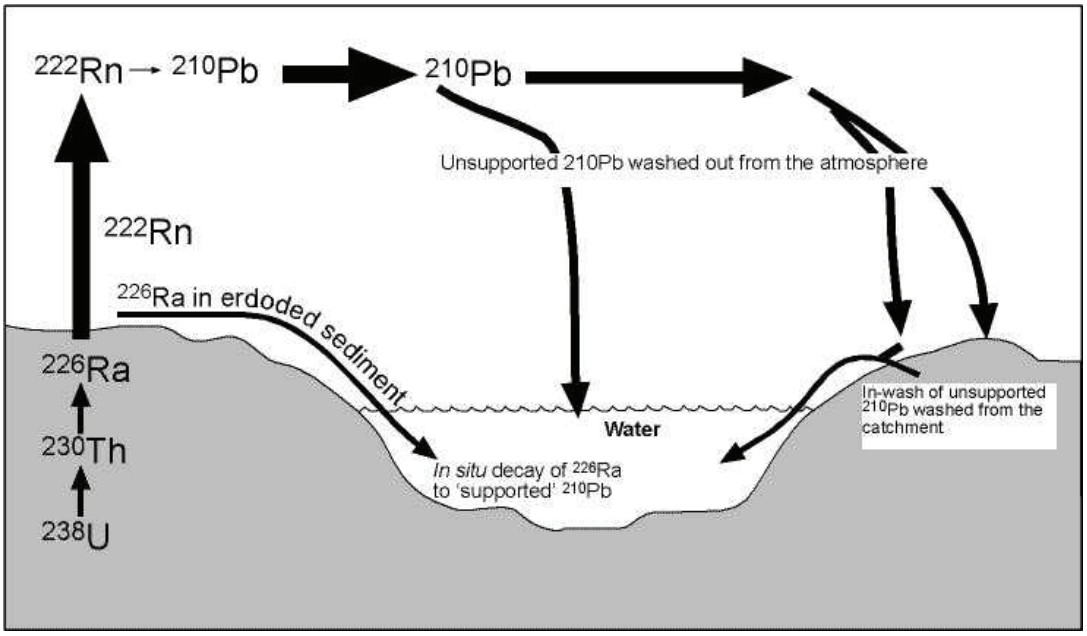

Figure 10. ^{210}Pb Sources (Oldfield and Appleby, 1984)

4.4.2 ^{210}Pb Age Models

In this study two common age models were compared to interpret sediment ages the constant flux/constant sedimentation rate model (CFCS) and the constant rate of supply model (CRS). For each core the models were compared, for all of the cores used in this study the CRS model was chosen for age determination. Both models give nearly identical results for cores with continuous sedimentation.

The CRS model adheres to a number of assumptions. Flux of unsupported ^{210}Pb to the sediments from the atmosphere is constant. ^{210}Pb within the water column is quickly transported to the sediment surface though adsorption to sinking particles. The unsupported ^{210}Pb content is exclusively from atmospheric sources. ^{210}Pb is assumed to not re-distribute once reaching the sediment surface. Lastly, that the decay of ^{210}Pb follows the decay law with a predictable rate of 0.03114 y^{-1} (Appleby, 2001). As the concentration of initial unsupported^{210}Pb changes due to sedimentation, the relationship between the two varies inversely as long as the ^{210}Pb flux remains constant (Appleby, 2001). Described by Appleby and Oldfield (1978) the calculations for the CRS model follows.

$$A = {}_m\int^{\infty} Cdm = {}_x\int^{\infty} \rho C dx \qquad \text{Equation 1.}$$

In Equation 1, the cumulative unsupported ^{210}Pb activity A is calculated to depth x, alternatively the cumulative dry mass m (ρ = dm/dx is the dry weight/wet volume ratio). By inserting t = 0 in the above equation we calculate the ^{210}Pb inventory for A(0), the residual ^{210}Pb in the entire record as in Equation 2.

$$A = A(0)\, e^{-\lambda t} \qquad \text{Equation 2.}$$

$$t = 1/\lambda \ln (A(0)/A) \quad \text{Equation 3.}$$

Rearrangement of Equation 2 to solve for time (t) is given in Equation 3. Both A and A(0) are calculated by integration of the ^{210}Pb profile. Using the CRS model, sedimentation rate at a given time is shown in Equation 4.

$$r = \lambda A/C \quad \text{Equation 4.}$$

The CRS ^{210}Pb model used to interpret the age of our sediments can be found as numerical results in Appendix A. Graphical representations for: ^{210}Pb activity vs depth are in Figs. 11-12 and CRS – age vs. depth are found in Figs. 13-14. Changes in sedimentation processes are visible in standard plots in Figs. 13-14. Variations are handled numerically with sediment accumulation rates (Fig. 18) (Appleby, 2001).

Core BH05-5MC was not included in the results, other than measured ^{210}Pb activities in Fig. 12. Measured by Jon Van Alstine, initial ^{210}Pb analysis for the top 5 cm of the core differed greatly from measurements of additional samples analyzed during our study, despite supported ^{210}Pb values at 10 cm depth remaining statistically constant, and a second suite of samples being measured. This difference, more than a simple bias, is apparent as a re-sampled point within the original interval is significantly different despite values of unsupported ^{210}Pb activity remaining comparable (activity at 10 cm depth).

The age versus depth profiles of cores calculated by the CRS method are shown in Figs. 13-14. All cores displayed continuous sediment accumulation. Core BH09-4MC shows dramatic changes in linear trends of age vs depth, in agreement with additional observations. Standard errors of age are plotted in Figs. 13-14 and calculated by

Equation 16 found in Sec. 4.4.4, calculation and descriptions of inventories required the use of the trapezium rule to handle the discontinuous sampling of intervals. These statistics and assumptions are described within the equations in Sec. 4.4.3.

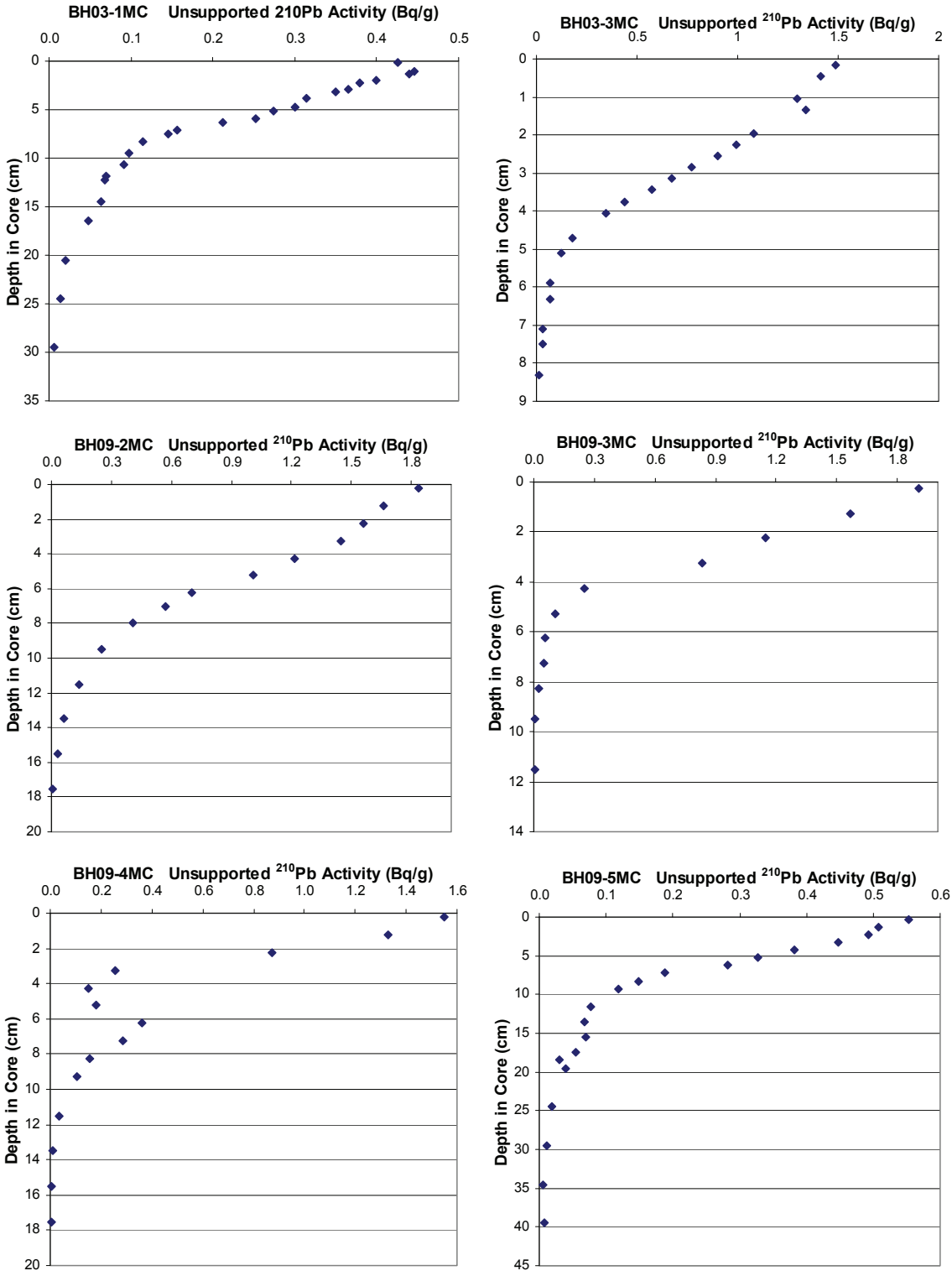

Figure 11. Unsupported ^{210}Pb Activity Profiles

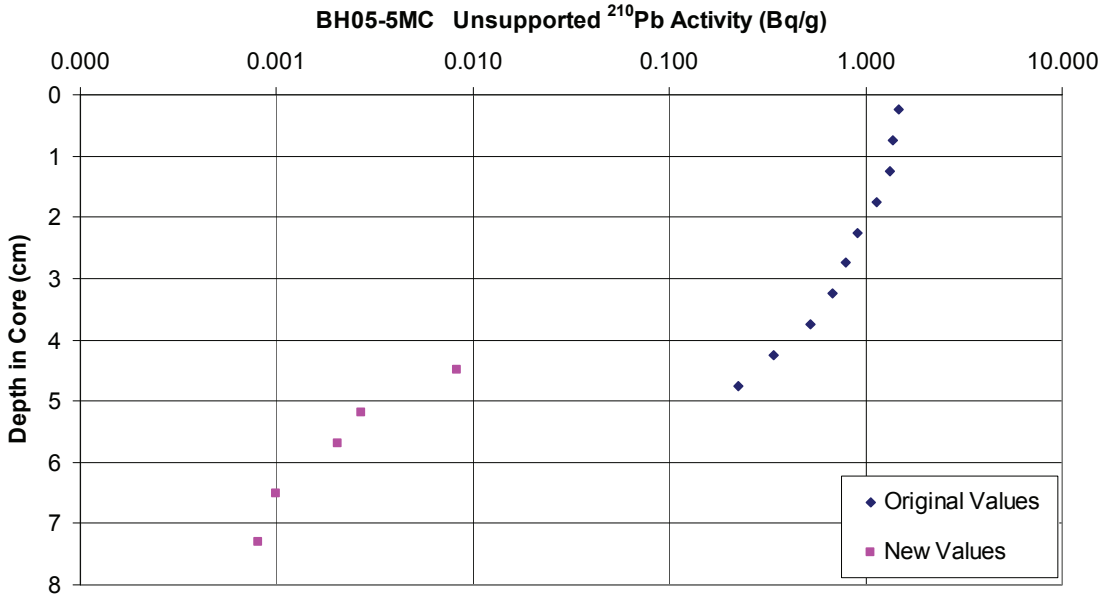

Figure 12. Semi-Log Unsupported ^{210}Pb Activity of Core BH05-5MC

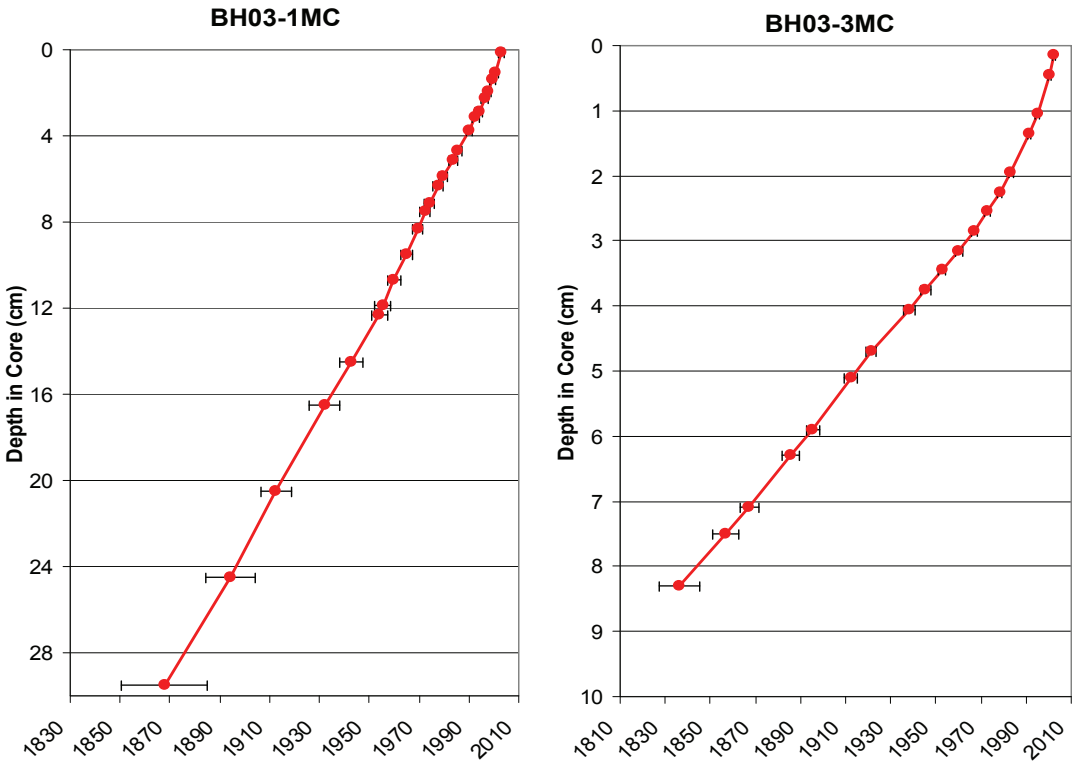

Figure 13. CRS – Age vs. Depth Profiles: 2003 Cores

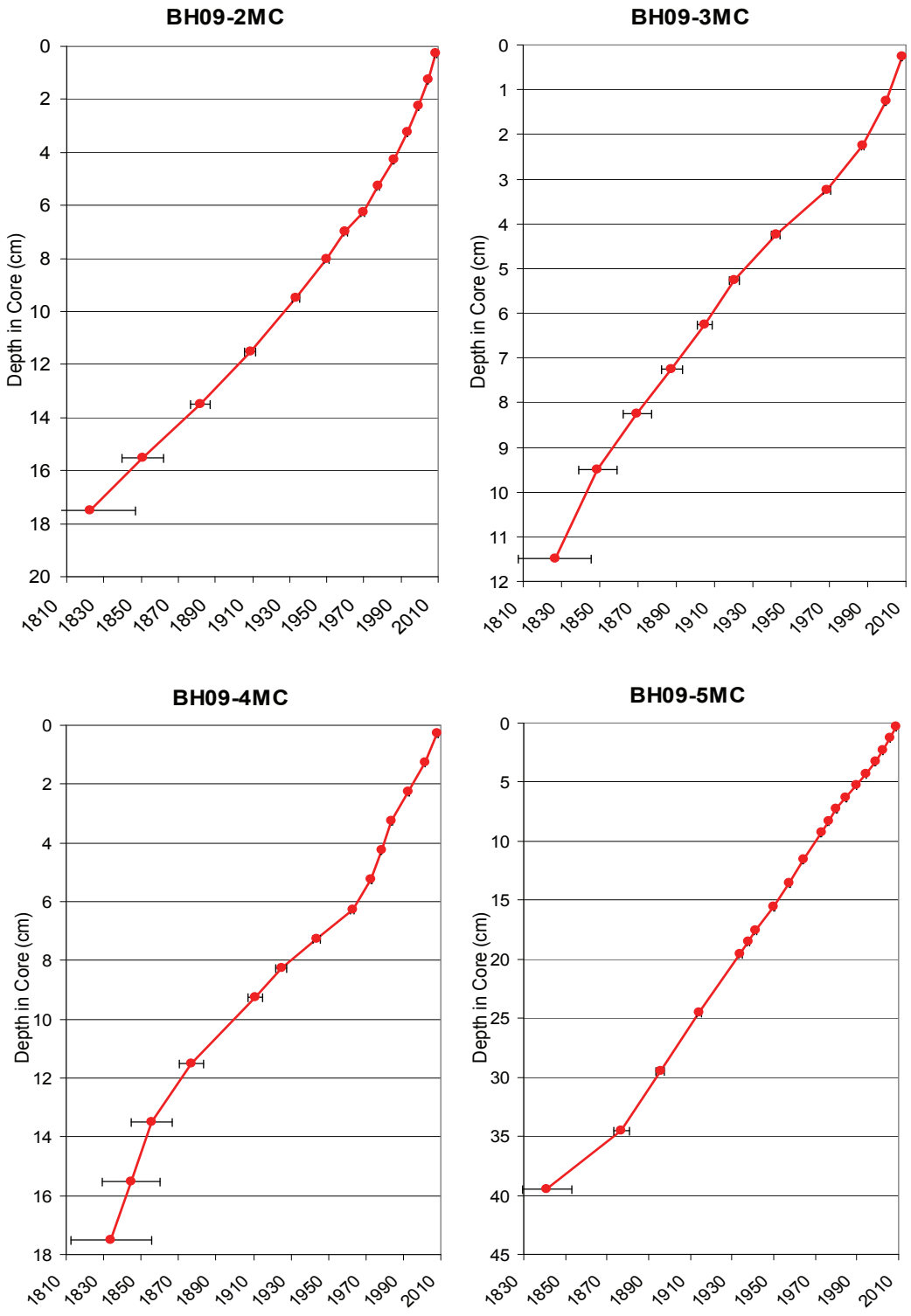

Figure 14. CRS – Age vs. Depth Profiles: 2009 Cores

4.4.3 ^{210}Pb Flux to Sediments

Calculating age using ^{210}Pb methods requires the assumption that the flux of ^{210}Pb for a given region, on yearly time scales is constant. Changes in calculations of flux values are the result of changes within the sedimentary process and must come from forces causing increased erosion or deposition to the sediments (Appleby, 2001). In Equation 5 we calculate the average flux of ^{210}Pb to the sediment.

$$P = \lambda A(0) \qquad \text{Equation 5.}$$

The flux of each core was calculated and appears in Fig. 15. In the equation P is the flux, λ the decay constant for ^{210}Pb (0.03114 y^{-1}) and A(0) is the ^{210}Pb inventory of the specific core for which flux is being calculated. According to Robbins (1982), ^{210}Pb flux to this region is estimated at 183 Bq/m^2yr, flux values larger than the estimate indicate systems in which sediment is accumulating and focusing (Van Alstine, 2006; Appleby, 2001). The cores in this study have larger flux ^{210}Pb than the regional estimate.

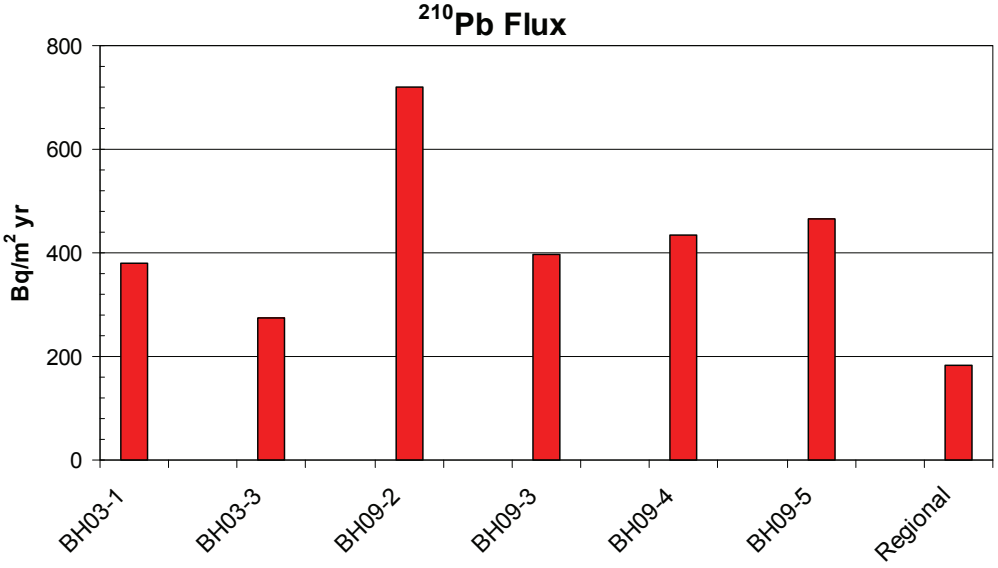

Figure 15. ^{210}Pb Flux of Cores

4.4.4 Dry Mass and Inventories of ^{210}Pb Calculations and Errors

The following formulas were necessary to complete the ^{210}Pb age model calculations. Measurements of dry density and grain size were not taken and require the following equations described in Oldfield and Appleby (1984).

$$DBD = M_{dsed} / (V_{dsed} + V_{water}) \quad \text{Equation 6.}$$

The dry bulk density (DBD) given as (g/cm^3) in Equation 6, and alternatively described in Equation 10, is calculated from the mass of the dry sediment (M_{dsed}), the volume of the dry sediment (V_{dsed}) and the volume of water (V_{water}).

$$V_{dsed} = M_{dsed} / D_s \quad \text{Equation 7.}$$

The volume of dry sediment was not measured directly; this value is calculated from the mass of dry sediment and the grain specific density of the dry sediment (D_s) as shown in Equation 7. The volume of water is simply calculated Equation 8.

$$V_{water} = M_{water} / D_{water} \quad \text{Equation 8.}$$

In Equation 9 shown below, density of the dry sediment (D_s) is calculated using percent organic matter (OM), estimated as twice the measured organic carbon content, and biogenic silica (BSi) which was estimated as 2%.

$$D_s = \%OM/100 + [2.0*(\%BSi/100)] + 2.65*[(100 - \%OM - \%BSi) / 100)] \quad \text{Equation 9.}$$

Equation 10 describes the dry bulk density (DBD), calculated from the percent water content (PW) of sample intervals by weight and the density of the dry sediment D_s.

$$DBD = [1 - (PW/100)] / \{[1 - (PW/100)] / D_s + (PW/100)\} \quad \text{Equation 10.}$$

$$W_{sed} = (DBD)(C_s)(X_n - X_{n-1}) \quad \text{Equation 11.}$$

The dry mass of the sediment interval ($W_{sed)}$ is calculated from the cross sectional area of the core (C_s), the DBD and the interval thickness in Equation 11.

The cumulative unsupported ^{210}Pb is handled in the following equations along with error of dating calculations, as in Appleby (2001). Equation 12 describes the generic formula of the ^{210}Pb inventory. C is the unsupported mass specific concentration of ^{210}Pb and X is the specific intervals depths midpoints.

$$\text{Inventory} = \sum C_i X_i \qquad \text{Equation 12.}$$

The stepwise calculation of the inventory is given using the trapezium rule in Equation 13. A_n is the inventory value for the specific depth, A_{n-1} is the previous (interval above) inventory value, C_n and C_{n-1} represent the concentration of ^{210}Pb in the current interval and previous respectively, and the depth of the two intervals midpoints is given by m_n and m_{n-1}.

$$A_n = A_{n-1} + 1/2(C_n + C_{n-1})(m_n - m_{n-1}) \qquad \text{Equation 13.}$$

Standard errors of inventories are the sum of what can be simplified to independent variables; the assumptions is that the trapezium rule has an independent variable as the rectangle rule described in Appleby 2001, as shown in Equation 14.

$$\sigma^2_{\hat{A}n} = \sigma^2_{\hat{A}n-1} + \sigma^2_{\Delta\hat{A}n} \qquad \text{Equation 14.}$$

Assuming a constant percentage error p in the dry mass increments, a reasonable value for this error is 7% and the expanded formula is shown below.

$$\sigma^2_{\hat{A}n} = (\sigma^2_{Cn} + p^2C_n^2)(m_n + m_{n-1})^2 \qquad \text{Equation 15.}$$

The equation below describes the calculation for the standard error of the age assignment; assumptions appear in full in Appleby (2001) regarding the inventory type

and the independence of variables. The formula uses the cumulative unsupported ^{210}Pb activity A, at depth zero A(0), and λ is the decay constant for ^{210}Pb, 0.03114 y^{-1}.

$$\sigma_t^2 = 1/\lambda^2[(\sigma_{A(0)}/A(0)) + (1-\{2A/A(0)\})(\sigma_A/A)^2] \qquad \text{Equation 16.}$$

4.4.5 Bulk Sediment Mass Accumulation Rates

The bulk sediment mass accumulation rates (MARs) are shown below in Fig. 17. Values shown were calculated as the total carbon mass divided by the time in years represented by the specific interval. The cores in the open lake maintain values between 0.01 – 0.03 g cm^{-2} yr^{-1}, the deviation in core BH09-4MC is assumed to be from iron tailings. Cores BH03-1MC and BH09-5MC show large shifts in accumulated material before more stable, values almost half of the prior maximum after ~1980.

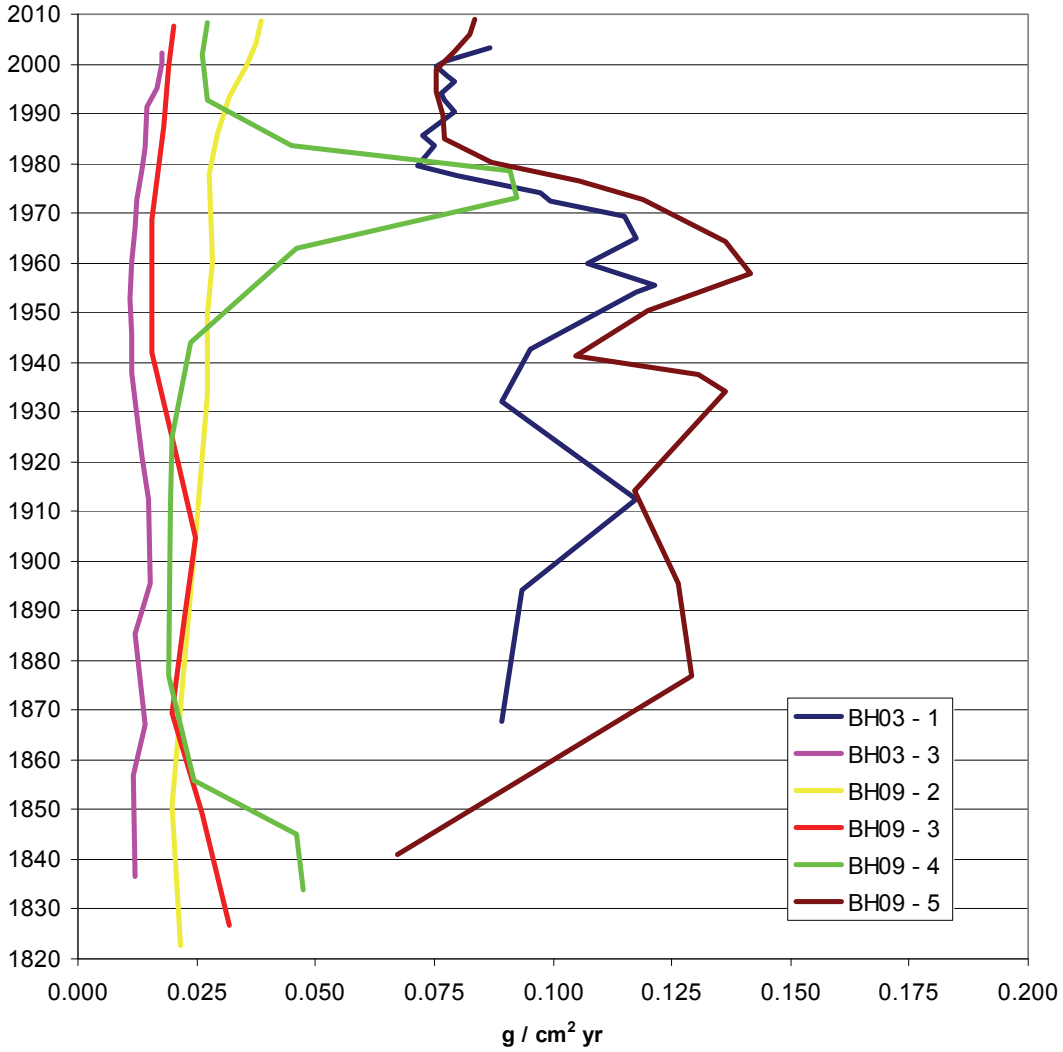

Figure 16. Sediment Mass Accumulation Rate

4.5 Concentrations of Total Organic C, Total N, and C/N

4.5.1 Total Organic Carbon (C_{org})

Total organic carbon (C_{org}) was measured for each sample interval as described in the methods. Cores are plotted as mass percent of the sediment sample (Fig. 17) and mass accumulation rate (Fig. 18) versus age, raw data is given in Appendix B. Organic carbon content ranged from ~1.0 to 4.0 % of the sediment by mass with accumulation rates of 25 to 375 mg C / cm^2 yr among cores. Duplicate analysis of every 5^{th} sample gave a standard error 0.01 wt%, largest variation among duplicates was 0.16 wt%. Calibration curves, utilizing 5 standards were run after every 3 samples and are shown in Sec. 4.5.3, Table 2. Shared among all the plots was remineralization of carbon in the top layers of the sediment.

Core BH09-4MC shows sediments that have been capped, within the 1955-1985 timeframe, giving limited metabolism/remineralization, in agreement with additional observations. Data prior to 1850 are suspicious; with values larger than expected. The remaining open water cores BH03-3MC, BH09-2MC, and BH09-3MC display similar behavior, decreasing approximately 1% in carbon content from the top to the bottom of the sampling interval, from 3.5% to roughly 2.25%. Only core BH09-2MC had its lowest values found in the early to mid 1900s and not at the bottom of the sampling interval. Accumulation plots suggest carbon flux peaking during the 1960s in cores BH03-3 and BH09-5 despite oxidative metabolism of C in the sediments.

Figure 17. Total Organic Carbon vs. Age

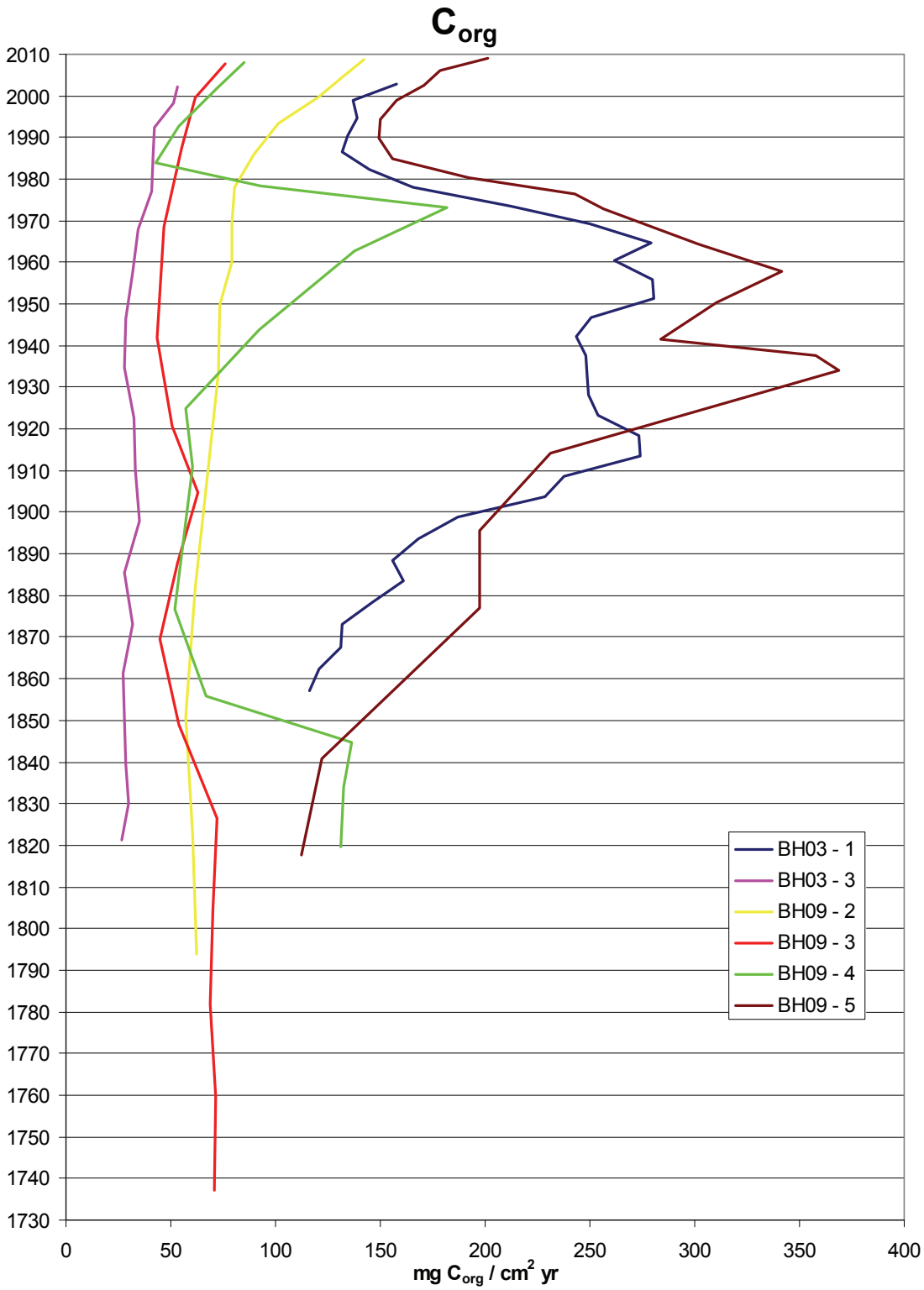

Figure 18. MAR Organic Carbon vs. Age

4.5.2 Total Nitrogen (N_{total})

Total nitrogen ($N_{total)}$ was measured for each sampling interval. Cores are plotted as mass percent of the sediment sample in Fig. 19 and as mass accumulation rate in Fig. 20 versus age; raw data is given in Appendix B. The values ranged between 0.1 and 0.45% for all the cores or mass accumulation rates of 3 to 23 mg N / cm^2 yr. Predicted loss of N through diagenetic metabolism is evident in all of the cores. Every 5^{th} sample was run in duplicate giving a standard error 0.001 wt%, the largest variation among duplicates was 0.008 wt%. Statistics of the calibration curves, utilizing 5 different standards, run every 3^{rd} sample are located in Table 2 in Sec. 4.5.3. Shared among all the plots was remineralization of nitrogen with initial depth.

Similar to carbon measurements (Sec. 4.5.1), organic compounds containing nitrogen appear to have been diluted from the mid 1950s to the mid 1980s in core BH09-4MC. The core's nitrogen values are well defined between 0.30 and 0.35% from the early 1800s to the mid 1950s, declining due to dilution, and return to 0.40% in the most current sediments. Similar to C_{org} trends, the open water cores of BH03-3MC, BH09-2MC, and BH09-3MC had loss of nitrogen, roughly 0.20% mass, from top to the bottom of the sampling intervals. MAR's of N describe 50% loss from measurements of the most current intervals. Core BH09-2MC produced a minimum nitrogen value of ~0.30% in the early 1900s. The cores sampled from the far western basin, BH03-1MC and BH09-5MC, track well together with mid 1800 values of ~0.12% they display an increase to a local maximum in the mid 1900s of ~0.18%. A rapid 0.05% decline in the following 2 decades was then followed with an increase from the 1980s to values of ~ 0.25%.

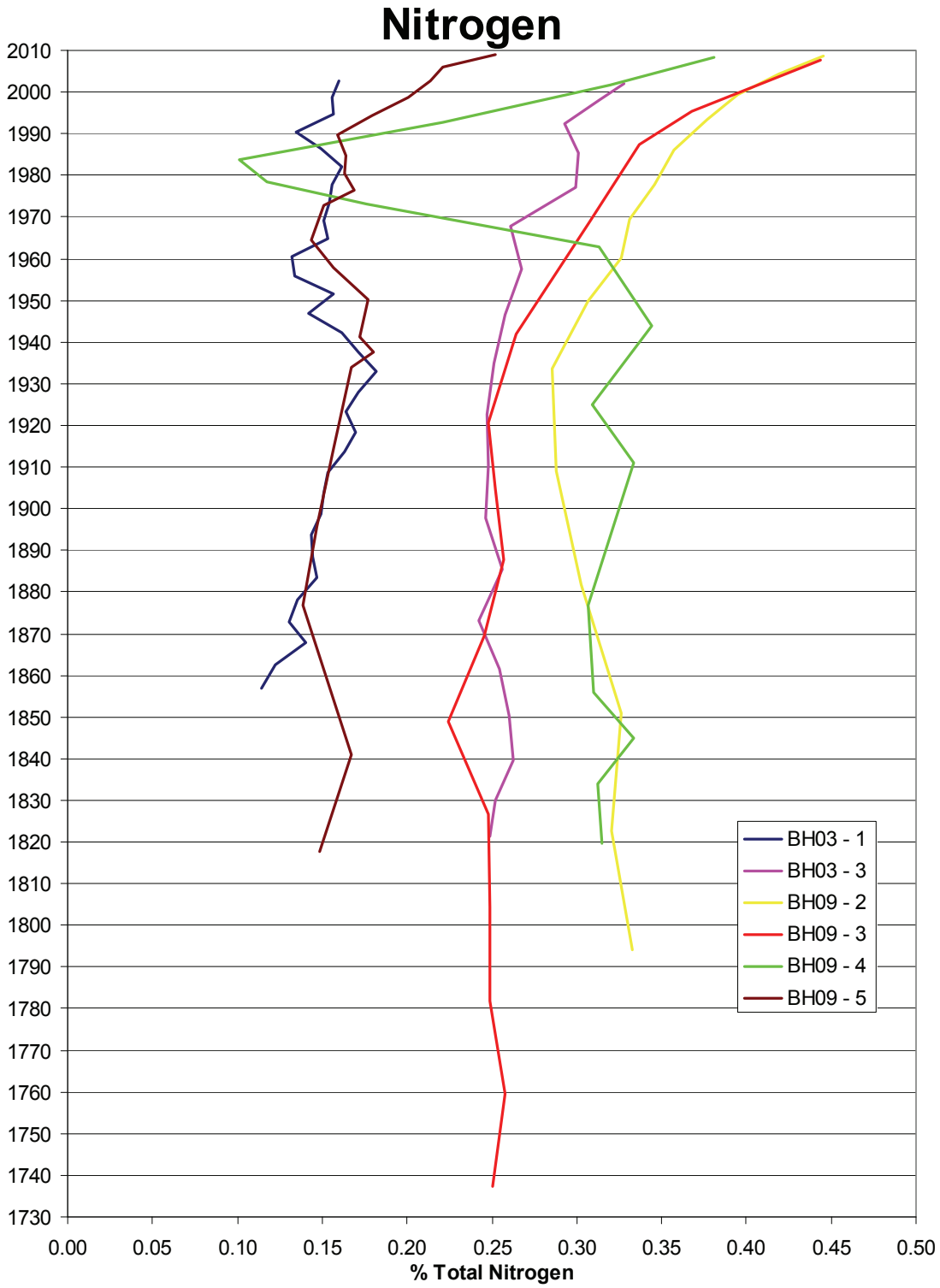

Figure 19. Total Nitrogen vs. Age

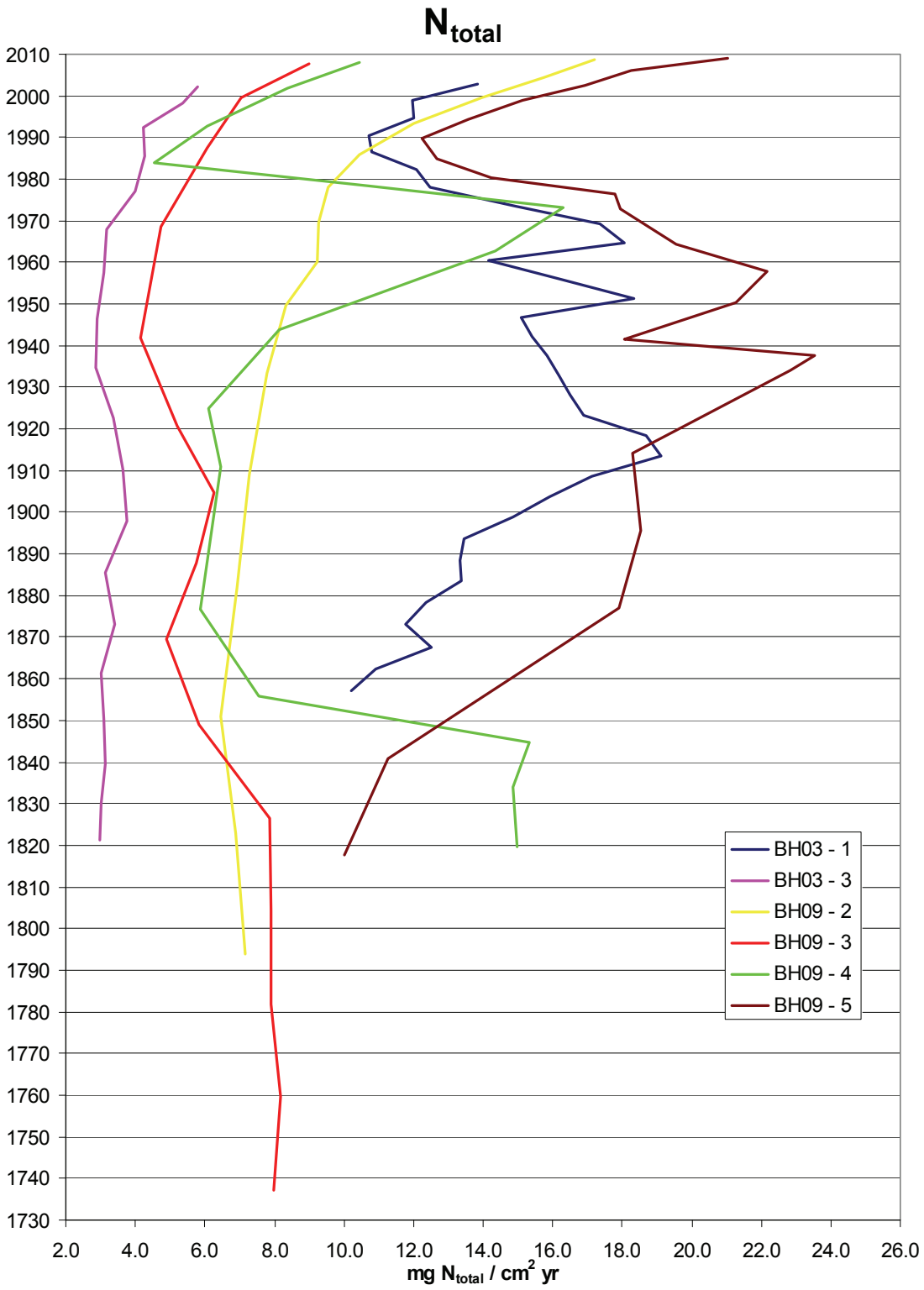

Figure 20. MAR Nitrogen vs. Age

4.5.3 C/N Ratio

The following plot found in Fig. 22 shows the ratio of mass percent organic carbon to mass percent nitrogen versus age. The intervals shown are the same as those of carbon (Figs. 17-18) and nitrogen (Fig. 19-20). Roughly every 5th sample was run in duplicate to determine error; the average of these duplicate points is plotted. Carbon measurements gave a standard error 0.01 wt%, largest variation among duplicates was 0.16 wt%. Duplicate nitrogen measurements gave a standard error 0.001 wt%, the largest variation among duplicates was 0.008 wt%. Statistics of known standards used as calibration spikes were run every 3rd sample (Table 2), raw data is in Appendix B.

Cores BH03-3MC, BH09-3MC, and BH09-4MC displayed similar behavior with C/N values around 9.0 increasing in the early 1900's to a maximum of roughly 10.0 in the 1960-70s. This maximum was followed by a steady decline to the current values near 8.0, core BH09-2MC does not display a maximum during the middle of the 20th century. Core BH09-02MC matches well to the other open water cores listed above in terms of starting and ending values of the C/N ratio. Cores BH03-1MC and BH09-5MC had measured values near 11.0 in samples from the early 1800s, this trend continued until a sharp increase in the late 1800s reaching a maximum around 1960. This maximum was followed by a steady decline to current values of ~9.0, lower than historical (~11.0).

Core	Carbon Calibration r^2	Nitrogen Calibration r^2
BH03-1MC	0.985466	0.995260
BH03-3MC	0.991530	0.995817
BH09-2MC, 3MC	0.991637	0.996958
BH09-4MC, 5MC	0.991059	0.989984

Table 2. Bulk Organics: Calibration Curve r^2 Table

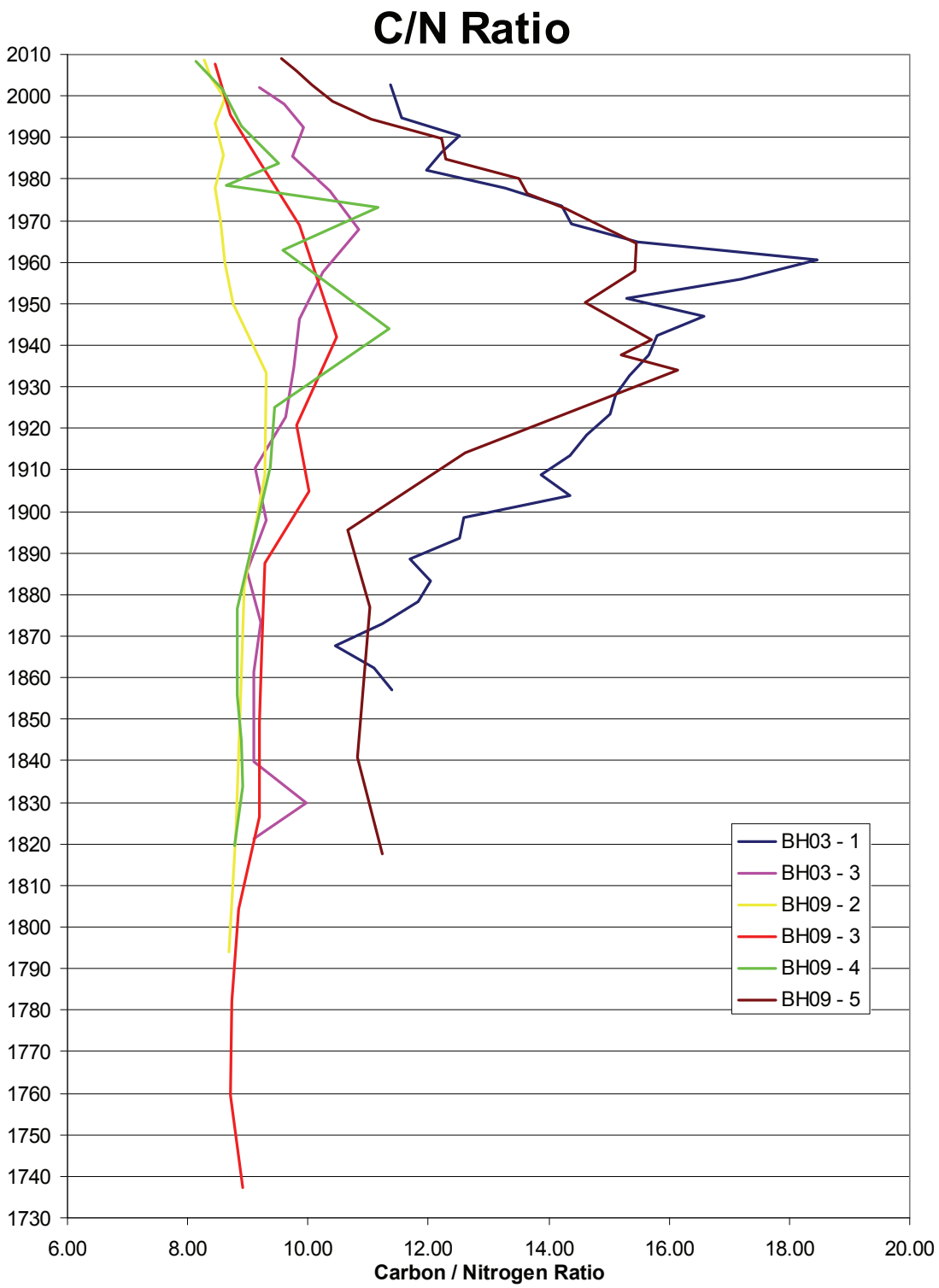

Figure 21. C/N Ratio of Cores vs. Age

4.6 Carbon and Nitrogen Isotopes

4.6.1 $\delta^{13}C$ Values

Changes in the concentration of stable carbon isotopes presented as $\delta^{13}C$ values were measured in intervals of interest in the 6 sediment cores, values are plotted versus age (Fig. 22). Duplicate analysis was performed every 5th samples down core, the average of these replicates is plotted. Duplicate measurement of $\delta^{13}C$ values had a standard error of 0.07‰, with largest variation among duplicates was 0.09‰. A complete set of numerical $\delta^{13}C$ values is given in Appendix B, the calibration curve statistics using 5 standards, run every 3rd sample is given in Table 3, Sec. 4.6.1.

Isotopic data are presented in delta notation. In this notation the ratio is the stable isotope concentration of the sample to the concentration of a reference standard, is used as calculated in the formula below.

$$\delta^{13}C = [(^{13}C/^{12}C_{sample})/(^{13}C/^{12}C_{VPDB}) - 1] \times 10^3 \qquad \text{Equation 17.}$$

The reference standard used for isotopic carbon values is Vienna PeeDee Belemnite (VPDB); use of this standard results in neagative $\delta^{13}C$ values for typical photosynthetic products as a result of the standard's isotopic composition.

The ratio of ^{13}C to ^{12}C found in atmospheric CO_2 is widely acknowledged to be influenced by historic and continued burning of fossil fuels. The CO_2 released from combustion of these fuels is depleted in ^{13}C compared to atmospheric values. A correction factor is necessary to interpret $\delta^{13}C$ data within this historical context for measurement containing bias due to the 'Suess Effect' (Hodell and Schelske, 1998; Verburg, 2007). The formula found in equation 18 the following page was used for an

estimation of $\delta^{13}CO_{2(atm)}$ for a given date (Y=year) within this study despite similar, simplified models.

$$\delta^{13}CO_{2(atm)}(Y) = 7.7738118 * 10^{-16} * Y^6 - 1.2222044 * 10^{-11} * Y^5 + 7.1612441 * 10^{-8} * Y^4 - 2.1017147 * 10^4 * Y^3 + 0.33316112 * Y^2 - 273.715025 * Y + 91703.261 \quad \text{Eq. 18.}$$

The equation was fit to a pool of 160 measurements originating from studies by Friedli et al. (1986), Francey et al. (1999), Keeling et al. (2001) and Langenfelds et al. (2002) and compiled by Verburg (2007). Observations from 1692 through 2000 gave the equation with an r^2=0.979, P=0, and n=160. The Verburg equation is suggested to be used no earlier then 1700 A.D., the equation used by Schelske and Hodell has a suggested limit of 1840 A.D. The correction factor for our measurements was the estimated $\delta^{13}CO_{2(atm)}$ change between 1700 and a given year, this bias (calculated by Eq. 20) was subtracted from the original $\delta^{13}C$ value.

In general, after correction all cores displayed general vertical behavior of $\delta^{13}C$ data prior to 1890 (Fig. 22). Data points display a measureable rise through the 1900s. This increase was followed by a recovery to lower concentrations into the 1980s. Since the 1980s all cores display a significant increase in ^{13}C concentration, with recent values larger than that of the mid 1900 peak.

Core BH03-3MC early values oscillate near -26.5‰. Starting around 1900 the concentration of ^{13}C within the core increased at nearly a linear rate through the most recent measurement. The core does not display a local maximum in the mid 1900s as observed in the remaining cores. The most recent measurement near -24.4‰ is an increase of over +2‰ from early measurements. Core BH09-2MC displays the least

amount of change of all the cores during the early 1900 period, early values fluctuate near -26.1‰ rising to roughly 25.7‰ nearly 20 years prior to the maximum in other cores. Values of approximately -25.9‰ in 1960-70 increased steadily through 2010 having the largest increase over the most current decade to a value of nearly -24.5‰.

Core BH09-3MC shows the increase of ^{13}C incorporation earliest of all the cores. Starting values of approximately -26.8‰ rose nearly 1‰ in the mid 1900s before a very minimal recovery, the second increase of +1‰, approaches -24.8‰. BH09-4MC starts to increase starting in 1910 from sustained values of approximately -26.6‰, reaching a maximum in the middle of the century the maximum of -25.6‰ falls to -26.0‰ in the mid 1980s before a subsequent increase to present values of nearly -25.4‰. This increase of only 1.2‰ was the smallest overall increase in $\delta^{13}C$ values of all the cores.

Cores BH03-1MC and BH09-5MC displayed very similar and somewhat distinct behavior from the other cores. The cores started at values of approximately -26.3‰, starting increased in near 1905 and 1915 respectively. Each core appears to have peaked in the early 1960s, later then the previous cores, with values of -24.8 and -25.0‰ respectively. Values dropped in 1980 and 1990, followed by a more recent increase; the most recent values are approximately -24.7 and -24.5‰. These cores show an overall increase of +2‰ since 1900, most similar to core BH03-3MC.

Core	Carbon Calibration r^2	Nitrogen Calibration r^2
BH03-1MC	**0.998880**	**0.992884**
BH03-3MC	**0.999198**	**0.993039**
BH09-2MC, 3MC	**0.998853**	**0.987113**
BH09-4MC, 5MC	**0.998430**	**0.981942**

Table 3. Isotope: Calibration Curve r^2 Table

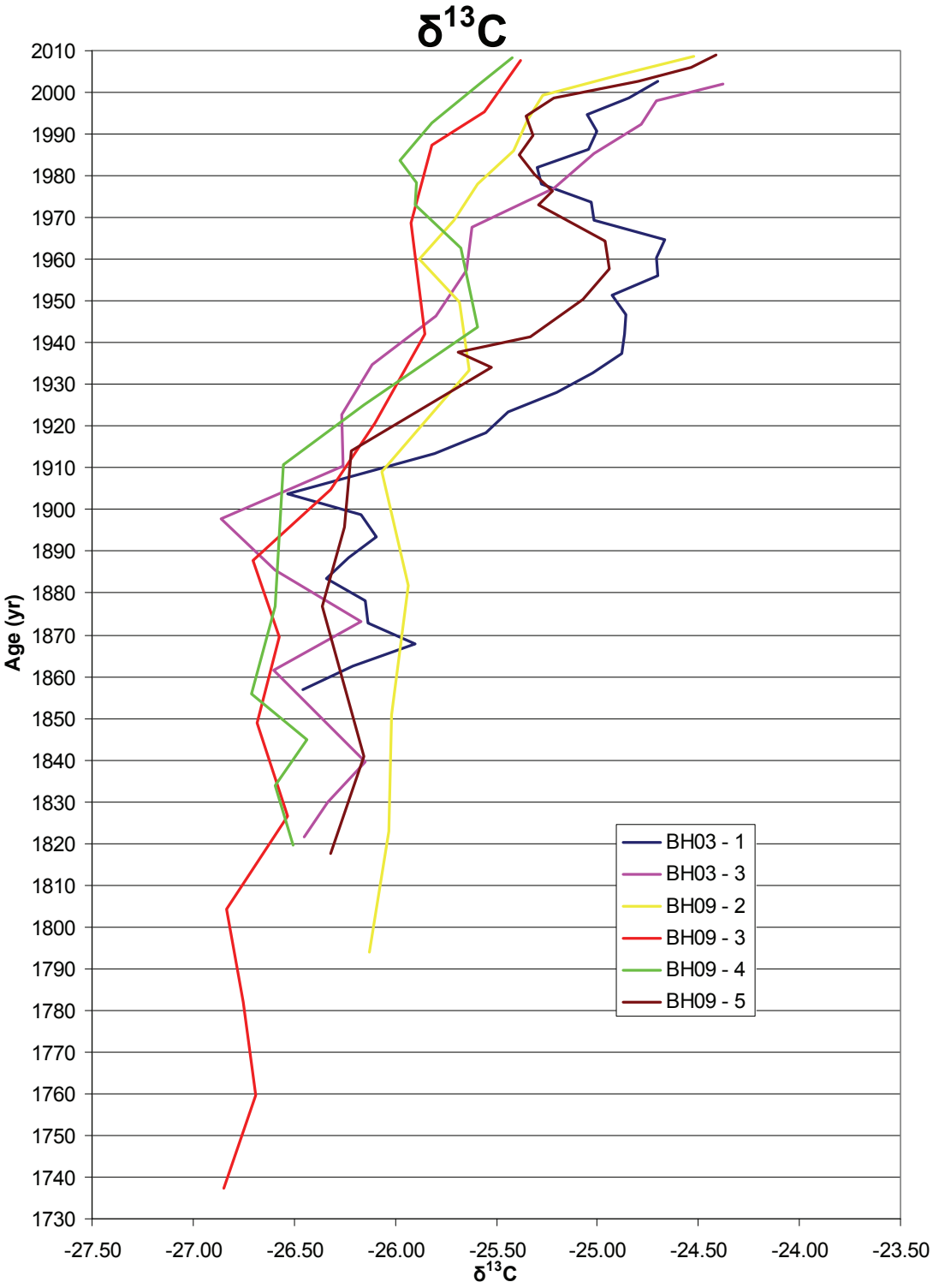

Figure 22. $\delta^{13}C$ vs. Age for all Cores

4.6.2 $\delta^{15}N$ Values

The stable nitrogen isotope compositions are given as $\delta^{15}N$ values, these were measured for intervals of interest within the 6 sediment cores. Values are plotted versus age in Fig. 23. Duplicate analysis was performed every 5 samples. Duplicate measurement of $\delta^{15}N$ values had a standard error of 0.02‰, the largest variation among duplicates was 0.18‰. A complete set of numerical $\delta^{15}N$ values is given in Appendix B, the calibration curve statistics using 5 standards, run every 3rd sample is given in Table 3, Sec. 4.6.1. The reference standard used for isotopic nitrogen measurements is atmospheric nitrogen.

Cores BH03-1MC and BH09-05MC display similar behavior, initial values show limited deviation from averages of 1.6 and 2.1‰, respectively, for values in the 1800s. Both cores display increased ^{15}N content beginning around and 1920 and 1935, these increases appear to reach a maximum around 1960 with values of 3.0 and 2.5‰. Recovery from this ^{15}N increase appears by the early 1990s. Both cores appear to show a recent increase with values at the top of each core at 2.4 and 2.2‰ respectively.

Core BH03-3MC shows limited variability among measurements; the suite of points averages ~3.8‰ for all depths. The low of 3.3‰ in approximately 1900 and a high of ~4.1‰ appear in the most recent measurements.

Core BH09-2MC has a profile decreasing with values of 3.5‰ in the mid 1800s giving a almost linear decrease to 2.2‰ by 2000. The most recent measurement show a +0.5 increase to 2.8‰ at the top of the core.

BH09-3MC has initial values during the early 1800s of about 3.3‰, increasing to about 3.8‰ by 1930 the trend then decreases to present values of nearly 3.0‰. This decrease is similar to cores BH03-2MC and BH09-4MC.

Core BH09-4MC similar to several of the other cores displays a decrease. Values of nearly 4.0‰ from the early 1800s steadily decrease in a somewhat linear fashion to present values of roughly 3.4‰. Similar to core BH09-3MC, this core shows a slight increase from the trend during the mid 1900s.

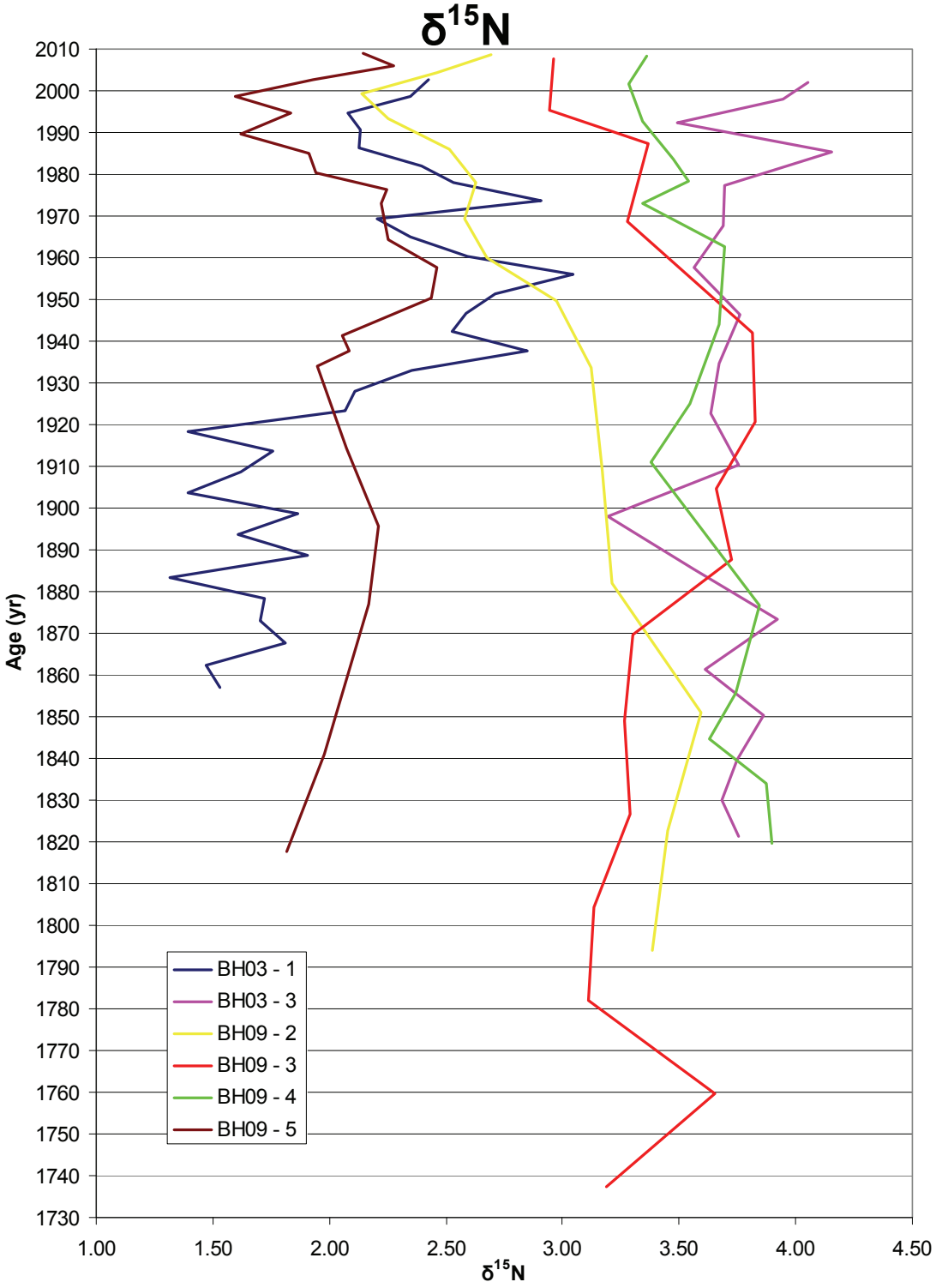

Figure 23. $\delta^{15}N$ vs Age for all Cores

4.6.3 $\delta^{13}C$ vs. C/N

C/N and $\delta^{13}C$ are plotted against one another in Fig. 24. Cores display general patterns depicting differences in regional environments and the burial of biological material. BH03-1 and BH09-5 in particular show an increase in C/N with heavier $\delta^{13}C$ values, although the highest $\delta^{13}C$ values are found in cores BH03-3 and BH09-2, C/N ~9.

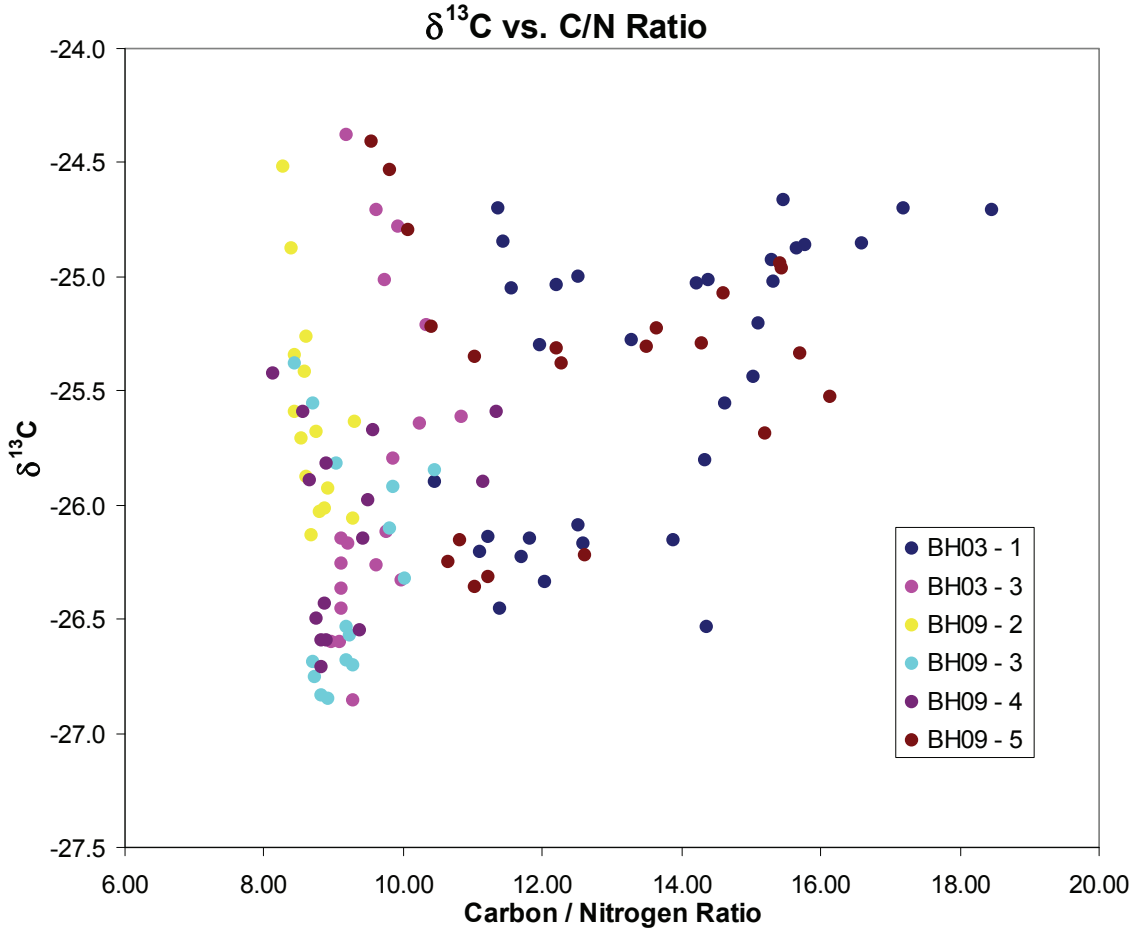

Figure 24. $\delta^{13}C$ vs. C/N Ratio

4.6.4 ^{15}N vs. C/N

C/N and $\delta^{15}N$ plotted against one another as shown in Fig. 25. Far western cores BH03-1MC and BH09-5MC show general grouping with higher C/N ratios at lower $\delta^{15}N$ values. The remaining cores BH03-3MC, BH09-2MC, BH09-3MC and BH09-4MC are all grouped in a much tighter fashion highlighted by lower and less variable C/N ratios and higher ^{15}N concentrations.

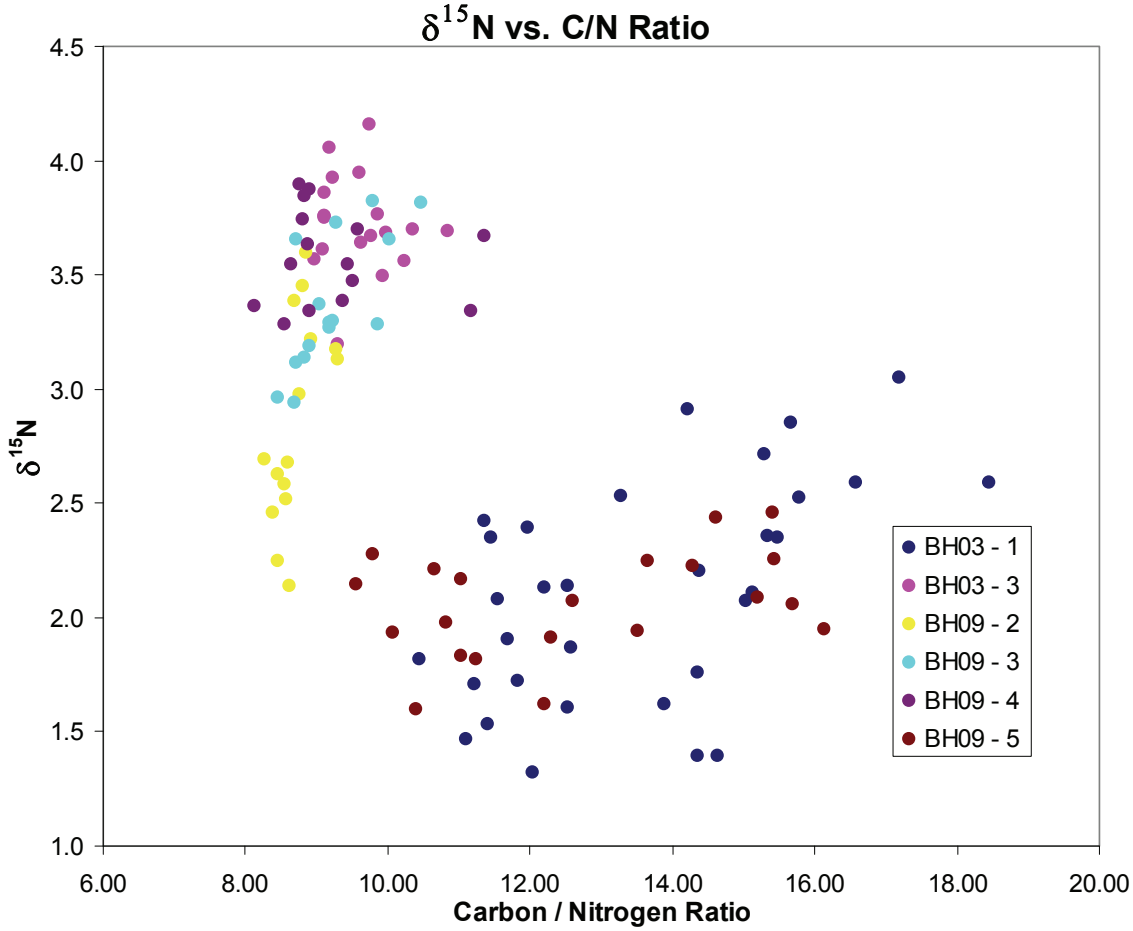

Figure 25. $\delta^{15}N$ vs. C/N Ratio

4.6.5 $\delta^{13}C$ vs. $\delta^{15}N$

$\delta^{13}C$ and $\delta^{15}N$ were plotted against one another as shown in Fig. 26. Linear trends fit to the data did not show strong statistical support, those trends with r^2 values > 0.6 did not match among cores with apparent trends. Therefore calculations are not included; more relevant to systems with strong 'eutrophic' behavior, fitting followed workup similar to Lake Ontario sediments (Hodell and Schelske; 1998).

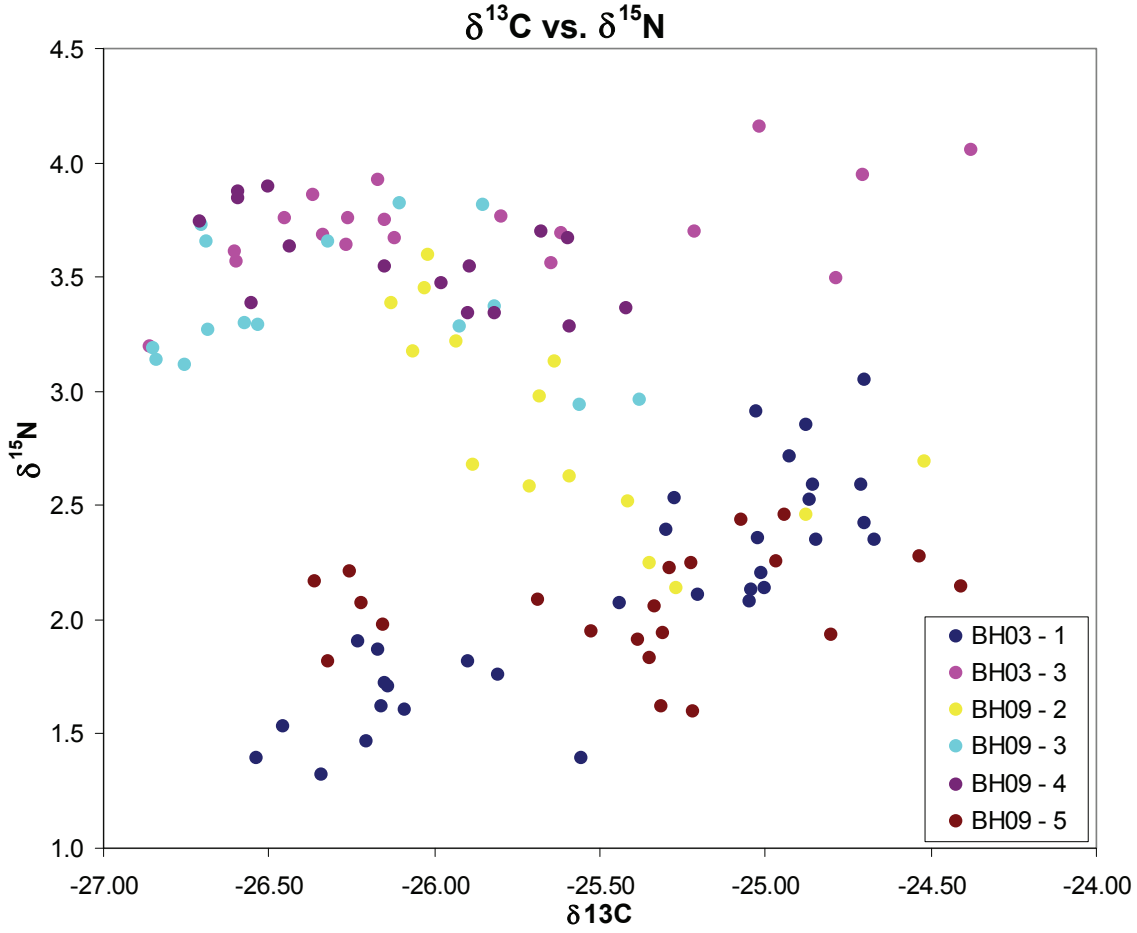

Figure 26. $\delta^{13}C$ vs. $\delta^{15}N$

4.7 Quantification of n-alkane Biomarkers

4.7.1 Aquatic n-alkanes

Alkanes with a lower number of carbon atoms (C_{15-23}), produced primarily by aquatic non-vascular plants, are shown in Figs. 27-29; data is listed in Appendix C. The plots are presented as mass accumulation rates (ng cm^{-2} yr^{-1}), of specific n-alkanes, grouped by core with values plotted vs. depth. Fig. 29 represents the total mass of C_{17-21}. Analysis will first describe n-alkane behavior of a single core, secondly comparing specific n-alkane behavior among cores. There is most interest in C_{17}, C_{19} and C_{21}; the following descriptions will focus on these alkanes.

Core BH03-1MC (Fig. 27) shows a general increase in accumulation of aquatic n-alkanes starting after 1870s, lasting until the 1950s. C_{17} and C_{19} show stronger maxima in the late 1800s of +0.04 and +0.09 ng cm^{-2} yr^{-1}, respectively, from initial values. This increase is followed by a 30 year period of lower rates. A second stronger maximum after 1930 (reaching maximum values at different times depending on the chain length) is evident in all chain lengths. C_{15} appears to have reached a maximum accumulation rate by the mid 1940s; the remaining alkanes display a maximum in the mid 1950s. This increase is followed by subsequent decline in all cores to mid 1800 values. The core's C_{15}, C_{21}, and C_{23} MARs describe current accumulation rates slightly larger than values of the 1850s. C_{17} and C_{19} MARs show a recent increase since the 1990s, with values similar to those of the early 1900s. Error is based on replicate analysis and comparison of internal standard among samples. Core BH03-1MC's n-alkane MARs standard error is

estimated to be within 14.0 % of the mean, calculated from the measured concentrations of internal standard among samples from this core.

Core BH03-3MC (Fig. 27), while limited in temporal resolution, shows a general increase in deposited aquatic n-alkanes starting after 1930s, although it should be noted that the majority of the data points contained very little measureable n-alkane and therefore interpretations should be made cautiously. C_{15} displays an increase reaching a maximum in the 1970s followed by a return to values similar to the early 1900s by the late 1900s. Alkanes C_{17}, C_{19}, C_{21}, and C_{23} show a strong maximum in the late 1970s. The only deviation among the data points, displaying an increasing trend, this increase is followed by reversal to lower values by the late 1980s. Current values appear only slightly higher then values of the mid 1800s. The estimated error among measurements is less than 5.1 % of the measured mean of the internal standard for core BH03-1MC.

Core BH09-3MC (Fig. 28) does not show similarity in trends among n-alkane MARs as the prior cores did. C_{15} initially shows very low biomarker accumulation rates, until an increase in the 1890s continuing until 1970, then a decline through the 1980 and a second increase to values of ~0.0001 ng cm^{-2} yr^{-1} presently. C_{17} exhibits values of 0.02 to 0.03 ng cm^{-2} yr^{-1} followed by decline after 1920, to a minimum circa 1970 followed by an increase with recent values similar to that of the 1850s. C_{19} shows a very similar profile to C_{17} with a less intense decline through the 1970s. Current MAR values show accumulation of approximately 0.06 ng cm^{-2} yr^{-1}. C_{21} shows a decline starting in the late 1800s, values increase slightly throughout the 1900s with a larger increase post 1970, current values are almost twice that of mid-1800 values at 0.065 ng cm^{-2} yr^{-1}. C_{23}

displays a recent increase starting in the late 1980s, from rather stable values early, with current values of approximately 0.017 ng cm^{-2} yr^{-1}, more than 3x larger than mid-1800 values. The estimated error among measurements is less than 10.6 % of the measured mean of internal standard for core BH09-3MC.

Core BH09-5MC (Fig. 28) presents trends similar to core BH03-1MC. C_{15} shows very low levels of biomarker until an increase in the early 1900s, variable behavior in the middle of the century and a decline through the 1980s. C_{17} describes values of 0.02 to 0.03 ng cm^{-2} yr^{-1} early oscillating through the mid 1900s with relatively stable values since 1950. C_{19} shows a very similar profile to C_{17} with a decline in the 1970s, current values show MAR of approximately 0.06 ng cm^{-2} yr^{-1} although recent values display fluctuation. C_{21}'s values are largely indicative of sediment MAR following an increase during the 1900s followed by decrease since ~1990. The standard error for core BH09-5MC is less than 12.8 % of the measured mean of MAR values shown, 6 of the 10 data points were processed in duplicate to calculate error of replicates, average deviation was less than 8.0 % of calculated means of the measured internal standard.

The total MAR for C_{17}, C_{19}, and C_{21} believed to best define the trends of the aquatic portion of short chain n-alkanes was plotted in Fig. 29. Cores BH03-1 and BH09-5 both have variable values between 0.15 and 0.35 ng $C_{17\text{-}21}$ / cm^2 yr, the average of values may indicate an increase through the mid-1900 and subsequent decline to present, error is estimated to be less than 14.0 and 12.8 % of mean values shown respectively. Core BH03-3 displays behavior suspicious of error with an increase maximum of ~0.7 ng $C_{17\text{-}21}$ / cm^2 yr, twice the largest values measured for cores BH03-1

and BH09-5. BH09-3 displays values ~0.1 ng $C_{17\text{-}21}$ / cm^2 yr until 1920, a slight decline during the mid 1900s that returns to values similar to the oldest measurements in the most recent sediments.

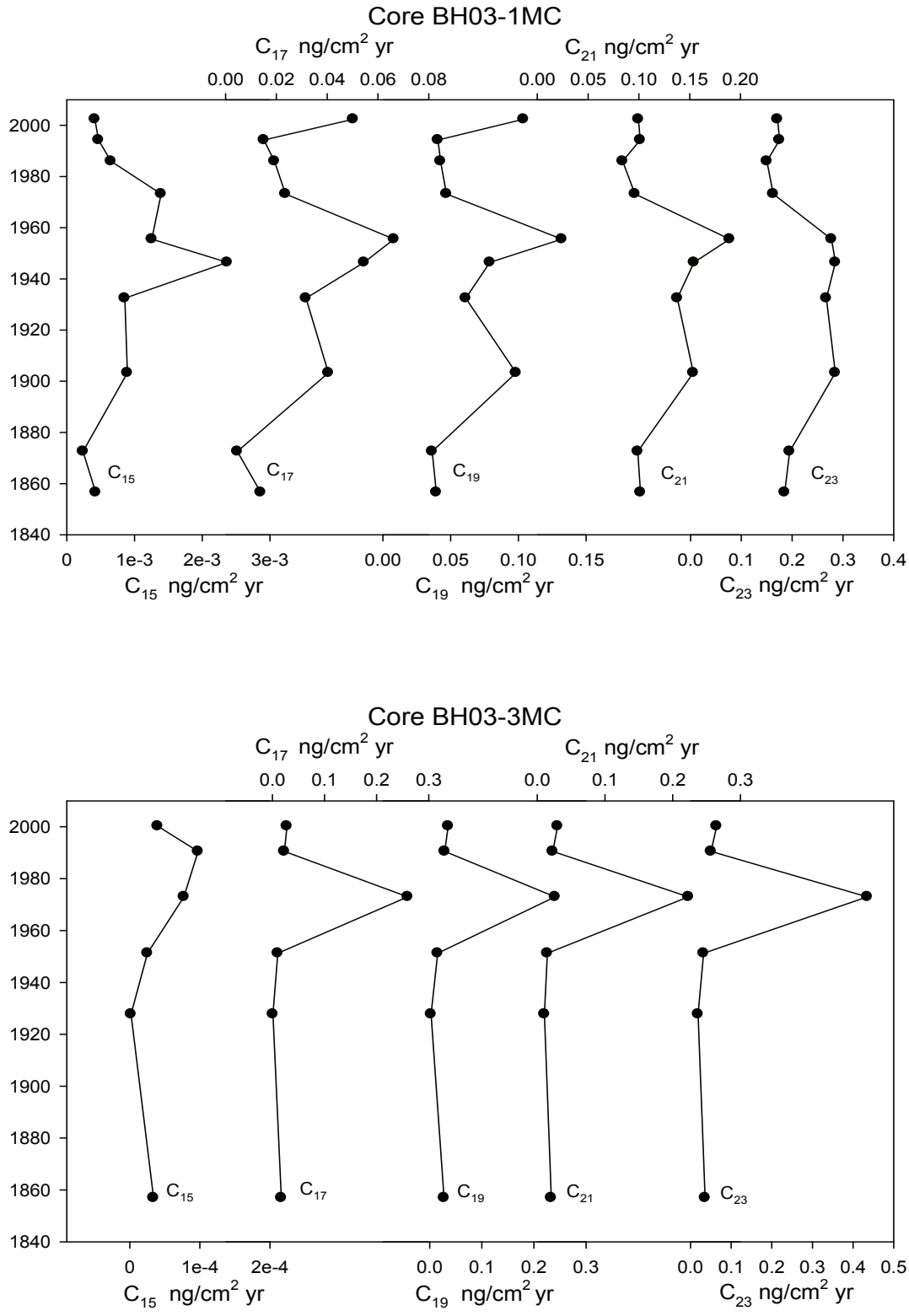

Figure 27. Aquatic n-alkanes: Cores BH03-1MC and 3MC

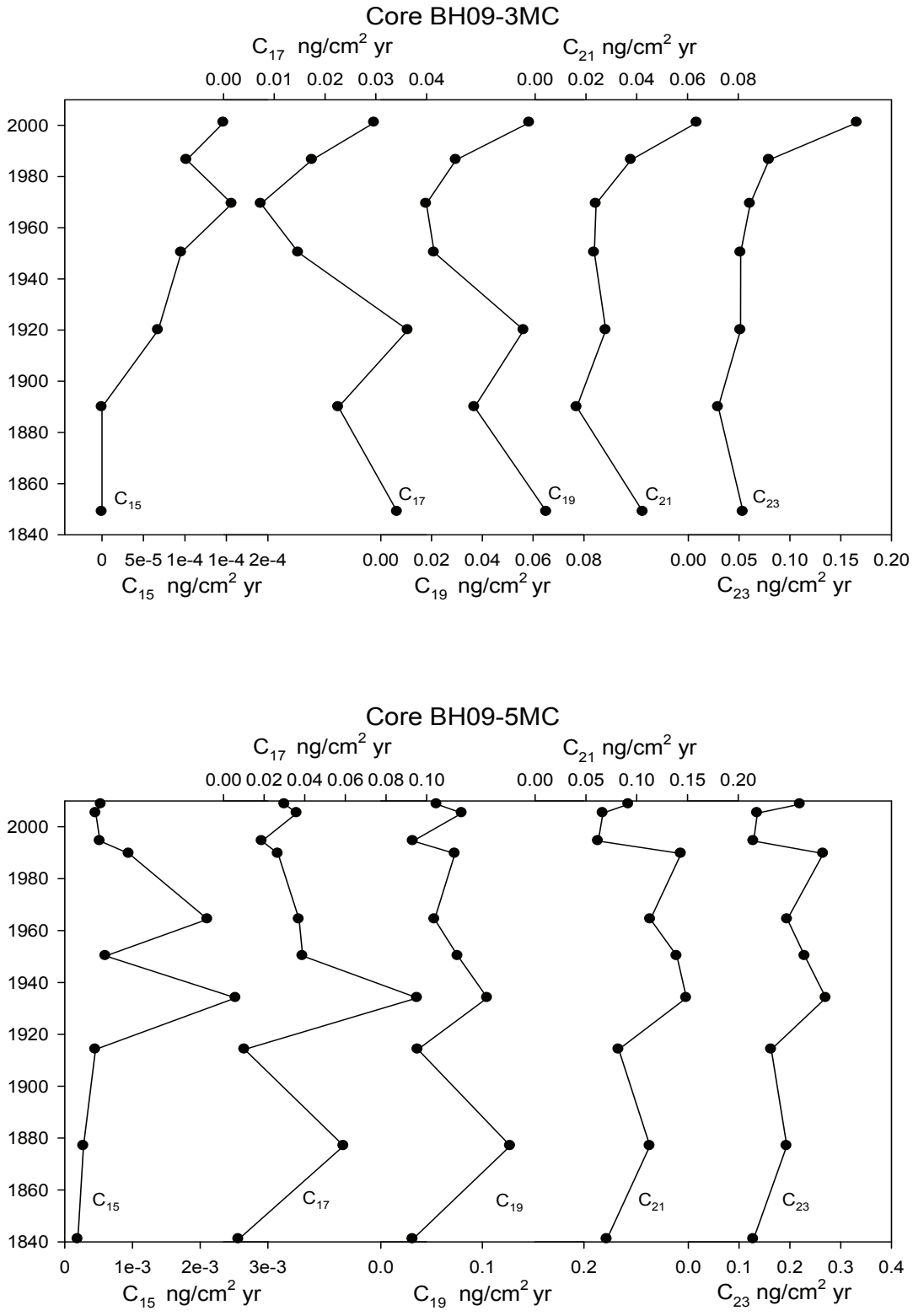

Figure 28. Aquatic n-alkanes: Cores BH09-3MC and 5MC

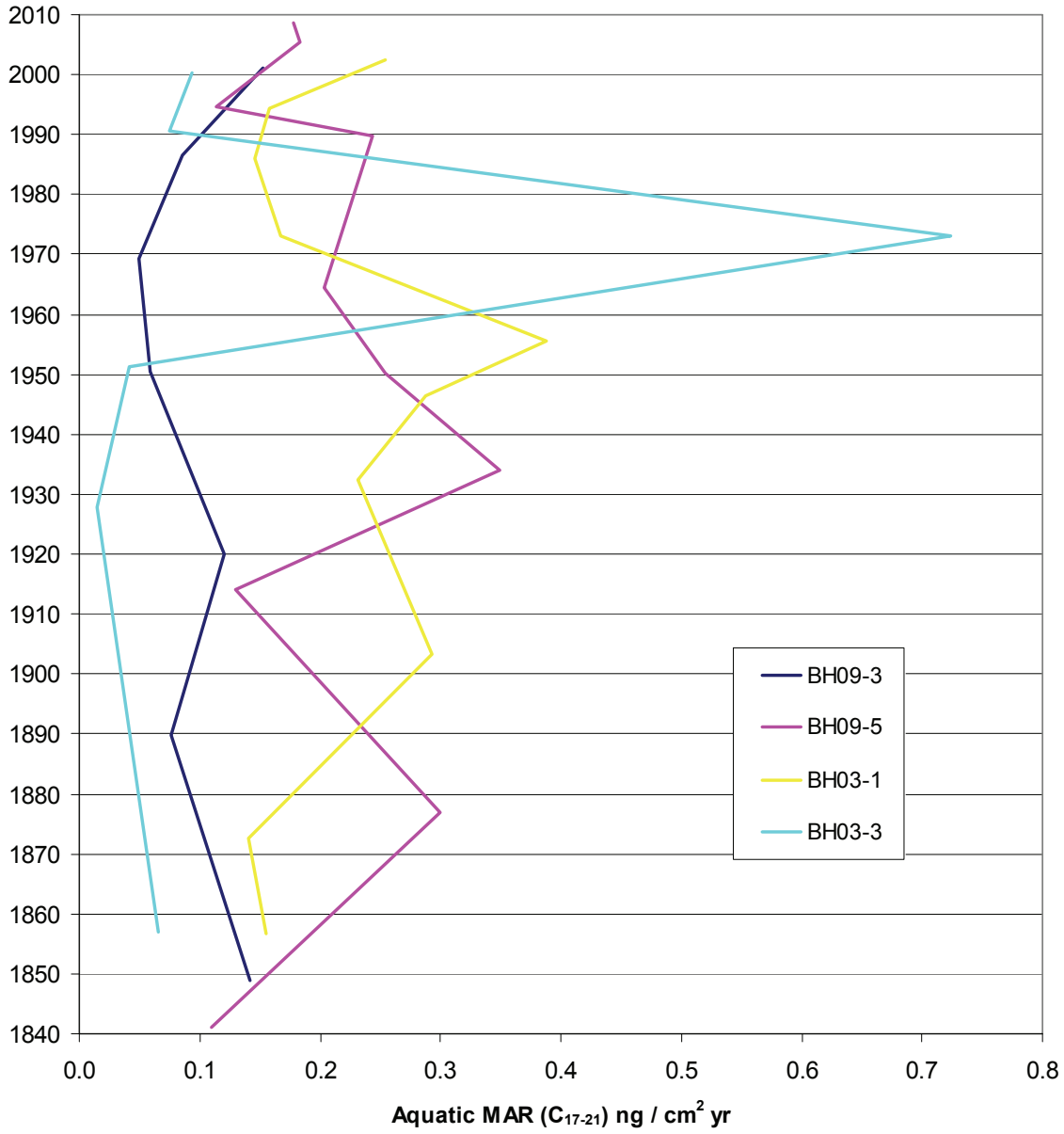

Figure 29. Total C_{17-21} MAR vs Age

4.7.2 Terrestrial n-alkanes

Alkanes with a higher number of carbon atoms (25-33) are primarily the result of growth of terrestrial photosynthetic organisms. MARs for these alkanes are shown in Figs. 30-32; raw data is listed in Appendix C. The plots are presented as mass accumulation rates (ng cm^{-2} yr^{-1}) of specific n-alkanes, grouped as cores with values plotted vs. depth. Fig. 32 represents the summed MARs for alkanes C_{27-31}. Of most interested are the C_{27}, C_{29} and C_{31} alkanes; descriptions will focus on these alkanes.

Core BH03-1MC (Fig. 30) shows a gradual increase through the mid-1900s followed by decline and steady values since the late 1970s. C_{27}, C_{29}, and C_{31} MARs have initial values of 0.35, 0.3 and 0.2 respectively, all increase in the late 1800s to a maximum in the 1950s of 0.7, 0.6 and 0.5 ng / cm^2 yr. Calculation from replicate analyses and comparison of internal standards among runs determined the largest standard error of n-alkanes of core BH03-1MC to be within 14.0 % of the mean of MAR values calculated.

Core BH03-3MC (Fig. 30) exhibits long chain alkane trends similar to aquatic short chain n-alkanes. MARs in the 1950-1970 intervals are six times larger than values found prior and after. C_{27}, C_{29}, and C_{31} all have early values (through the 1800s and into the early 1900s) of ~ 0.1 ng / cm^2 yr. Compound MARs reach maxima in the late 1970s of 1.0, 0.65 and 0.45 ng / cm^2 yr respectively, current values appear slightly larger than values of the mid 1800s. The standard error is better than 5.1 % of the measured mean of MAR values from calculation of internal standards. BH09-3MC (Fig. 31) shows general increase in accumulation of terrestrial n-alkanes starting after the 1880s. C_{29} appears to

show a stronger local maximum, +0.1 ng cm^{-2} yr^{-1} from initial values, than other chain lengths in the early 1900s followed by a 30 year period of lower rates. A second stronger increase appears post 1930 (in all long chain alkanes in this core), most significantly, in the most recent measurements. C_{25}, C_{31}, and C_{33} describe current accumulation rates slightly larger than values of the 1850s. C_{27} and C_{29} show recent increase since the 1990s. The standard error among measurement of core BH09-3MC internal standards is estimated to be within 10.6 % of the measured mean of MAR values.

In core BH09-5MC (Fig. 31), 6 of the 10 data points were processed in duplicate to calculate error of worked up replicates, average error was less than 8.0 wt.% of calculated means. Abundance values of the terrestrial n-alkanes appear similar to the trends of aquatically derived C_{21} and C_{23} shown in Fig. 28. Recent values since the 1990s are similar to the rates of the 1800s with a dramatic recent increase for the most recent sediments. The standard error for core BH09-5MC long chain values is less than 12.8 % of the measured MAR values shown calculated from the internal standard.

Total MAR rates for C_{27}, C_{29}, and C_{31}, best represent trends of the terrestrial portion of long chain n-alkanes (Fig. 32). Core BH03-3 has unusual n-alkane abundances; the same very large peak observed in individual alkanes observed in Figs. 28 and 29 is apparent in terrigenous n-alkane values. Core BH09-3 displays general increase over the measured time interval with current values of ~1.0 ng $C_{27\text{-}31}$ / cm^2 yr. Core BH09-5 displays an increasing trend shown in n-alkanes longer than C_{21} starting in the late 1800s, multiple maximum values during the mid-1900s give way decrease by the 1980s.

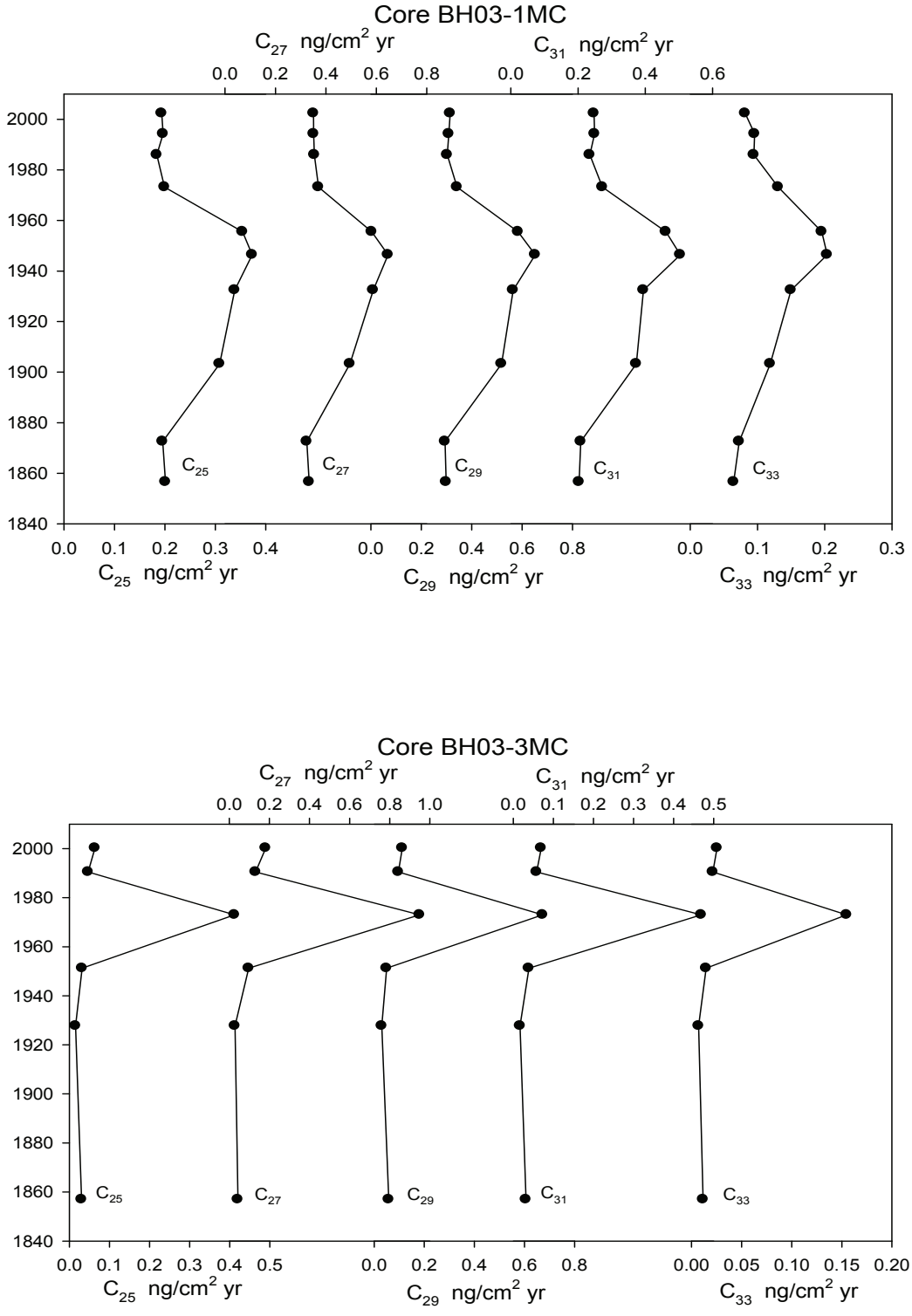

Figure 30. Terrestrial n-alkanes: Cores BH03-1MC and 3MC

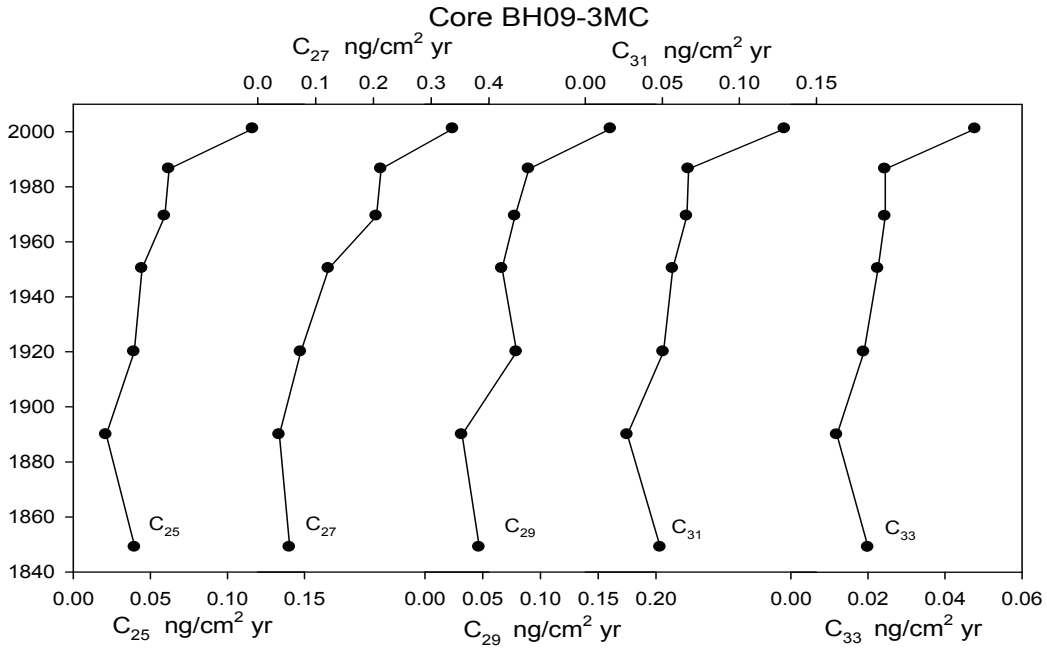

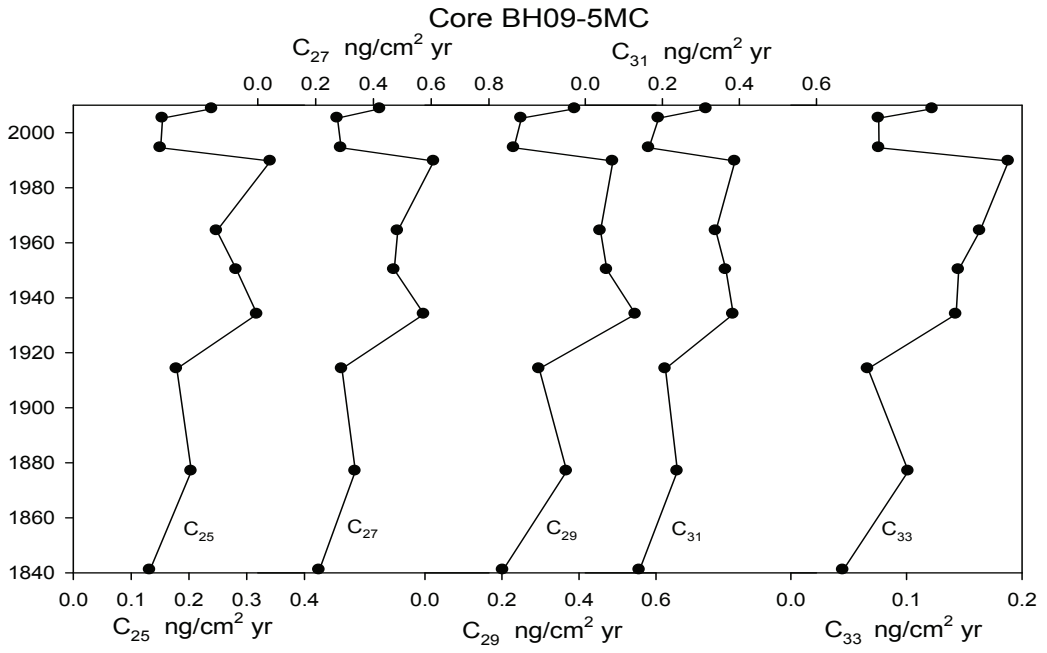

Figure 31. Terrestrial n-alkanes: Cores BH09-3MC and 5MC

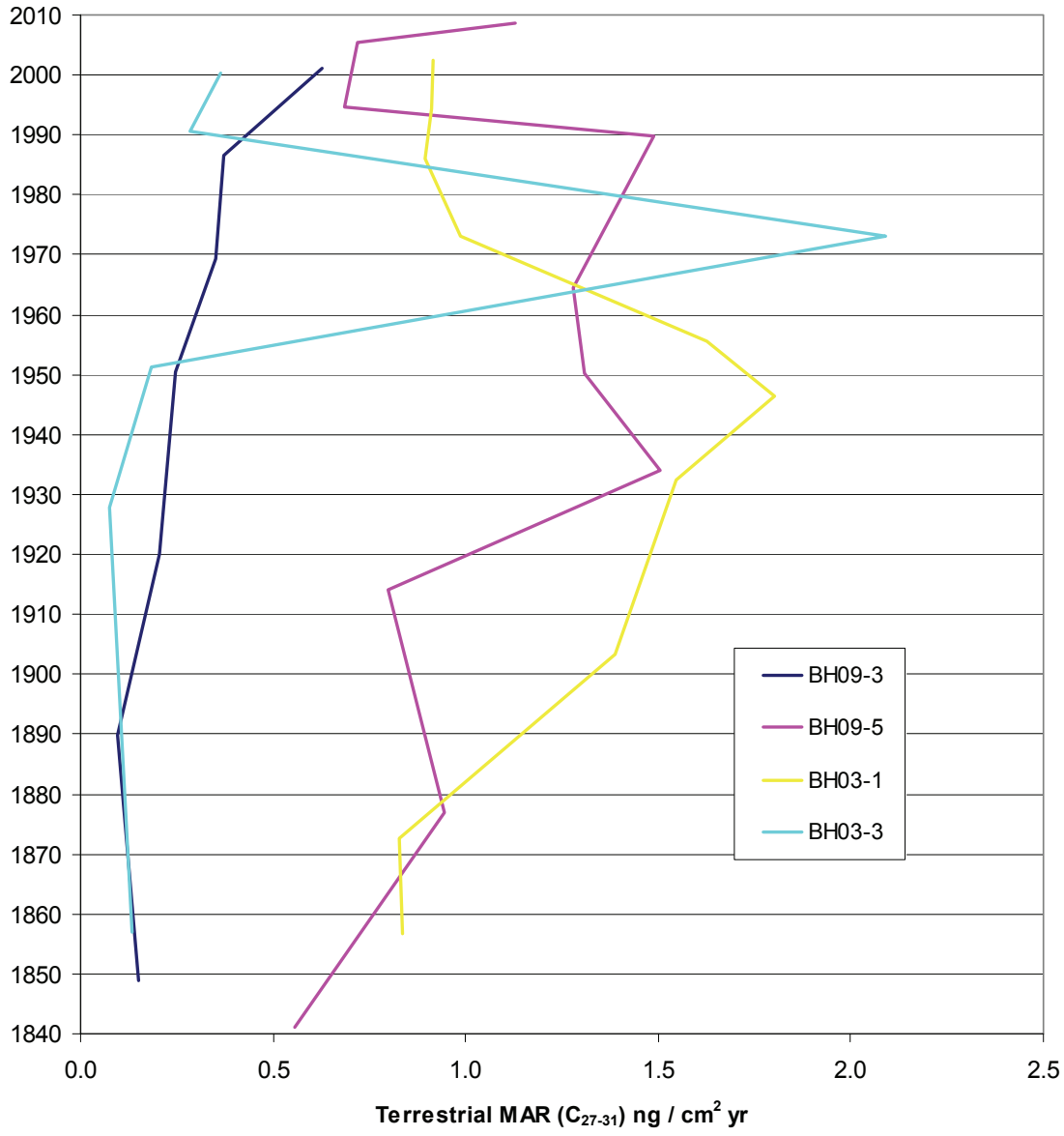

Figure 32. Total C_{27-31} MAR vs Age

4.7.3 Carbon Preference Index and Average Chain Length

The Carbon Preference Index (CPI) was calculated for each core to examine the odd over even carbon chain length predominance. The index is used to look at the dominance of biologically, predominantly photosynthetic n-alkanes, which are mainly odd carbon number compounds, while petroleum sources add both odd and even number n-alkanes in the same n-alkane chain length range. Bray and Evans (1961) described the index for terrestrial compounds C_{24} to C_{34} in length in the following Equation 20, used to calculate the CPI for terrestrial n-alkanes in Fig. 33. A modified CPI, to treat aquatic produced n-alkanes is shown in Equation 21.

$$CPI_{terrestiral} = \tfrac{1}{2}*[(C_{25}+C_{27}+C_{29}+C_{31}+C_{33})/(C_{24}+C_{26}+C_{28}+C_{30}+C_{32}) + (C_{25}+C_{27}+C_{29}+C_{31}+C_{33})/(C_{26}+C_{28}+C_{30}+C_{32}+C_{34})] \quad \text{Equation 20.}$$

$$CPI_{aquatic} = \tfrac{1}{2}*[(C_{17}+C_{19}+C_{21})/(C_{16}+C_{18}+C_{20}) + (C_{17}+C_{19}+C_{21})/(C_{18}+C_{20}+C_{22})] \quad \text{Equation 21.}$$

CPI values > 3 describe samples with no significant petroleum contamination where as CPI ~1 represents contamination mainly by petroleum, matured organics having undergone catagenic processing (Bray and Evans, 1961). The aquatically derived CPI Equation 21 yields lower values (CPI > 2) for uncontaminated conditions; fewer compounds are measured and averaged in this equation along with compounds that inherently have lower concentrations.

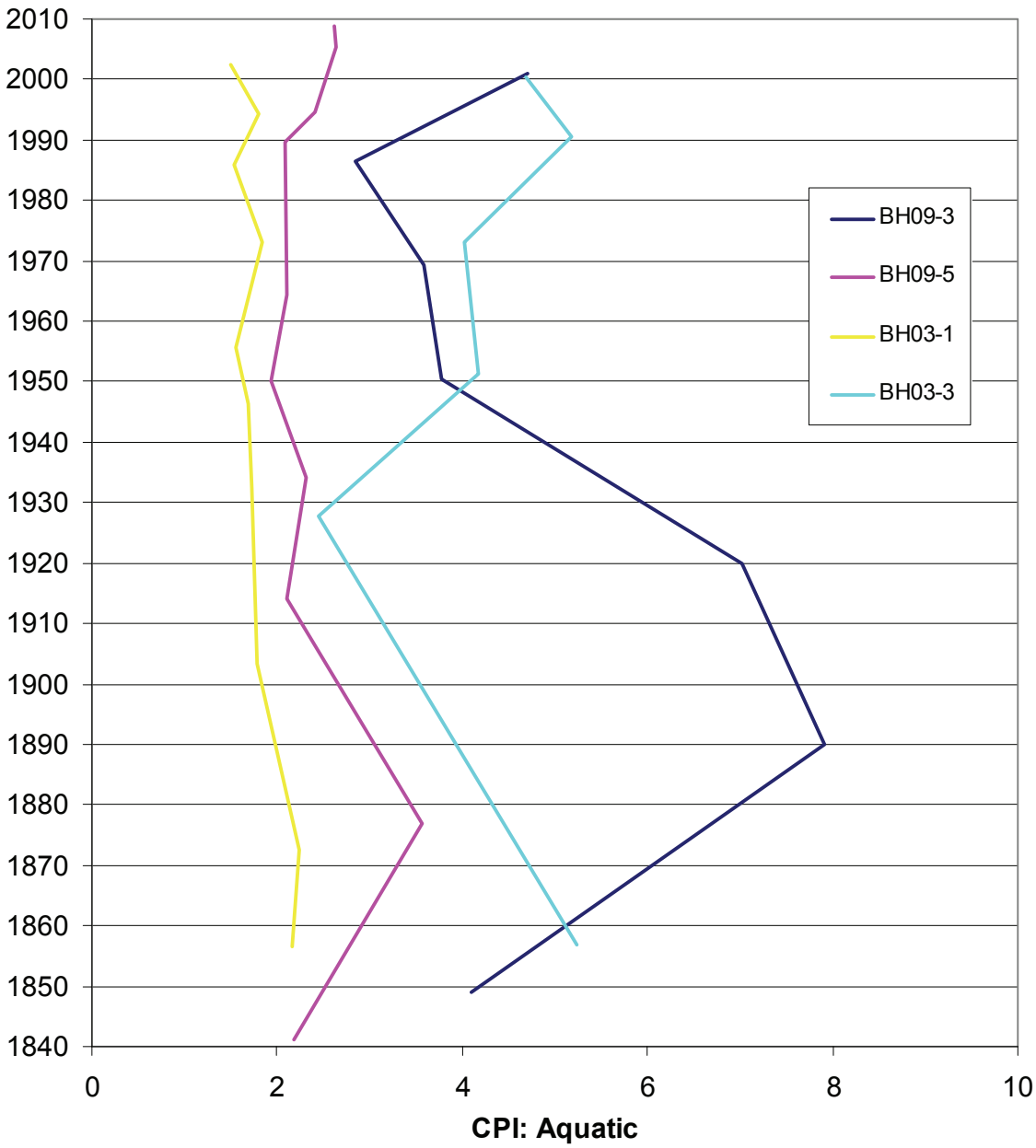

Figure 33. Aquatic: Carbon Preference Index

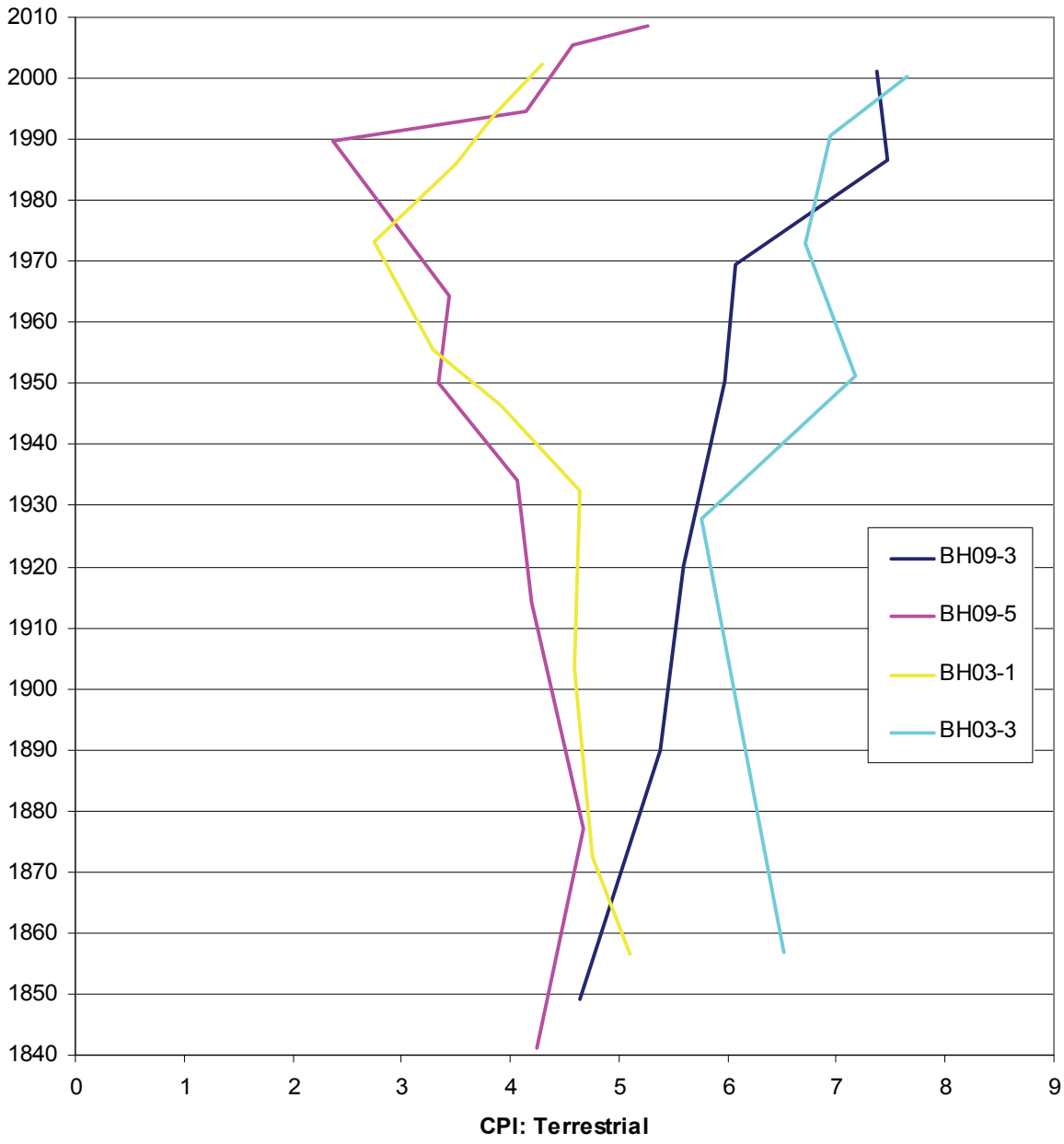

Figure 34. Terrestrial: Carbon Preference Index

Average chain length (ACL) of n-alkanes may be used to distinguish changes within the source pool over time; increase of the ACL value can indicate increasing aridity or temperature (Rommerskirchen *et al*., 2003, Castañeda *et al*., 2009b). The generic formula found in Equation 23 can be tailored to determine ACL values for n-alkanes sources that are not well described by Equation 22 ($C_{23\text{-}33}$). In this study we investigated both aquatic $C_{15\text{-}21}$ along with the entire range (aquatic to terrestrial) of measureable photosynthetically derived n-alkanes $C_{15\text{-}33}$. Plots in Fig. 35 describe the aquatic, terrestrial and complete n-alkane pools.

$$ACL_{23\text{-}33} = (23[C_{23}]+ 25[C_{25}]+ 27[C_{27}]+ 29[C_{29}]+ 31[C_{31}]+ 33[C_{33}]) / ([C_{23}]+[C_{25}]+[C_{27}]+[C_{29}]+[C_{31}]+ [C_{33}]) \quad \text{Equation 22.}$$

$$ACL_{\{n \text{ to } (n+i)\}} = (n[C_n]+\ldots+(n+i)[C_{(n+i)}]) / ([C_n]+\ldots+[C_{(n+i)}]) \quad \text{Equation 23.}$$

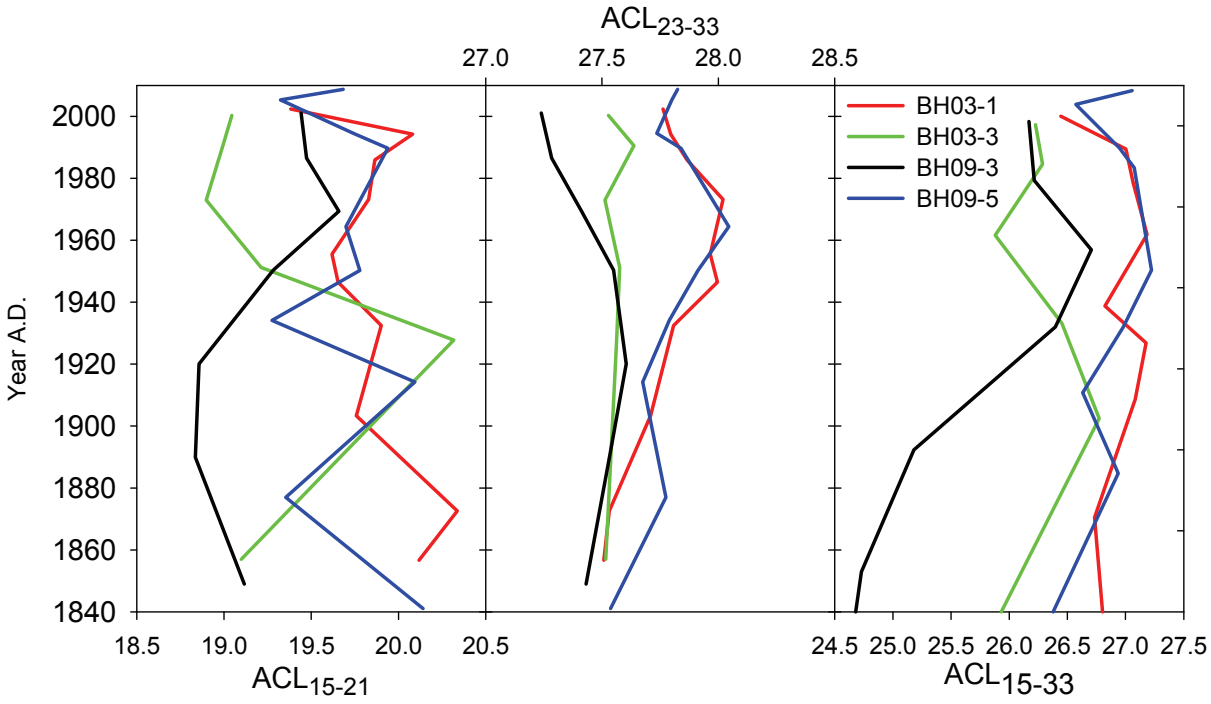

Figure 35. Average n-alkane chain length

4.7.4 Terrestrial Aquatic Ratio: Primary Source Determination

Source determination and the predominance of terrestrial vs. aquatic (T/A) compounds is estimated in multiple ratio metric measurements. Less general than the C/N ratio of bulk organics, the T/A ratio of n-alkanes shows the relationship of n-alkanes, which are not likely to undergo differential degradation, as can occur with C/N ratios.

$TAR_{HC} = (C_{27\text{-}31}/C_{17\text{-}21})$ Equation 24. C_{29}/C_{17} Ratio Equation 25.

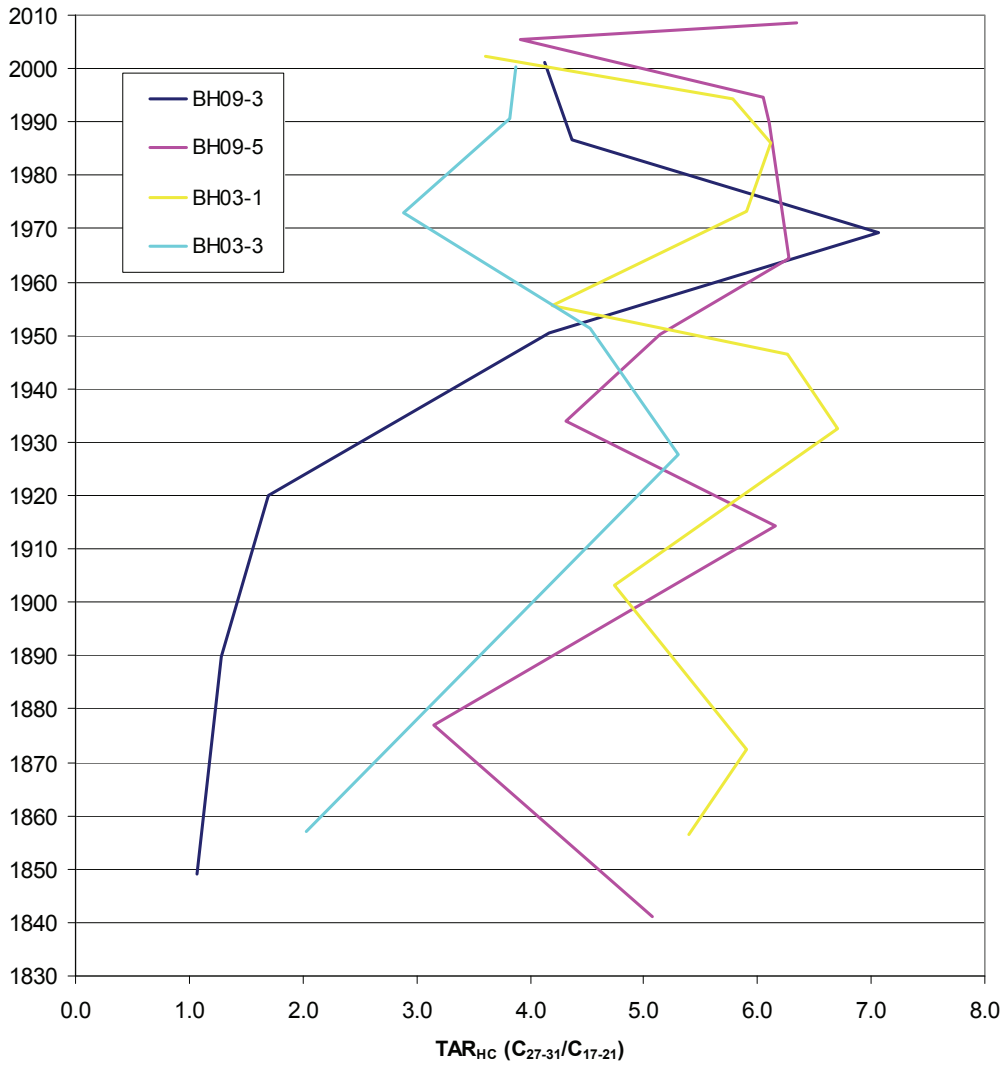

Figure 36. TAR_{HC} ($C_{27\text{-}31}/C_{17\text{-}21}$) vs. Age

Equations 24 and 25 describe ratios of measured concentrations of n-alkanes (Meyers, 1997; Castañeda, 2009b).

$$TAR_{HC} = (C_{27\text{-}31}/C_{17\text{-}21}) \qquad \text{Equation 24.}$$

$$C_{29}/C_{17} \text{ Ratio} \qquad \text{Equation 25.}$$

Values are unitless in both cases; the change may reflect increase or decrease of either source within the ratio. Meyers (1997) observes several studies indicate the TAR_{HC} values may over represent terrigenous organics, which was the motivation for the inclusion of the C_{29}/C_{17} Ratio and comparison of the C/N Ratio (Fig. 21, Section 4.5.3).

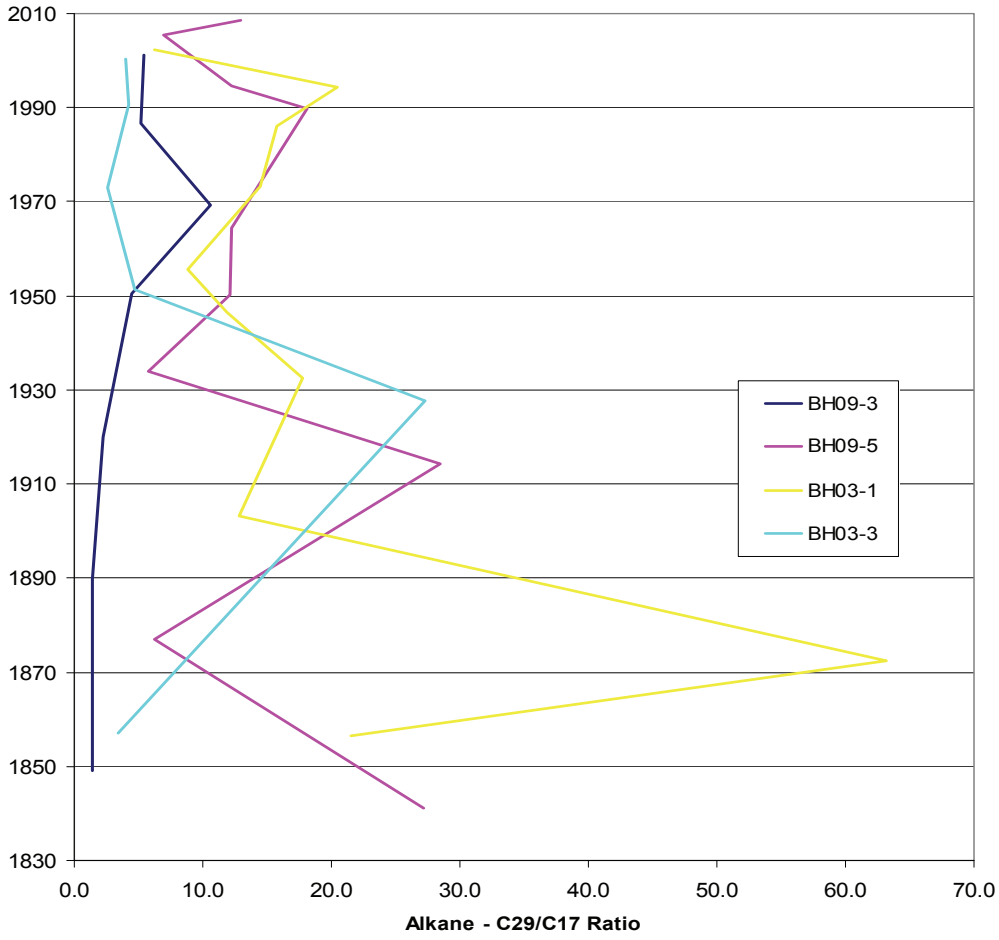

Figure 37. C_{29}/C_{17} Ratio vs. Age

4.8 Isotopic Composition of n-alkane Biomarkers

The carbon isotopic composition of the n-alkanes is shown in Figures 38 and 39. Both aquatic (Fig. 38) and terrigenous (Fig. 39) n-alkane $\delta^{13}C$ values were plotted along with $\delta^{13}C_{org}$ for reference. Cores BH03-1 and BH09-5, shown respectively, were measured for n-alkane specific $\delta^{13}C$; raw data is contained within Appendix D. For simplicity, discussion of aquatic n-alkanes is limited to C_{17}, C_{19} and C_{21} and that of terrestrial n-alkanes to C_{27}, C_{29} and C_{31}. Replicate analysis of selected samples of cores BH03-1 and BH09-5 gave standard errors less 0.83 and 0.68‰ respectively for odd chain n-alkanes and the internal squalene standard.

Both cores indicate that aquatic alkanes become ^{13}C enriched over the period of increase suggested by $\delta^{13}C_{org}$. Significantly light values of C_{17} samples from the late 1800s, in both BH03-1 and BH09-5, display large deviation among replicates. Average values for C_{17} from this early period are approximately -38 and -42‰ respectively, exceedingly light for typical photosynthetic n-alkanes. $\delta^{13}C$ of aquatic n-alkanes in both cores increased by greater than +2‰ during the 20th century. This increase was followed by decline, similar to the bulk $\delta^{13}C_{org}$ proxy. Like $\delta^{13}C_{org}$ values; sedimented aquatic n-alkanes are becoming heavier since 1970, particularly apparent in BH03-1.

Terrestrial $\delta^{13}C$ values in Fig. 39, of both BH03-1 and BH09-5, describe conditions of fluctuating isotopic concentration, slightly larger than the estimated error of measurement. Values for all terrestrial n-alkanes, in the mid 1800s, decrease at the end of the century until ~1940s. This decrease appears to be approximately -1.5‰ in all plotted compounds on average. Since the 1940s measurements oscillate, somewhat in

unison between the cores, current values of nearly -31‰ appear to describe slightly increased ^{13}C concentration of recent samples across terrigenous source n-alkanes lengths.

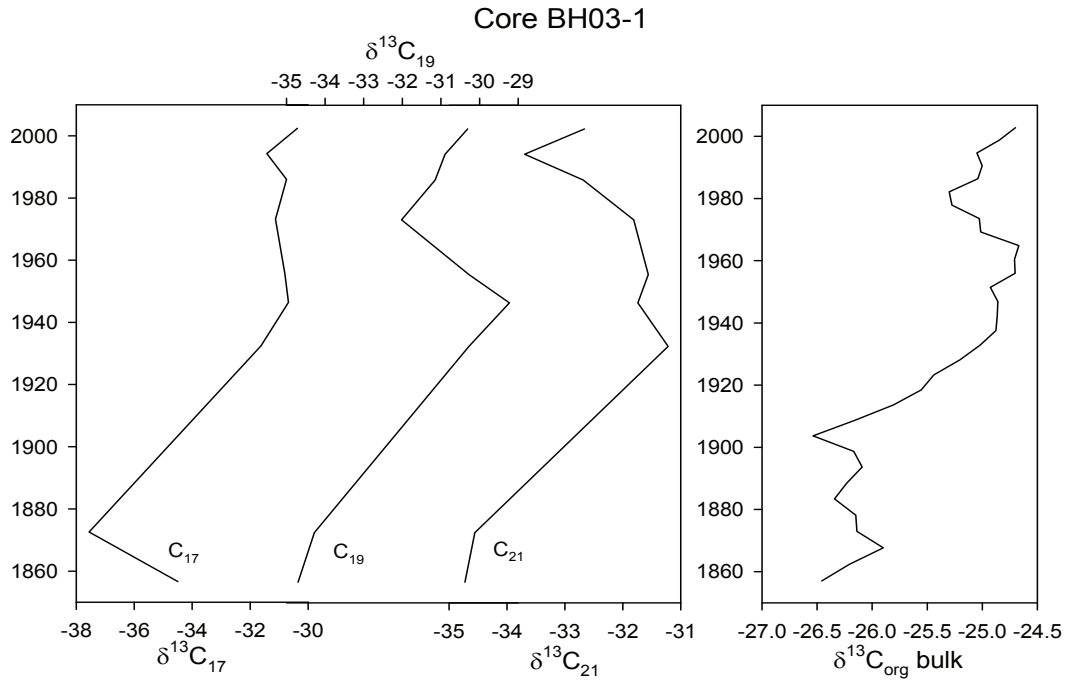

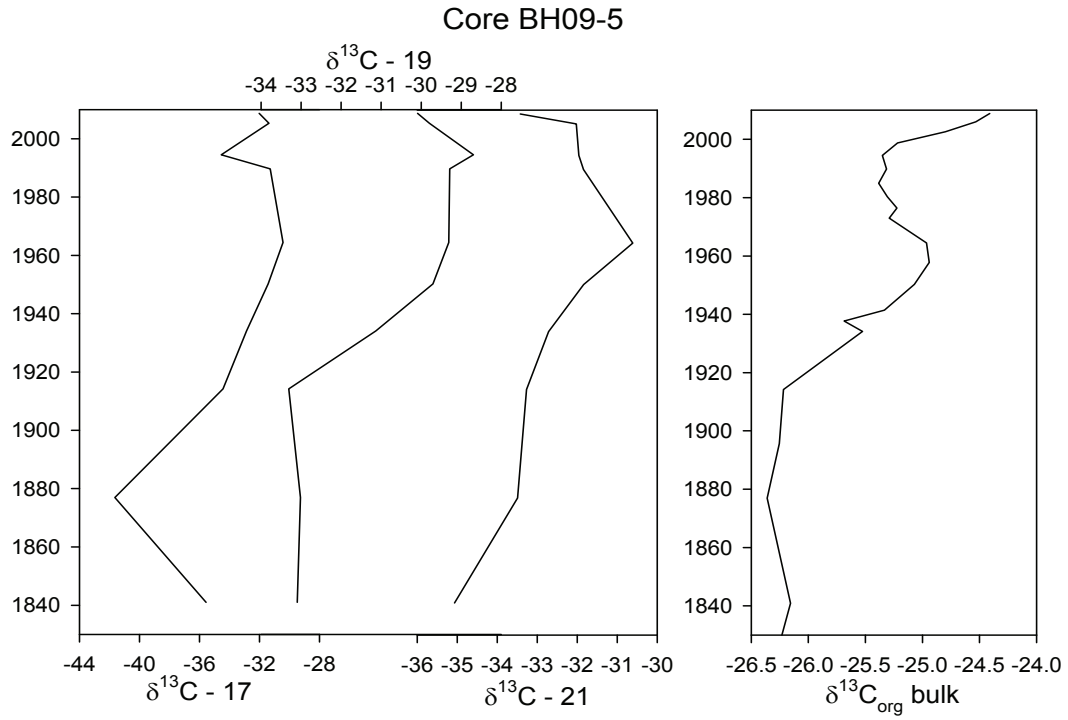

Figure 38. Aquatic $\delta^{13}C$ for Cores BH03-1MC and BH09-5MC

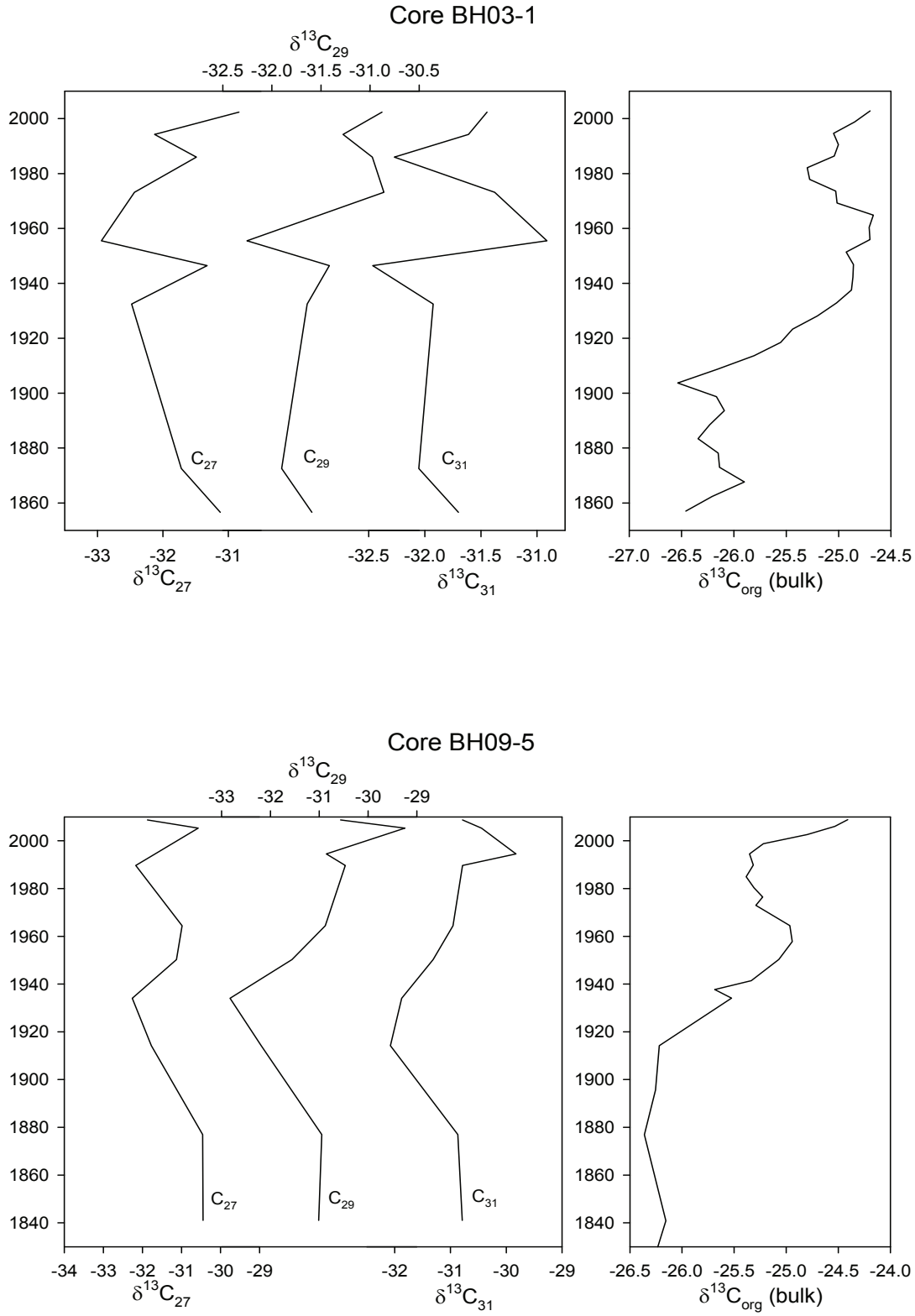

Figure 39. Terrestrial $\delta^{13}C$ for Cores BH03-1MC and BH09-5MC

4.9 Significant Trends of Individual Cores

The following plots in Figs. 40-45 represent the significant trends of measured organics in individual cores plotted over the time interval of measurements, early 1800s to the most recent sediments. Cores are presented in the order they appear in much of the results (BH03-1, BH03-3, BH09-2, BH09-3, BH09-4 and BH09-5). Plot trend lines are color coded with the corresponding measurement type and range of values. Plots alternate with x-axis labels above and below the figure, moving left to right across a plot.

Each core was represented by the most relevant measurements suggesting nutrient or productivity change including: Sedimentation Rate, TOC, TN (Total Nitrogen), $\delta^{15}N_{bulk}$, $\delta^{13}C_{org}$, and C/N Ratio. Cores for which n-alkane biomarker abundance was measured are described by aquatic and terrigenous total plots as well as representative ratios, TAR_{HC} and C_{29}/C_{17} Ratio. Cores BH03-1 and BH09-5 for which carbon isotopic composition was measured of the individual n-alkane biomarkers include data for C_{17}, C_{19}, C_{21} and C_{27}, plotted along $\delta^{13}C_{org}$ for comparison; these cores have two plots (with some proxies shared among charts) found as Figs. 41 and 46, BH03-1 and BH09-5 respectively.

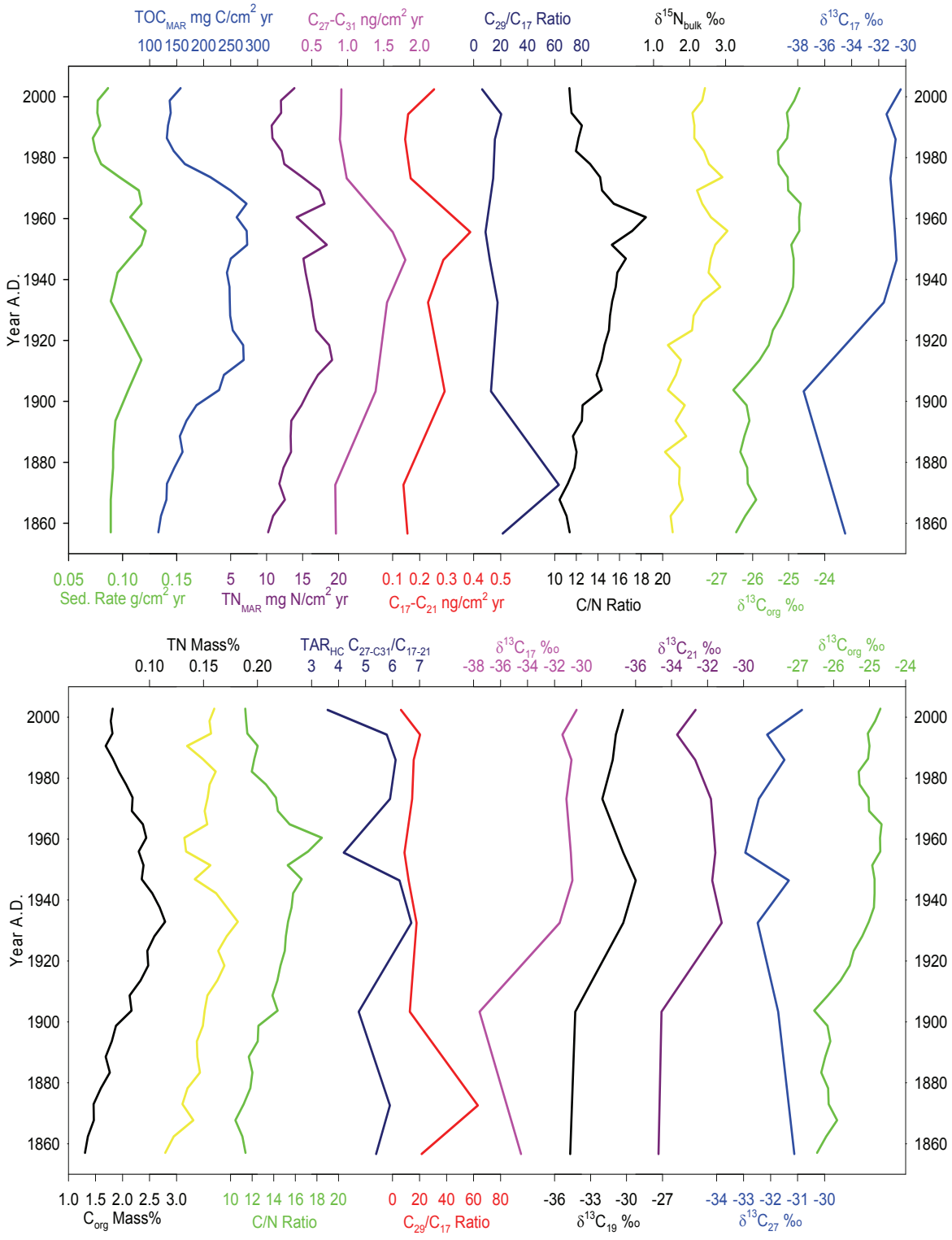

Figure 40. Core BH03-1MC Significant Trends (Both Plots)

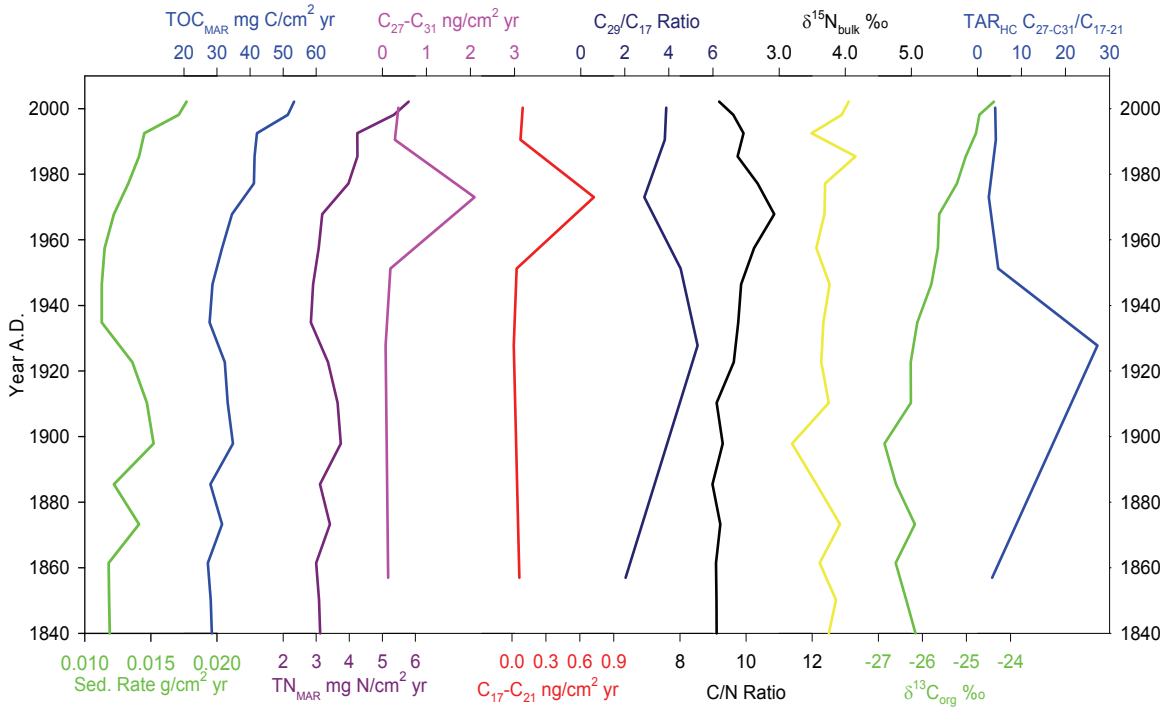

Figure 41. Core BH03-3MC Significant Trends

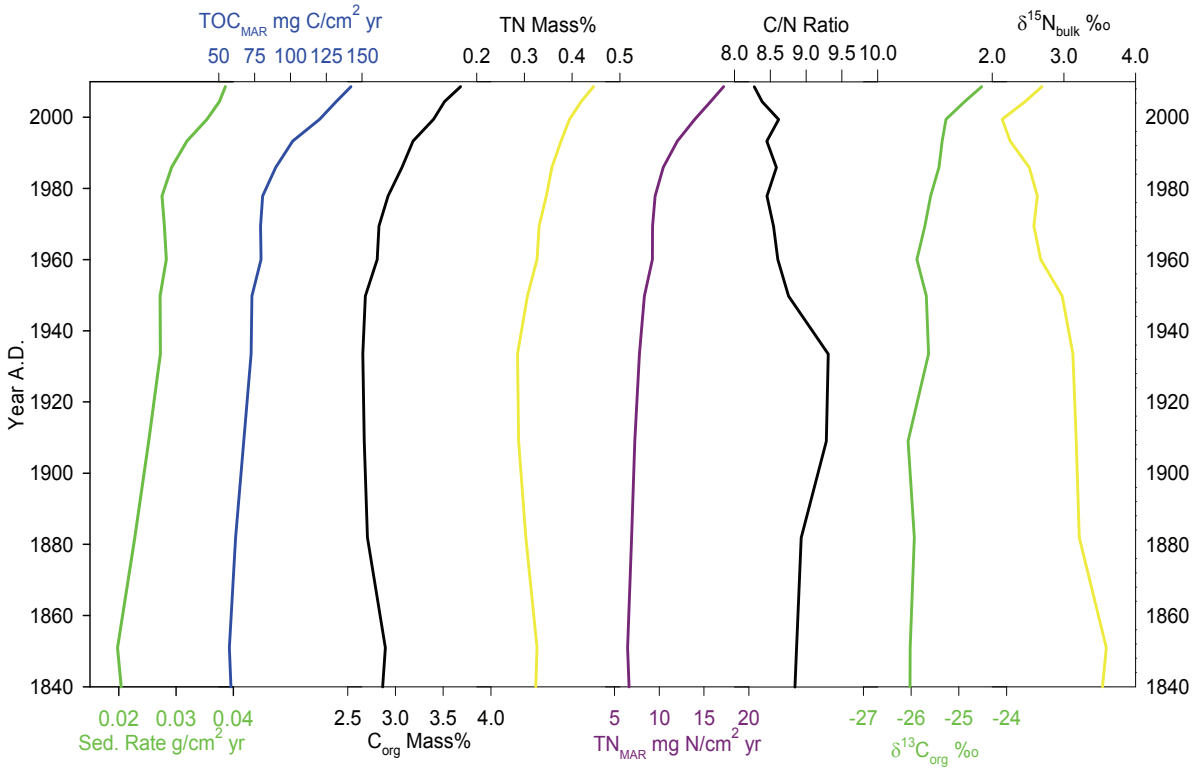

Figure 42. Core BH09-2MC Significant Trends

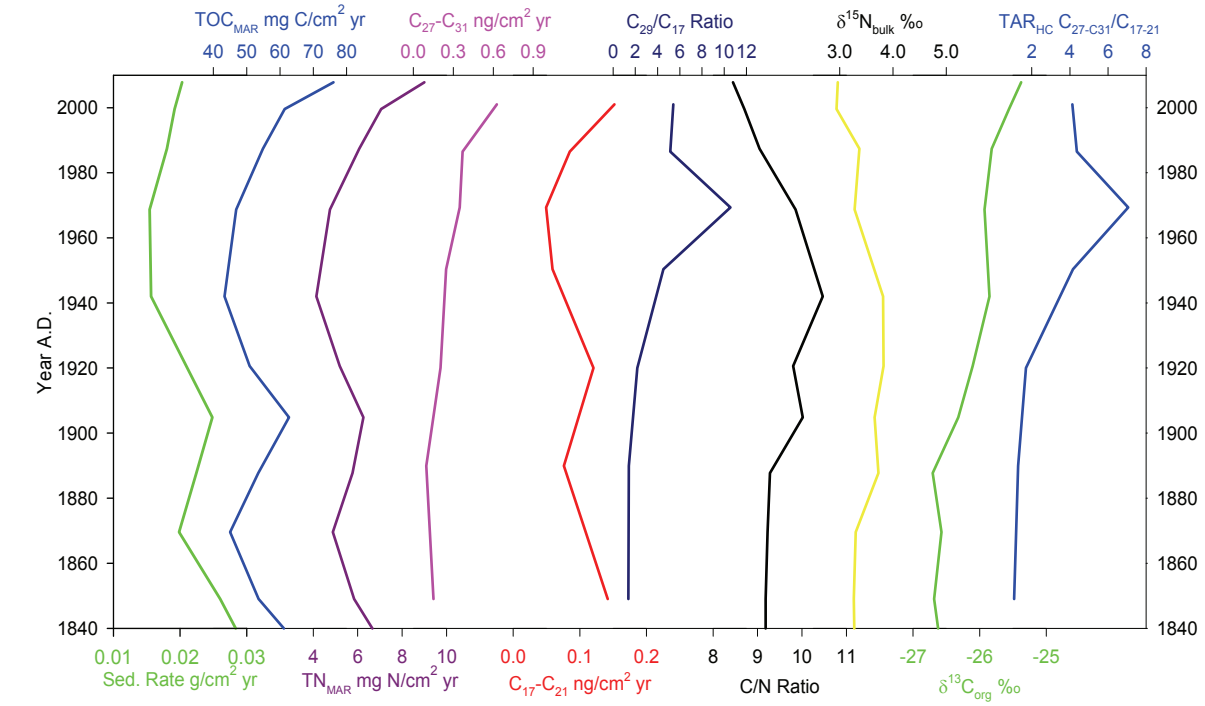

Figure 43. Core BH09-3MC Significant Trends

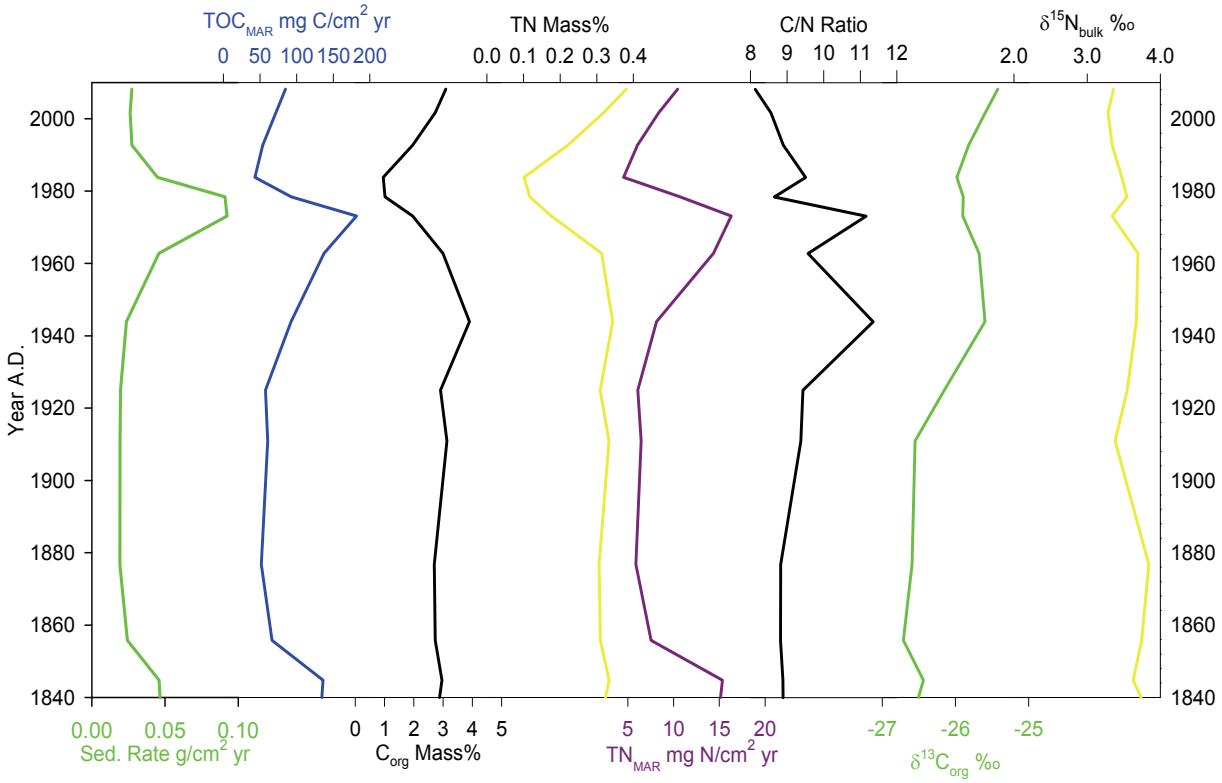

Figure 44. Core BH09-4MC Significant Trends

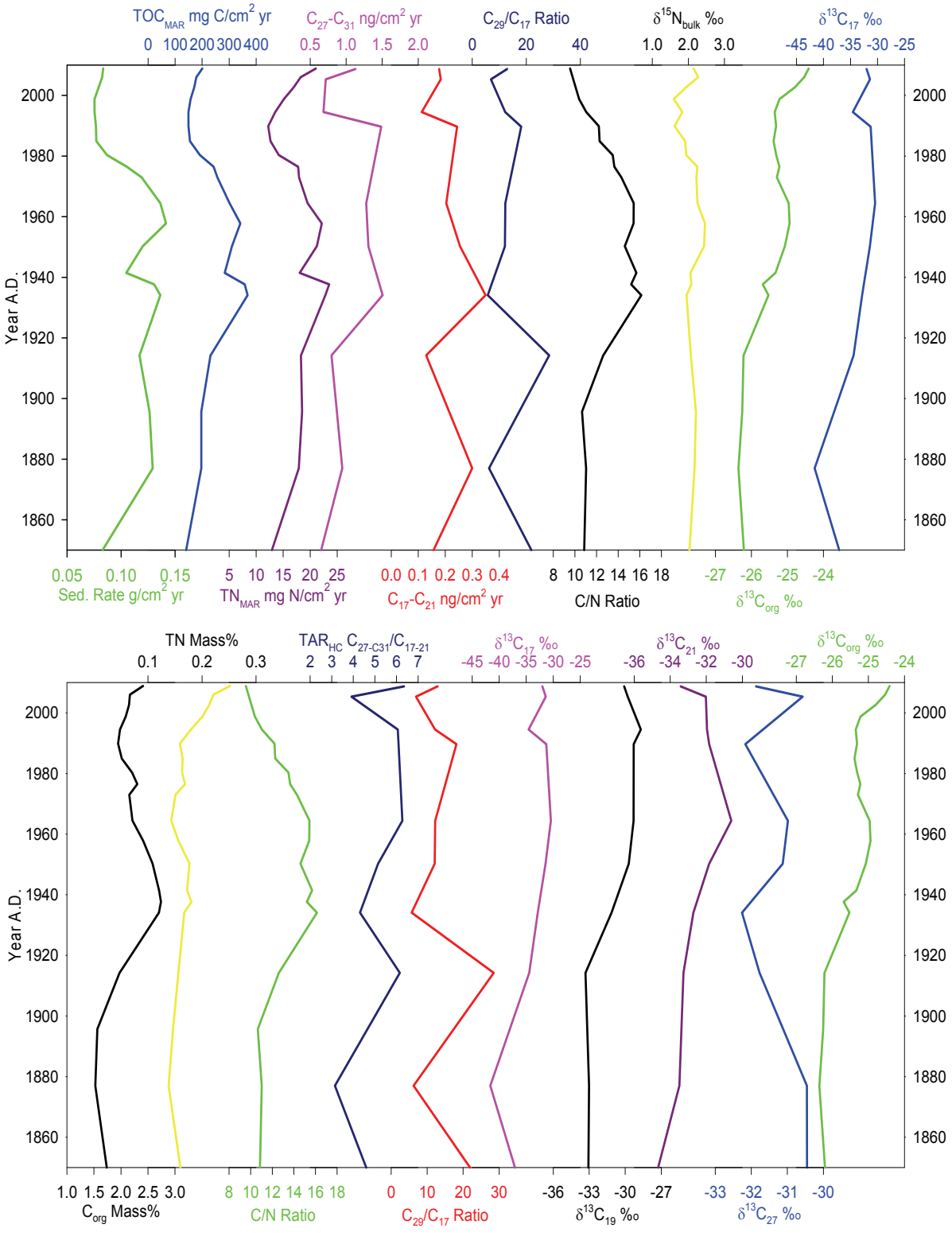

Figure 45. Core BH09-5MC Significant Trends (Both Plots)

5. Discussion

5.1 Sediment Cores

Continuous sedimentation was evident for the cores used in this study. This judgment was based primarily on the low variability in sedimentation rates determined by ^{210}Pb with no obvious breaks in the record of radioactive decay. Other relevant evidence was ideal initial seismic reflection profiles of all sampling sites (prior to sampling) and expected loss of porosity/water content with depth (Fig. 9). Cores displayed consistent mineral distribution and horizons (Sec. 4.1) along with magnetic susceptibility data suggesting continuous sedimentary processes (Sec. 4.2). Concentration of magnetic material within the presumed oxic/anoxic boundary, regardless of visual verification of a distinct metal oxide horizon (Figs. 3-8), was measured in all cores. Larger than the regional ^{210}Pb flux average in all cores (183 Bq/m^{2}yr, Robbins, 1982) (Fig. 15) also indicates continuous sedimentation. Changes in chemical trends along similar time intervals (Sec. 4.5-4.9) act as a time marker shared among cores. Cores were dated using stratigraphy of ^{210}Pb and the CRS model for age assignment. Of seven original cores selected, six were measured for elemental and isotopic concentration of C and N. Four cores were selected for quantification of n-alkane biomarker, of which 2 were further measured for specific δ^{13}C analysis of individual n-alkane compounds.

Cores BH03-1 and BH09-5 were taken from sites in close proximity and can be considered duplicates (Fig. 2), used to test the validity of age assignments and analytical precision, they displayed strong agreement. These cores had relatively high sedimentation rates (Fig. 16, Table 1). Both were recovered from the more developed

western arm of the basin, at sites affected by significant input from the watersheds of the St. Louis and Nemadji Rivers and the cities of Duluth MN and Superior WI. The remaining cores, BH03-1, BH09-2, BH09-3, and BH09-4, represent conditions more typical of off-shore open-water locations.

Core BH05-5, sampled near the Western Lake Superior Mooring (47^{o} 21' 19" N, 89^{o} 28' 50" W), was not analyzed for any chemical proxies as we were unable to assign dates due to significantly different ^{210}Pb concentrations (more than an order of magnitude between adjacent sampled layers). Inability to use this core is unfortunate as the location is centered among the other sampling sites, potentially offering observations with the most open water behavior. It is recommended that a new core be taken from this location and analyzed for the parameters in the study as this location is also the most frequently sampled water column station in Lake Superior. This site may offer the best location to detect trends in the recent past that may be relevant to the interpretation of the most recent deposition in Lake Superior.

Of the 6 cores examined extensively, BH09-4MC was the only core to have large fluctuations in sedimentation rate not associated with physical processing or changes in organic deposition. This core contained an interval (2-6 cm depth, spanning 1962 to 1987) that was impacted by taconite mining activities along the north shore of Minnesota, including the harbors of Silver Bay and Taconite Harbor, with primary operation circa 1955-1980. Mine tailings from the taconite process were added directly to the lake during that time and likely account for the significant increase in sediment material diluting organics and dramatic increase in measured magnetic susceptibility values (Fig.

7). The iron rich tailings provide a means of physically capping the sediments. Return of the organics contained within and below the affected strata to the overlying water column was limited and highlighted by large unanticipated values (Figs. 17 and 19). These trends associated with mining in Lake Superior cores neighboring BH09-4, have also been observed in other studies (Li, 2011). The large change in sedimentation rate in core BH09-4MC between ~1840-1860 (Fig. 16) may be an artifact stemming from the choice of the supported ^{210}Pb values used in CRS calculations (Appleby, 2001) providing estimates of sedimentation rate during this early period that are higher than actual values. Over the interval there were no evident changes in sediment composition that would provide a possible cause for an accelerated rate of sedimentation.

Core BH09-3's sedimentation rate also increased significantly over this early time interval, probably for a similar reason. Due to the dramatic change in sediment rate and composition (e.g. lower water content as well as lower C and N in the later 1900s), discussion of core BH09-4's chemical trends is complicated by the likely influence of a local sedimentation source during this period of mining effluents to the lake. With the exception of the presented mining effects BH09-4 shows similarity to that of open water sites BH03-3, BH09-2 and BH09-3 in general behavior over the longer record.

Cores BH09-2, 3, and 4 collected in 2009 had core tops treated with Zorbitrol, samples and measurements were unaffected because extruded samples were taken immediately after coring on shipboard. These samples were used exclusively for intervals less than 20 cm depth in core. Estimates of sediment accumulation rates suggest consistent regional influences and low rates of sedimentation (approx. 0.02 g/cm^2 yr) for

the pelagic regions of Lake Superior (Fig. 18) at sites BH03-3, BH09-2, BH09-3 and BH09-4 (with the exception of the time period of elevated sedimentation rate affected by local mining practices).

In contrast, cores BH03-1 and BH09-5 describe increasing sediment accumulation through the mid 1800s by roughly 0.05 g/cm^2 yr. Higher, fluctuating sedimentation rates through the 1970s were followed by dramatic decline by 1980, values of both cores are ~0.08 g/cm^2 yr and both show a slight increase in the present century. Wastewater treatment by the Western Lake Superior Waste Disposal (WLSSD) concerns the majority of industrial and residential sources of the St Louis River at present. The facility came online in 1978 and is likely responsible for much of the change in observed sedimentation rate and buried organics, as both increased during the early to middle 1900s (WLSSD, 2011).

5.2 Anthropogenic Change

Logging and early settlement within the catchment, which was well underway by 1850, had little impact on the C and N content of sediments or their stable isotopic signatures even at the sites closest to Duluth-Superior. Observation of the sedimentary record suggests deforestation may have affected sedimentation rates in the western end of the lake by the late 1800s, in agreement with historical records of logging intensity moving east to west along the south shore of the lake, with the majority of operations slowing towards the end of the century (White and Mladendoff, 2004). Nutrient input by deforestation, suggested by increasing terrestrial biomarker accumulation (Figs. 30-31)

and increased C/N (Fig. 21), pales in comparison to the greater effects to come later. This greater nutrient input (post 1900) is attributed to the influence of increasing population in the urban areas of Duluth-Superior and associated agricultural activity in the St. Louis and Nemadji river basins. Bulk sediment C and N stable isotope composition vary little in the late 1800s but change significantly starting in the first few decades of the 1900s. These changing isotopic signatures are consistent with a new source of nitrogen affecting the western end of the lake associated with higher rates of primary productivity; indicative of increased phosphorus concentrations from urbanization.

C_{org} MAR (Fig. 18) increased slowly by the mid 1800s accelerating into the early 1900s may be attributed to urbanization because the increase is most apparent in the far western basin consistent with a growing population center in Duluth-Superior. The earliest sedimentation rate estimates for the mid 1800s (Fig. 16) agree with open water cores away from Duluth-Superior displaying little or no increase while cores BH03-1 and BH09-5 in the far western basin show sedimentation increases in this time period. Although there is little change in the organic content of the sediments the increasing sedimentation rates indicated that C_{org} deposition was also increasing. N_{total} (Figs. 20 and 21) displays trends similar to that of C_{org} with increased sedimentation of nitrogen starting in the early 1900s, slightly later than the increase in C_{org}. The lag of N_{total} in BH03-1 and BH09-5 correlates with an increase in C/N (values exceeding 15) likely indicative of terrigenous input in the late 1800s as a result of logging and agricultural land clearance at the time (White and Mladendoff, 2004). C/N values of open water

cores BH03-3, BH09-2, BH09-3, and BH09-4 fall within the range typical of aquatic predominance (4-10) increasing in the late 1800s (Meyers, 1997). Isotopic trends of C and N, discussed more thoroughly in the following sections, display steady values throughout the late 1800s, prior to marked increase by 1910. Interestingly, the increase in C/N suggesting an increase in terrigenous material, likely including soil debris and wastes (Talbot, 2001), is not accompanied by increased loading of ^{15}N. Similarly, $\delta^{13}C$ values did not change until after the turn of the century when they became more ^{13}C enriched suggesting increasing aquatic primary productivity. Deforestation would have been expected to mobilize terrestrial material with isotopic values in the range of -28 to -26‰ from the forested vegetation cover consisting primarily of C_3 photosynthetic vegetation. However, during this early historical period $\delta^{13}C$ of organic matter was already in this range and so the sedimentary organic carbon isotopic signature would be insensitive to changes. Therefore, evidence of a clear impact of deforestation and logging rests only on the increase in mass sediment rate in the mid 1850s in the western most part of Lake Superior which was accompanied by an increase in C and N loading to the westernmost part of the lake. Away from these western sites there is little or no evidence for an impact of logging within the bulk organic matter of these sediment records.

In the westernmost sites the abundance of long chain n-alkanes increases throughout the late 1800s as measured by C_{27}, C_{29}, and C_{31} (Figs. 31-32). These n-alkanes (with odd chain length predominance) are specific to terrestrial vegetation (Eglinton and Hamilton, 1967) and are indicative of increasing terrestrial organic matter

inputs through this time period as mass sedimentation rates increased. Cores BH03-3 and BH09-3 further to the east displayed little change in these biomarker compounds over the period, suggesting that maximum inputs were in the western end of the lake. BH03-1 and BH09-5 terrestrial biomarkers increase prior to 1900 although only BH09-5 shows subsequent decline in the early 1900s, while BH03-1 increases steadily through the 1950s. Disagreement between the two closely sampled cores is somewhat discouraging, linked perhaps to low concentrations of these compounds, to differences in calculated but low sedimentation rates and to consequent poor resolution in sample intervals.

The carbon preference index (CPI, Figs. 33-34), should indicate potential sample contamination from fossil fuel residues. Terrigenous plots demonstrate values >3, signifying a considerable dominance of odd chain length alkanes, indicating primarily fresh organic matter uncontaminated by petroleum hydrocarbons (Bray and Evans, 1961). The average chain length (ACL, Fig. 35) suggests the significance of C_{27} in the terrigenous (C_{23-33}) component of alkanes (Rommerskirchen *et al.*, 2003). The ACL_{15-33} displays the prominent chain length to vary near 27, indicative of the abundance of long chain compounds relative to aquatic.

The terrigenous to aquatic ratio of n-alkanes (TAR_{HC}, Fig. 36) show the relative change in source material contributions. BH03-1 and BH09-5 do not correlate until ~1950 when both cores display increased terrigenous impact and then a recent decline by 2000. Lack of agreement between these cores, prior to 1900, suggests limited impact of logging and land use upon this ratio. Shown in Fig. 37 is the direct ratio of C_{29}/C_{17} which has also been used to observe changes in terrigenous to aquatic source contribution

(Meyers, 2003). This ratio (although noisy) shows a stronger influence of terrestrial material early in the record with substantial decline by the early 20th century. BH03-1 is largely influenced by the low abundance of C_{17} in the late 1800s, with arbitrary values larger than 62. This ratio swing is similar to the signal observed during agricultural land-clearing in Ontario ~1900 by Meyers *et al*. (1980). Core BH09-5 matches nicely with BH03-1 post 1950s; the increasing T/A ratio through 1990 appears to be driven by a smaller contribution of C_{17}. BH03-3 and BH09-5 increase in the late 1800s indicating relatively higher terrigenous input. BH09-3 which is centrally located in the lake, exhibited only a weak increase that may not be statistically significant.

5.3 Nitrogen Cycling

The measured increase of nitrate in the Lake Superior water column from 5 uM to nearly 30 uM in the last century is subject for concern as the effects and cause of reactive N loading to Lake Superior are largely unknown (Ivanikova *et al*., 2007, Sterner *et al.,* 2007). The sedimentary record in these cores will provide insight to the possible change in N sources to the lake and how they relate to observed water column changes. The $\delta^{15}N$ within the sedimentary record shows little change in all cores from the 1840s through the end of the 19th century, suggesting stable N sources during the period of active logging and deforestation. The significant changes in N content and $\delta^{15}N$ all post date 1910 when the documented increase in nitrate concentrations in the lake began to occur and were likely not related to deforestation (Talbot, 2001). Isotopic variations in N among cores lacks agreement, appearing to be largely related to regional

environmental controls, indicating non-uniform N cycling throughout Lake Superior. In the western most sites near Duluth-Superior $\delta^{15}N$ increases well after the turn of the century and well after the evidence of increased N loading at these sites through the 1800s which is the only evidence of an impact of land use changes in this part of the lake. The rise in $\delta^{15}N$ is nearly concurrent with the rise in $\delta^{13}C$ values (Fig. 23) and this is best explained by the effect of population growth and increased urbanization in Duluth-Superior. A rise in $\delta^{15}N$ such as that observed here is a well known consequence of sewage influence which would also result in increased P loading and higher primary production in the westernmost end of Lake Superior. The $\delta^{15}N$ decline among cores, post 1980, is likely in response to mandated improvements in sewage treatment. The increase in the most recent decade is problematic and may suggest some further change in N cycling in the western end of the lake in recent years.

Away from the two westernmost coring sites there is a long term decline in $\delta^{15}N$ (or no change at BH03-3) that is most simply explained by the increase in isotopically light atmospheric deposition of N which has increased across the entire region (Ostrom *et al*., 1998). Measurement of $\delta^{15}N$ within the sediment record away from the western end displays distinct differences based on location of sample sites shown in Fig. 23. BH09-2 and BH09-4 become progressively ^{15}N depleted over the entire sample interval, the largest decrease after 1940 consistent with known changes in regional atmospheric deposition of fixed N (Ostrom, 1998). BH09-2's N isotope composition became ^{15}N depleted most significantly from (3.5 to 2.0‰) by 2000 in agreement with in-lake nitrification (Sterner *et al.*, 2007), since 2000 values become heavier with ~0.5‰

increase. BH03-3 plots steady values with small fluctuations over time, the heaviest values among all the cores, averaging 3.75‰. Cores BH03-1 and BH09-5 show significant increase starting in the 1920s, likely indicating both loading from heavier anthropogenic sources and increased primary productivity. $\delta^{15}N$ increases during putative P-loading from sewage through the first half of the 20th century, likely reflecting isotopically heavier sewage sources to the N pool (Finlay *et al.*, 2007). The observed $\delta^{15}N$ increase reaches its maximum during the 1960s before decline through the 1980s. P-loading resulting from the poorly treated sewage would stimulate nitrate utilization and increase burial of N by aquatic algae (Ivanikova *et al*., 2007).

Trends of $\delta^{15}N$ in the 1980s vary; BH09-5's values are lighter than those of the 1800s while BH03-1's values are significantly heavier. Values of the open water cores BH03-3, BH09-2, 3, and 4 all display similar behavior with lower minimum values during the late 1980-90s as well as the late 1800s, probably a response to the increased role of isotopically light N in the lake (Finlay *et al.*, 2007). All cores display some small $\delta^{15}N$ increase, with varying intensity, in measurements of the last 20-30 years. The sampling sites experiencing a prior minimum concentration of ^{15}N ~1990 now show a recent increase, a reflection that N cycling that has continued to change within Lake Superior (Sterner *et al.*, 2007; Talbot, 2001;Urban *et al*., 2007).

5.4 Productivity Trends

P-availability is known to control productivity within Lake Superior (Guildford *et al*., 1994) with Fe playing a co-limiting role at least during artificially stimulated primary

production (Sterner *et al*., 2004; Ivanikova *et al*., 2007). Lake wide P-loading, represented by measured increases in productivity is displayed in cores representative of open water locations show a general increase in C_{org} MAR since the early 1900s, and also inferred by $\delta^{13}C_{org}$, which is often considered a primary productivity proxy (Schelske and Hodell, 1991, 1995). Open water sites peaked during the 1930-40s followed by little to no measureable decrease since; cores representative of the moderately urban environment of the western region of the lake display productivity peaking in the mid-1960s followed by substantial decline. Recovery from P loading, shown by decreases in BH03-1 and BH09-5, is most apparent by the 1980s with a lowering of $\delta^{13}C_{org}$ values (Hodell and Schelske, 1998). The increase of $\delta^{13}C_{org}$ in the measurement of all cores in the most recent sediments is puzzling. In agreement with P-loading, increased sedimentation of short chain n-alkanes and associated compound specific isotopic composition suggests increased aquatic primary production (Meyers, 1997).

Carbon content (C_{org}, Figs. 17-18) illustrates expected loss by remineralization in the most recently deposited sediments at the top of the core; strongest within the oxygenated portion of the sediments as expected (Burdige, 2007). Logarithmic decrease of carbon content was most apparent above the oxic/anoxic boundary, identified in the cores by the dispersed Mn and Fe horizons, demonstrating consistently higher rates of remineralization within oxygenated sediments (Richardson and Nealson, 1989). BH03-1 and BH09-5 both display significant increase of carbon content post 1880s, peaking in the mid 1930s at values of ~2.75% C by mass, nearly twice the initial concentrations observed in the 1800s. Increased carbon concentration is consistent with increased

productivity and increased sedimentation of organic material (Burdige, 2007). In general, a maximum in carbon concentration during the 1930s decreases linearly through 1980, returning to values slightly larger than values of the mid 1800s. A possible recent increase since 1990 is likely exaggerated by sedimentation rate and diagenetic processes affecting the most recent sediments. If remineralization of carbon within the most recently sequestered sediments is anticipated values may be consistent with rates in the late 1800s. BH03-3, BH09-2, and BH09-3 display slight positive deviation from vertical. The apparent decrease in BH09-3 starting in the early 1900s, reaching a minimum ~1950, is largely influenced by sedimentation rate. Observations indicate the largest increase and change near the western end of the basin, C_{org} highlights significant change due to urban population inputs to the watershed in the early 1900s.

N_{total} (Figs. 19-20) displays similar trends to organic carbon. Total nitrogen plotted as MAR values increases with sedimentation of organics starting in the middle of the 1800s. The C/N ratio of open water cores BH03-3, BH09-2, BH09-3, and BH09-4 is within the typical aquatic range of 4-10 (Meyers, 1997). Cores BH03-1 and BH09-5 display a significant increase exceeding a ratio of 15 in the 1960s, C/N increases with $\delta^{13}C$ profiles possibly indicating increasing terrestrial inputs along with increasing P availability. However there is no evidence of a strong increase in terrestrial input from the analysis of alkanes in fact aquatic alkanes become relatively more important than terrestrial alkanes post 1930 (Fig. 38) so other explanations must be examined for the increase in C/N. This lag of N relative to C within sedimented organics may be an indication of nitrogen limitation within phytoplankton community during increased

productivity, as available N would likely be assimilated into aquatic producers (Ivanikova *et al*., 2007). Algal growth, under N limited conditions, is possible with high C/N ~20 in cellular compounds (Hecky *et al*., 1993; Talbot and Laerdal, 2000) and sedimented organics. However, N limitation seems unlikely given the observed increase in nitrate concentrations through the past century. Another alternative is that the increased input of organic matter into the sediments stimulated denitrification during this period and resulted in lower C/N ratios.

$\delta^{13}C$ of bulk organic matter, an aquatic productivity proxy, matched well with bio-available P in Lake Ontario and Erie (Schelske and Hodell, 1991, 1995; Hodell and Schelske, 1998). Plot of $\delta^{13}C_{org}$ for all cores (Fig. 22) indicate similar nutrient limited production responding to loading and recovery of P. The most ^{13}C enriched OM was found within the most recent measurements in all cores, while recent productivity has been shown to be declining (Urban *et al*., 2007). Carbon isotope values between -27 and -24.5‰ measured within these cores is consistent with that of sedimented aquatic organic material measured in Lakes Erie and Ontario in bulk samples (Schelske and Hodell, 1991, 1995: Hodell and Schelske, 1998). Core BH03-3 is the only open water site that displays an increasing trend but no productivity maximum during the mid 1900s. It shows a linear increase from the late 1800s through ~2000 of +2.0‰, but values do not decline to indicate recovery from P enrichment. The remaining cores from off shore sites, BH09-2, BH09-3 and BH09-4, display significant increase of +0.5‰ starting ~1900 and reaching maxima in the 1930-40s. This productivity peak gives way to recovery from nutrient enrichment by ~1960-1980. All cores display a second increase post 1980;

current values average +1.5‰. A significant lag in peak productivity is shown in BH03-1 and BH09-5 as values appear to reach a maximum ~1960 of +1.0‰ compared to values of the 1800s, two decades later than the open water sites. In response to P loading, this maximum is followed by subsequent recovery by 1980 as observed in the lower great lakes after bi-national agreement to limit P loading from point sources (Hodell and Schelske, 1998). All cores showed an increase in $\delta^{13}C_{org}$ observed since 1980 exceeding even values of the 1960s maxima. These puzzling trends and interpretation of recent $\delta^{13}C_{org}$ increase are discussed in Sec 5.5.

$\delta^{15}N$ values are in agreement with productivity increasing in the mid 1900s as high values indicate increased anthropogenic input associated with population (Talbot, 2001). $\delta^{13}C$ vs. C/N (Fig. 24) describes bulk sediment samples primarily consisting of organic matter from lacustrine algae (Meyers, 1994), values from -27.0 to -24.5‰ and 8 to 19, respectively, are consistent with measurement of Lake Ontario algae validating the use of $\delta^{13}C_{bulk}$ (Hodell and Schelske, 1998; Silliman *et al*., 1996). $\delta^{15}N$ vs. C/N (Fig. 25) highlights major differences in cores, BH03-1 and BH09-5 reflecting associated urban conditions. Increase in the C/N ratio of bulk sediment, indicating increased terrestrial input and potential N limitation, correlates well with the increase in $\delta^{15}N$ suggesting increased anthropogenic source material (Talbot, 2000). $\delta^{13}C$ vs. $\delta^{15}N$ (Fig. 26) did not show a strong statistical relationship upon initial equation modeling of productive time periods (observed by $\delta^{13}C_{org}$) despite success in analysis of bulk Ontario sediments by Hodell and Schelske (1998). Evidence of increased productivity in Lake Superior is significantly less than that experienced by Lake Ontario and the lower great lakes,

suggesting that while primary productivity in Lake Superior has been impacted by human development in the watershed, the impact has been much lower than in the lower lakes.

The temporal resolution of biomarker samples was limited due to the need for large samples and the more labor intensive nature of the work relative to bulk measurements, resulting in time intervals as large as 25 years in core BH03-3. Intervals in BH09-3 represent 15 years of accumulation each while sample intervals in BH03-1 and BH09-5 reflect 5 and 4 year periods respectively. C_{15} was measured in low abundance; therefore, interpretation and significance is limited while C_{23} is not directly attributed to aquatic production (Cranwell *et al.*, 1987). BH03-3 (Figs. 28 and 29) showed strong increase in apparent accumulation of all n-alkanes from 1950 through 1970, following 1970 n-alkane abundance decreases to prior levels, in agreement with P-loading and isotopic measurements (Urban *et al*., 2007). BH09-3's continuous record, an average of many years within each interval, provides evidence of a faithful record by deviation of C_{15} from other chain lengths. BH03-1 and BH09-5 both display increase and decrease since the mid 1800s. Maximum accumulation of short chain alkanes is evident in the 1960s and by 1930s respectively in these two cores. In reference to inferred nutrient loading and the time scale observed by $\delta^{13}C_{bulk}$, BH03-1 appears to show better agreement by n-alkane measurement. Increase, evident from the late 1800s in cores is followed by decease with values that have remained relatively stable since the 1980s. BH09-3's plots decrease from earliest measurements through the 1960s, and then increase through the most recent measurements, appearing to contradict aquatic production of other cores. Fig. 29 displays the total accumulation of C_{17}, C_{19}, and C_{21}

chain lengths in an attempt to amplify their signal. Although BH03-1 and BH09-5 represent comparable trends in the same region, values fluctuate but appear to lack significant shared trends, suggesting limited productivity information is discernable especially considering error among duplicate measurements.

C_{27}, C_{29}, and C_{31} as terrestrial indicators (Figs. 30-32) are associated with potential nutrient input from terrestrial vegetation. BH03-3 displays behavior similar to that of short chains with a dramatic spike from the 1950-1970. BH03-1 and BH09-5 indicate increase in the early 1900s although display disagreement as decrease is observed by the 1960s and 1990 respectively. Core BH09-3 highlights a prominent increase, 3 fold from 1850 to 2000. Fig. 33 plots of total accumulation rates of C_{27}, C_{29}, and C_{31} simply highlights previously described features of individual chain lengths. BH03-1 and BH09-5 track within the same range (but cross 4 times) over 10 similar sample points, mismatched time intervals among samples may exaggerate dissimilarity.

CPI values larger than 3 describe significant predominance of terrestrial alkanes (Bray and Evans, 1961); aquatic compounds may be equally well represented by values larger than 2. The $ACL_{15\text{-}33}$ displays the prominent chain length to vary between 26 and 27 indicating the abundance of long chain compounds relative to aquatic and selective preservation of N deficient terrestrial material during sedimentary processes (Burdige, 2007; Meyers, 1997).

According to TAR_{HC} (Fig. 37), BH09-3 has greater influence of terrigenous input through 1970 followed by subsequent decline by the late 1980s. BH03-1 and BH09-5 do not correlate well until ~1950 when both cores displayed increased terrigenous input

from the turn of the century followed by decline by 2000. Currently BH09-5's TAR_{HC} and C_{29}/C_{17} ratios appear to have increase since ~2000, the lone core with such a current sample interval measured. BH03-3's trends fluctuate largely, suggesting an increase in the late 1800s and peaking during the 1930s, followed by a decline by 1970 and recent increase.

Isotopic analysis of n-alkanes (Fig. 38) from BH03-1 and BH09-5 provides as additional productivity check, without diagenetic interference (Hayes, 1993). Although trends display general agreement, $\delta^{13}C$ values of specific aquatic biomarker compounds range from -40 to -30 per mil, lighter than $\delta^{13}C_{bulk}$ (O'Leary, 1981; Collister *et al*., 1994). $\delta^{13}C_{17}$ measurements in both cores are limited by measureable material during the late 1800s with low values approaching -43‰ in BH09-5. For $\delta^{13}C_{17}$, productivity peaks in the mid 1900s are evident in both BH03-1 and BH09-5 although significant recent increase within the last 20 years is only observed in BH03-1. BH03-1 and BH09-5 show similar behavior in respect to $\delta^{13}C_{19}$ and $\delta^{13}C_{21}$; an increase in the early 1900s reaching a maximum ~1960 before declining. $\delta^{13}C$ of terrestrial n-alkanes (Fig. 39) is primarily constrained between values of -33 and -30, associated with the signature of C_3 land plants (O'Leary, 1981). Both cores display similar fluctuating trends depicting evidence of changes in source material contribution over time. Although long chain n-alkanes make up the principal portion of the n-alkane measured within the sediments, long chain $\delta^{13}C$ values do not match $\delta^{13}C_{bulk}$ trends, suggesting a greater influence of aquatic OM on the bulk organic carbon isotopic composition, and supporting the use of $\delta^{13}C$ of bulk OM as a proxy for aquatic primary productivity in this system.

Rates of increased production in the largely oligotrophic system of Lake Superior, driven primarily by P loading associated with urbanization of the watershed, largely agree with hypothesized increases in primary production as indicated by $\delta^{13}C$ productivity proxy. Starting in the early 1900s productivity peaked in the mid 1900s with the western portion of the basin showing the greatest effect of enrichment upon productivity while there is no evidence of increased P loading arising from logging in the late 1800s having a direct effect on production. Increased levels of long chain n-alkane biomarkers indicative of increase terrestrial input from deforestation do not match $\delta^{13}C_{bulk}$ and productivity trends of the mid 1900s so although terrestrial inputs were relatively more important in the late 1800s they may not have had a strong imprint on bulk organic C isotopic signatures.

5.5 Recent Trends

Despite recent increase in both $\delta^{13}C_{bulk}$ and $\delta^{15}N_{total}$ long term oligotrophication of the lake is suggested since at least the 1980s; as this study hypothesized. Recent $\delta^{13}C$ increase since 1980 is perplexing and may not indicate production changes in the most recent measurements. In opposition to this interpretation of the $\delta^{13}C_{org}$ sedimentary record, since 1980, direct indicators of modern productivity (such as chlorophyll concentrations) have been in decline since at least the 1970s (Urban *et al*., 2005). The recent increase measured in Lake Erie's $\delta^{13}C$ is attributed to the arrival of zebra muscles (Schelske and Hodell, 1995), which is not a significant event in Lake Superior. Change in sedimentary $\delta^{13}C_{org}$ is not likely the result of diagenetic processing of the sediments,

resulting in ^{13}C enrichment, such increases in $\delta^{13}C_{org}$ have not been reported to be significant (Hayes, 1993; Hodell and Schelske, 1998). Change of contribution of the major species of the phytoplankton community is hypothesized as a possible explanation which would require targeted research. Species selection within the community may change measured $\delta^{13}C$, despite steady nutrient availability. The 10‰ difference between aqueous carbon dioxide and bicarbonate (Mook *et al*., 2004) suggests that increased contribution of any phytoplankton that prefers bicarbonate could have a dramatic effect on the resulting OM. Warming of Lake Superior's surface waters is widely acknowledged as an ongoing change to the lake (Austin and Colman, 2007); such change may have the potential to catalyze species selection as algae are likely impacted by changes to the uppermost water column. Compound specific isotopic analysis of aquatic alkanes does not show ^{13}C enrichment since ~2000; BH03-1 increases through 2000 while BH09-5 sampled more recently does not. The average chain length of aquatic alkanes appear to show consistent change (lowering) over this puzzling time period; however the trend appears later than that observed by $\delta^{13}C_{bulk}$.

Trends of $\delta^{15}N$ in the 1980s vary but all cores display recent small $\delta^{15}N$ increase, suggesting flux of the N pool (Talbot, 2001). Most sampling regions experienced a prior minimum concentration of ^{15}N ~1990, a reflection that N cycling that has continued to change within Lake Superior despite suggestion that measurement of nitrate are rather stable (Sterner *et al.*, 2007; Urban *et al*., 2007).

6. Conclusions

Sediment cores, representative of the larger lake basin, provide a means to investigate a faithful history of nutrient and productivity changes within Lake Superior over the past 1-2 centuries. Despite small sample size, reasonably high analytical precision and temporal resolution were obtained amongst samples from cores with relatively high sedimentation rates. Six multi-cores were collected during research voyages during the summers of 2003 and 2009. Sub-sampled intervals were representative of multiple years, acting to minimize interpretation errors from deviation due to seasonal variability.

The bulk concentrations of organic C and N along with the isotopic compositions of both elements are widely established proxies used to determine changing source material and growth conditions. These indicators were found appropriate to interpret historic change in primary productivity as the buried organic material in the lake is predominantly aquatically produced. In particular the use of $\delta^{13}C_{bulk}$ productivity proxy, used in similar paleo-productivity studies of Lakes Erie and Ontario in the 1990s, is well suited for the P limited primary production of Lake Superior. The quantification of n-alkane abundances, a measure of historic source specific production, presented challenges in both resolution and broad-spectrum significance (i.e., did not yield clear results). In contrast, the $\delta^{13}C$ of biomarkers derived from algae is an unequaled source specific productivity measurement that verifies aquatic productivity drove the trends of bulk OM.

Early land use changes including logging within the Lake Superior catchment were found to provide limited initial nutrient input to Lake Superior. Increasing n-alkane

biomarker accumulation and increased C/N ratios suggest land use changes became noteworthy in the late 1800s, in agreement with historical records. Bulk isotopic compositions of C and N changed little during this early historical period. Despite a well documented increase in nitrate within the lake's water column throughout the 1900s, $\delta^{15}N$ within the sedimentary record shows little change during the end of the 1800s and into the 1900s. In general, change in $\delta^{15}N$ lacks agreement among cores suggesting the cycling of N is largely influenced by regional environmental factors.

Lake wide P-loading is most significant near the population center of Duluth-Superior in comparison to open water core locations. Productivity increased from the early 1900s, and peaked during the 1930-40s as indicated by measurement of $\delta^{13}C_{bulk}$ as well as the accumulation rate and $\delta^{13}C$ of short-chain n-alkanes (algal biomarkers). Cores representative of the moderately urban environment of the western region display stronger productivity peaking in the mid-1960s, with $\delta^{13}C$ values heavier than other regions of the lake by ~1.7‰. A substantial shift to lighter $\delta^{13}C$ values post mid-1960s suggests that decreasing P availability is closely related to the implementation of a wastewater treatment facility brought online in the late 1970s and government mandated P reductions.

Despite a recent increase in both $\delta^{13}C_{bulk}$ and $\delta^{15}N_{total}$, overall oligotrophication of the lake is suggested since the 1980s. The $\delta^{13}C$ increase since 1980 is perplexing and appears largely unrelated to P-availability. Additional work is necessary to surmise the root of such recent changes that deviate from what may be expected behavior of a P-limited system with continually declining P concentration.

References:

Allender, E. and L. Granina., 1997. Biogeochemical phosphorous mass balance for Lake Baikal, southeastern Siberia, Russia. *Marine Geology* **139**: 5-19.

Appleby, P.G. and Oldfield, T., 1978. The calculation of lead-210 dates assuming a constant rate of supply of unsupported ^{210}Pb to the sediment. *Catena* **5**:1-8.

Appleby, P.G., 2001. Chronostratigraphic techniques in recent sediments, In: W.M. Last & J.P. Smol (eds), *Tracking Environmental Change Using Lake Sediments Volume 1: Basin Analysis, Coring, and Chronological Techniques*, pp. 171-203. Kluwer Academic Press, Dordrecht, The Netherlands.

Austin, J. and S. Colman. 2007. Lake Superior summer water temperatures are increasing more rapidly than regional air temperatures: a positive ice-albedo feedback. Journal *of Geophysical Letters* **34**.

Baker, J., S. Eisenreich, and B. Eadie., 1991. Sediment trap fluxes and benthic recycling of organic carbon, polycyclic aromatic hydrocarbons, and polychlorobiphenyl congeners in Lake Superior. *Environ. Sci. Tech*. **25**:500-509.

Bennett, E.B., 1986. The nitrifying of Lake Superior. *Ambio* **15**:272-275.

Bray, E.E. and Evans, E.D., 1961. Distribution of n-paraffins as a clue to recognition of source beds. *Geochimica et Cosmochimica Acta* **22**:2-15.

Burdige, David J., 2007. Preservation of Organic Matter in Marine Sediments: Controls, Mechanisms and an Imbalance in Sediment Organic Carbon Budgets?. *Chemical Reviews* **107**:467-485.

Burkhardt, S., U. Riebesell, and I. Zondervan. 1999. Effects of growth rate, CO_2 concentration, and cell size on the stable carbon isotope fractionation in marine phytoplankton. *Geochimica et Cosmochimica Acta* **63**:3729-3741.

Caraco, N.F., 1995. Influence of human populations on phosphorus transfer to aquatic systems: a regional scale study using large rivers, In: H. Tiessen (Ed.), *Phosphorus in the Global Environment: Transfer, Cycles and Management*, pp. 235-244. Wiley, New York.

Cartwright, J.A., N.J. Wattrus, D.E. Rausch, and A. Bolton., 2004. Recognition of an early Holocene polygonal fault system in Lake Superior: Implications for the compaction of fine grained sediments. *Geology* **32**:253-256.

Castañeda, I., J P. Werne, and T.C. Johnson., 2007. Wet and arid phases in the southeast African tropics since the last glacial maximum. *Geology* **35**:823-826.

Castañeda, I., J.P. Werne, T. Johnson, and T. Finlay., 2009a. Late Quaternary vegetation history of southeast Africa: the molecular isotopic record from Lake Malawi. *Paleogeogrpahy, Paleoclimatology, Paleoecology* **275**:110-112.

Castañeda, I., J P. Werne, and T.C. Johnson., 2009b. Inflence of climate change on algal community structure and primary productivity of Lake Malawi (East Africa) from the Last Glacial Maximum to present. *Limnol. Oceanogr*. **54**(6, part 2):2431-2447.

Cerling, T., J. Harris, B. MacFadden, M. Leakey, J. Quade, V. Eisenmann, and J. Ehleringer., 1997. Global vegetation change thorugh the Miocene/Pliocene boundary. *Nature* **389**:153-158.

Chapra, S.C., 1977. Total phosphorus model for the Great Lakes. *Journal of Environmental Engineering Div.* **103**:147-161.

Collister, J., G. Riely, B. Stern, G. Eglinton, and B. Fry., 1994. Compound-specific $\delta^{13}C$ analyses of leaf lipids from plants with differing carbon dioxide metabolism. *Organic Geochemistry* **21**:619-627.

Cotner, J.B., B.A. Biddanda, W. Makino, and E. Stets., 2004. Organic carbon biogeochemistry of Lake Superior. *Aquatic Ecosystem Heath and Management* **7**:451-464.

Cranwell, P.A., 1981. Diagenesis of free and bound lipids in terrestrial detritus deposited in a lacustrine sediment. *Organic Geochemistry* **3**:79-89.

Cranwell, P.A., G. Eglinton, and N. Robinson., 1987. Lipids of aquatic organisms as potential contributors to lacustrine sediments-II. *Org. Geochem*. **11**:513-527.

Dabous, A.A. 2002., Lead-210 Geochronology and Trace Metal Geochemistry of Sediment Cores from Lake Overstreet and Upper Lake Lafayette, Leon County, Florida. *Environmental Geosciences* **9**(2):51-65.

Duarte, C.M., and Y.T. Prairie. 2005. Prevalence of heterotrophy and atmospheric CO_2 emissions from aquatic ecosystems. *Ecosystems* **8**:862-870.

Eglinton, G. and Hamilton, R.J., 1963. The distribution of alkanes, In: T. Swain (Ed.), *Chemical Plant Taxonomy*. Academic Press.

Eglinton, G. and Hamilton, R.J., 1967. Leaf epicuticular waves: *Science* **156**:1322-1335

Evans, J.E., 1980. ^{210}Pb Geochronology in Lake Superior Sediments: Sedimentation

Rates, Organic Carbon Deposition, Sedimentary Environments, and Post-Depostional Processed. M.S. Thesis, Univ. of Minnesota, Dept. of Geology and Geophysics, Minneapolis, MN. pp. 16-22.

Evans, J.E., T.C. Johnson, E.C. Alexander Jr., R.S. Lively, and S.J. Eisenreich., 1981. Sedimentation rates and depositional processes in Lake Superior from Pb210 geochronology. Journal of Great Lakes Research **7**:299-310.

Fee, E.J., J.A. Shearer, E.R. DeBruyn, and E.U. Schindler., 1992. Effects of lake size on phytoplankton photosynthesis. *Canadian Journal of Fisheries and Aquatic Sciences* **49**:2445-2459.

Finlay, J.C., R.W. Sterner, and S. Kumar., 2007. Isotopic evidence for in-lake production of accumulating nitrate in Lake Superior. *Ecological Applications* **17**(8):2323-2332.

Flood, R.D., and T.C. Johnson., 1984. Side-scan targets in Lake Superior – evidence for bedforms and sediment transport. *Sedimentology* **31**:311-333.

Freeman, K.H., 2001. Isotopic Biogeochemistry of Marine Organic Carbon. *Reviews in Mineralogy and Geochemistry* **43**(1):579-605.

Friedman, S.K. and Reich, P.B., 2005. Regional legacies of logging: Departure from presettlement forest conditions in northern Minnesota. *Ecological Applic*. **15**(2): 726-744.

Giger, W., C. Schaffner, and S.G. Wakeham., 1980. Aliphatic and olefinic hydrocarbons in recent sediments of Greifensee, Switzerland. *Geochi. Cosmochi. Acta* **44**:119-129.

Goossens, H., R.R. Duren, J.W. Leeuw and P.A. Schenck., 1989. Lipids and their mode of occurance in bacteria and sediments-II. Lipids in the sediment of a stratified, freshwater lake. *Organic Geochemistry* **14**:27-41.

Harris, D., W.R. Horwath, and C. Van Kessel., 2001. Acid fumigation of soils to remove carbonates prior to total organic carbon or carbon-13 isotopic analysis. *Soil Sci. Soc. Am. J.* **65**:1853-1856.

Hayes, J.M., 1993. Factors controlling ^{13}C content of sedimentary organic compounds: Principles and evidence, In: R.J. Parkes, P. Westbroek and J.W. de Leeuw (Eds.), *Marine Sediment, Burial, Pore Water Chemistry, Microbiology and Diagenesis*. Marine Geology **113**:111-125.

Hecky, R.E., 1993. The eutrophication of Lake Victoria. *Verh. Internat. Verein. Limnol.* **2**5:39-48.

Heinen, Erik Allen., 2002. Carbon and Nutrient Cycling in Western Lake Superior. M.S. Thesis, Univ. of Minnesota, Dept. of Geology and Geophysics, Minneapolis, MN

Hodell, D.A. and C. L. Schelske., 1998. Production, sedimentation, and isotopic composition of organic matter in Lake Ontario. *Limnol. Oceanogr*. **43**(2):200-214.

Ivanikova, N.V., R.M.L. McKay, G.S. Bullerjahn, and R.W. Sterner., 2007. Nitrate utilization by phytoplankton in Lake Superior is Impaired by Low Nutrient (P,Fe) Availability and Seasonal Light Limitation – A cyanobacterial Bioreporter Study. *Journal of Phycology* **43**(3):475-484.

Gruber N., Keeling C.D., Bacastow R.B., Guenther P.R., Lueker T.J., Wahlen M., Meijer H.A.J., Mook W.G., Stocker T.F., 1999. Spatiotemporal patterns of carbon-13 in the global surface oceans and the oceanic Suess effect. *Global Biogeochem Cycles* **13**:307-335.

Kendall, C. and E.A. Caldwell., 1998. Fundamentals of Isotope Geochemistry, In: C. Kendall and J.J. McDonnell (Eds.), *Isotope Tracers in Catchment Hydrology*, pp. 51-86. Elsevier Science B.v., Amsterdam.

Larson, A.M., 2007. The White Pine Industry in Minnesota. Minneapolis, MN, USA: University of Minnesota Press. p432.

Li, J. 2011. Diaenesis and sediment-water exchanges in organic-poor sediments of Lake Superior. MS Thesis, University of Minnesota.

McKenzie, A.J., 1985. Carbon Isotopes and Productivity in the Lacustrine and Marine Environment, In: Werner Stumm (Ed.), *Chemical Processes in Lakes*, pp. 99-118. Wiley-Interscience, New York.

Meyers, P.A., Bourbonnie, R.A., Takeuchi, N., 1980. Hyudrocarbons and fatty acids in two cores of Lake Huron Sediments. *Geochimica et Cosmochimic Acta* **44**:1215-1221.

Meyers, P.A., 1994. Preservation of source identification of sedimentary organic matter during and after deposition. *Chemical Geology* **144**:289-302.

Meyers, P.A., 1997. Organic geochemical proxies of paleoceanographic, paleolimnologic, and paleclimatic processes. *Organic Geochemistry* **27**:213-250.

Meyers, P.A., 2003. Applications of orgainic geochemistry to paleolimnological reconstructions: a summary of examples from the Laurentain Great Lakes. *Organic Geochemistry* **34**:261-289.

Minnesota Sea Grant. (2010, August 4). General Format. Retrieved from http://www.seagrant.umn.edu/superior/facts

Mook, W.G., J.C. Bommerson, and W.H. Staverman. 1974. Carbon isotope fractionation between dissobled bicarbonate and gaseous carbon dioxide. *Earth Planet. Sc. Lett.* **22**:169-176

Ngobi, G.N., T.C. Johnson, and P.A. Solheid., 1998. Environmental Magnetism of Late Pleistocene / Holocene Sequences from Lake Victoria, East Africa, In: John T. Lehman (ed.), *Environmental Change and Response in East African Lakes*, pp. 59-73. Kluwer Academic Publishers, Dordrecht, The Netherlands.

Nowaczyk, N.R., 2001. Logging of Magnetic Susceptibility, In: W.M. Last and J.P. Smol (Eds.), *Tracking Environmental Change using Lake Sediments Vol. 1: Basin Analysis, Coring, and Chronological Techniques*, pp. 155-170. Kluwer Academic Press, Dordrecht, Netherlands.

Oldfield, F. and Appleby, P. G., 1984. Empirical testing of ^{210}Pb-dating models for lake sediments, In: Haworth, E.Y. and Lund, J.W.G. (Eds.), *Lake Sediments and Environmental History*, p. 405. University of Minnesota Press, Minneapolis, Minnesota.

O'Leary, M.H., 1981, Carbon isotope fractionation in plants. *Phytochemistry* **20**:553-567.

Ostrom, N.E., D.T. Long, E.M. Bell, and T. Beals., 1998. The Origin and cycling of particulate and sedimentary organic matter and nitrate in Lake Superior. *Chemical Geology* **152**:13-28.

Ostrom, P.H., N.E. Ostrom, J. Henry, B.J. Eadie, P.A. Meyers, and J.A. Robbins., 1998. Changes in the tropic state of Lake Erie: discordance between molecular δ^{13}C and bulk δ^{13}C sedimentary records. *Chemical Geology* **152**:163-179.

Richardson, L.L. and Nealson, K.H., 1989. Distributions of manganese, iron and manganese-oxidizing bacteria in Lake Superior sediments of different organic carbon content. *Journal of Great Lakes Research*. **15**(1):123-132.

Rieley, G., R.J. Collier, D.M. Jones, G. Eglinton, P.A. Eakin, and A.E. Fallick., 1991. Sources of sedimentary lipids deduced from stable isotope analyses of individual compounds. *Nature* **352**:425-427.

Robbins, J.A., 1982. Stratigraphic and dynamic effects of sediment reworking by Great Lakes zoobenthos. *Hydrobiologia*. **92**:611-622.

Robbins, J.A. and B.J. Eadie., 1991. Seasonal cycling of trace elements, ^{137}Cs, ^{7}Be, and $^{239+240}$Pu in Lake Michigan. *Journal of Geophysical Research* **96**:17081-17104.

Rommerskirchen, F., Eglinton, G., Dupont, L., 2003. A north to south transect of Holcene southeast Atlantic continental margin sediments: relationship between aerosol transport and compound specific $\delta^{13}C$ land plant biomarker and pollen records. *Geochemistry, Geophysics and Geosystems* **4**:1101.

Rubinson, K.A. and J.F. Rubinson., 2000. *Contemporary Instrumental Analysis.* 1st Edition, pp. 111-117;529-533;673-694. Upper Saddle New Jersey: Prentice-Hall.

Schwark, L., K. Zink, and J. Lechterbeck., 2002. Reconstruction of post glacial to early Holocene vegetation history in terrestrial Central Europe via cuticular lipid biomarkers and pollen records from lake sediments. *Geology* **30**:463-466.

Schelske, C.L. and D.A. Hodell., 1991. Recent changes in productivity and climate of Lake Ontario detected by isotopic analysis of sediments. *Limnology and Oceanography* **36**:961-975.

Schelske, C.L. and D.A. Hodell., 1995. Using carbon isotopes of bulk sedimentary organic matter to reconstruct the history of nutrient loading and eutrophication of Lake Erie. *Limnology and Oceanography* **40**:918-929.

Schelske, C.L., E.F. Stoermer, and W.F. Kenny., 2006. Historic low-level phosphorus enrichment in the Great Lakes inferred from biogenic silica accumulation in sediments. *Limnology and Oceanography* **51**:728-748.

Silliman,J.E., Meyers, P.A., Bourbonniere, R.A., 1996. Record of postglacial organic matter delievery and burial in sediments of Lake Ontario. *Organic Geochemistry* **24**:463-472.

Sterner, R.W., T.M. Smutka, R.M.L. McKay, Q. Xiaoming, and E.T. Brown., 2004. Phosphorus and trace metal limitation of algae and bacteria in Lake Superior. *Limnology and Oceanography* **49**:495-507.

Sterner, R.W., E. Anagnostou, S. Brovold, G.S. Bullerjahn, J.C. Findlay, S. Kumar, R.M.L. McKay, and R.M. Sherrel., 2007. Increasing stoichiometric imbalance in North America's largest lake: Nitrification in Lake Superior. *Geophysical Research Letters* **34**.

Talbot, M.R. and T. Laerdal., 2000. The late Plestocene-Holocene Paleolimnology of Lake Victoria, East Africa, based upon elemental and isotopic analyses of sedimentary organic matter. *Journal Paleolimnology* **23**:141-164.

Talbot, M.R., 2001. Nitrogen Isotopes in Paleolimnology, In: W.M. Last and J.P. Smol (Eds.), *Tracking Environmental Change Using Lake Sediments. Volume 2: Physical and Geochemical Methods*, pp. 401-439. Kluwer Academic Publishers, Dordrecht, The Netherlands.

Tylmann, W., 2004. Estimating the Sedimentation Rates Using ^{210}Pb on the Example of Morphologically Complex Lake (Upper Lake Raduńskie, N Poland). *Geochronometria* **23**:21-26.

Urban, N.R., M.T. Auer, S.A. Green, X. Lu, D.S. Apul, K.D. Powell, and L. Bub., 2005. Carbon cycling in Lake Superior. *Journal of Geophysical Research* 110.

Urban, N.R., 2007. Nutrient cycling in Lake Superior: A retrospective and update, In: M. Munaware and R. Heath (Eds.), *The State of Lake Superior*. Ecovision World Monograph Series.

Van Alstine, Jon D., 2006. A High Resolution Study of the Spatial and Temporal Variability of Natural and Anthropogenic Compounds in Off Shore Lake Superior Sediments. M.S. Thesis, Univ. of Minnesota, Dept. of Geology and Geophysics, Minneapolis, MN.

Wakeham, S.G. and E.A. Canuel.. 2006. Degredation and Preservation of Organic Matter in Marine Sediments, In: J.K. Volkman (Ed.), *The handbook of Environmental Chemistry Vol. 2 Reactions and Processes Part N*, pp. 295-321. Springer Berlin Heidelburg, New York.

Weiler, R.R. 1978., The chemistry of Lake Superior. *Journal of Great Lakes Research* **4**:370-385.

Western Lake Superior Sanitary District (WLSSD). (2011, April 14). General Format. Retrieved from http://www.wlssd.duluth.mn.us/about_history.php

White, M.A. and Mladendoff, D.J., 2004. Old-growth forest landscape transitions from pre-European settlement to present. *Landscape Ecology* **9**: 191-205.

White, M.A. and Host, G.E., 2008. Forest disturbance frequency and patch structure from pre-European settlement to present in the Mixed Forest Providence of Minnesota, USA. *Canadian Journal of Forest Research* **38**: 2212-2226.

Appendix: A ^{210}Pb Concentration and CRS Age Model Data

Core BH03-1MC CRS Calculation

Center of Interval (cm)	Cum. Dry Mass (g/cm2)	Unsup. Activity (Bq/g)	Error of Unsup. Act. (±s.d.)	Date A.D.	Error of Age (±s.d.)	Sediment Accum. (g/cm2 yr)	Error of Sed. Accum. (±s.d.)
0.15	0.0482	4.26E-01	2.54E-02	2003.1	1.18	0.0866	0.00560
1.05	0.2462	4.45E-01	1.87E-02	2000.6	1.16	0.0770	0.00371
1.35	0.3251	4.40E-01	1.66E-02	1999.6	1.17	0.0755	0.00341
1.95	0.4904	4.00E-01	1.58E-02	1997.5	1.21	0.0778	0.00370
2.25	0.5780	3.80E-01	1.60E-02	1996.3	1.23	0.0792	0.00397
2.85	0.7608	3.65E-01	7.89E-03	1994.0	1.29	0.0766	0.00282
3.15	0.8570	3.50E-01	1.30E-02	1992.7	1.32	0.0770	0.00370
3.75	1.0546	3.14E-01	1.24E-02	1990.2	1.38	0.0794	0.00408
4.7	1.4031	3.00E-01	1.30E-02	1985.6	1.51	0.0725	0.00412
5.1	1.5490	2.73E-01	1.09E-02	1983.6	1.58	0.0749	0.00420
5.9	1.8446	2.53E-01	1.11E-02	1979.5	1.73	0.0714	0.00447
6.3	1.9971	2.12E-01	9.75E-03	1977.6	1.81	0.0801	0.00529
7.1	2.3163	1.56E-01	8.11E-03	1974.2	1.95	0.0972	0.00716
7.5	2.4793	1.45E-01	6.91E-03	1972.5	2.03	0.0993	0.00724
8.3	2.8162	1.14E-01	4.78E-03	1969.5	2.19	0.1150	0.00852
9.5	3.3395	9.69E-02	5.08E-03	1965.0	2.46	0.1176	0.01024
10.7	3.8858	9.15E-02	5.76E-03	1960.0	2.82	0.1071	0.01093
11.9	4.4155	6.96E-02	2.38E-03	1955.5	3.18	0.1215	0.01206
12.3	4.5890	6.89E-02	3.97E-03	1954.0	3.31	0.1174	0.01324
14.5	5.7624	6.29E-02	2.85E-03	1942.6	4.63	0.0953	0.01311
16.5	6.7202	4.86E-02	2.30E-03	1932.0	6.31	0.0891	0.01646
20.5	8.6837	1.98E-02	2.29E-03	1912.6	5.95	0.1174	0.02384
24.5	10.5608	1.42E-02	1.70E-03	1894.2	9.81	0.0934	0.02837
29.5	12.8872	6.57E-03	1.60E-03	1867.7	17.44	0.0891	0.04883

Supported Activity: 2 Samples

A_b	A(0)	(Bq/g)	(±s.d.)
6.57E-03	2.143985	4.06E-02	7.81E-04

Core BH03-3MC CRS Calculation

Center of Interval	Cum. Dry Mass	Unsup. Activity	Error of Unsup. Act.	Date A.D.	Error of Age	Sediment Accum.	Error of Sed. Accum.
(cm)	(g/cm2)	(Bq/g)	(±s.d.)		(±s.d.)	(g/cm2 yr)	(±s.d.)
0.15	0.0260	1.49E+00	6.48E-02	2002.2	0.71	0.0177	0.00080
0.45	0.0617	1.41E+00	5.64E-02	2000.2	0.73	0.0177	0.00074
1.05	0.1493	1.30E+00	3.82E-02	1995.0	0.79	0.0165	0.00055
1.35	0.2008	1.34E+00	4.56E-02	1991.4	0.84	0.0145	0.00055
1.95	0.3174	1.08E+00	3.49E-02	1983.2	0.84	0.0141	0.00051
2.25	0.3824	9.92E-01	3.22E-02	1978.4	0.92	0.0133	0.00050
2.55	0.4518	9.02E-01	2.78E-02	1972.8	1.03	0.0125	0.00048
2.85	0.5243	7.70E-01	2.27E-02	1966.9	1.18	0.0122	0.00050
3.15	0.6001	6.75E-01	2.40E-02	1960.3	1.38	0.0115	0.00056
3.45	0.6807	5.75E-01	1.96E-02	1952.8	1.67	0.0108	0.00058
3.75	0.7634	4.38E-01	1.34E-02	1945.5	2.05	0.0113	0.00070
4.05	0.8491	3.48E-01	1.52E-02	1937.9	2.55	0.0113	0.00090
4.7	1.0631	1.76E-01	7.53E-03	1921.3	2.19	0.0136	0.00093
5.1	1.1947	1.23E-01	6.94E-03	1912.3	2.80	0.0147	0.00132
5.9	1.4471	6.92E-02	4.51E-03	1895.4	2.92	0.0152	0.00149
6.3	1.5695	6.51E-02	3.36E-03	1885.4	3.91	0.0122	0.00138
7.1	1.8116	3.12E-02	2.75E-03	1867.2	4.25	0.0141	0.00196
7.5	1.9309	2.81E-02	2.77E-03	1857.0	5.70	0.0118	0.00205
8.3	2.1702	1.46E-02	2.25E-03	1836.5	9.01	0.0119	0.00327

Supported Activity: 4 Samples

A_b	A(0)	(Bq/g)	(±s.d.)
1.46E-02	2.017643	4.21E-02	1.04E-03

Core BH09-2MC CRS Calculation

Center of Interval	Cum. Dry Mass	Unsup. Activity	Error of Unsup. Act.	Date A.D.	Error of Age	Sediment Accum.	Error of Sed. Accum.
(cm)	(g/cm2)	(Bq/g)	(±s.d.)		(±s.d.)	(g/cm2 yr)	(±s.d.)
0.25	0.0720	1.84E+00	7.58E-02	2008.6	0.57	0.0386	0.0051
1.25	0.2286	1.66E+00	6.71E-02	2004.4	0.37	0.0376	0.0053
2.25	0.4051	1.56E+00	6.41E-02	1999.4	0.18	0.0354	0.0056
3.25	0.5994	1.45E+00	5.97E-02	1993.3	0.07	0.0319	0.0062
4.25	0.8155	1.22E+00	5.10E-02	1985.9	0.36	0.0292	0.0068
5.25	1.0371	1.01E+00	4.31E-02	1977.9	0.66	0.0276	0.0072
6.25	1.2744	7.02E-01	3.13E-02	1969.4	0.83	0.0280	0.0071
7	1.5395	5.71E-01	2.61E-02	1960.1	1.12	0.0283	0.0070
8	1.8189	4.10E-01	2.02E-02	1949.8	1.36	0.0272	0.0073
9.5	2.2633	2.49E-01	1.45E-02	1933.5	1.83	0.0273	0.0073
11.5	2.8822	1.37E-01	1.00E-02	1909.0	2.96	0.0252	0.0079
13.5	3.5004	6.00E-02	7.39E-03	1881.9	5.29	0.0228	0.0087
15.5	4.1135	3.10E-02	5.77E-03	1850.9	11.03	0.0198	0.0100
17.5	4.7186	6.90E-03	5.17E-03	1822.7	23.95	0.0215	0.0092

Supported Activity: 1 Sample

A_b	A(0)	(Bq/g)	(±s.d.)
6.90E-03	2.314985	8.10E-02	4.36E-03

Core BH09-3MC CRS Calculation

Center of Interval	Cum. Dry Mass	Unsup. Activity	Error of Unsup. Act.	Date A.D.	Error of Age	Sediment Accum.	Error of Sed. Accum.
(cm)	(g/cm2)	(Bq/g)	(±s.d.)		(±s.d.)	(g/cm2 yr)	(±s.d.)
0.25	0.0693	1.91E+00	7.83E-02	2007.8	0.32	0.0203	0.0028
1.25	0.2275	1.57E+00	6.45E-02	1999.6	0.24	0.0192	0.0029
2.25	0.4466	1.15E+00	4.75E-02	1987.4	0.92	0.0180	0.0031
3.25	0.7351	8.31E-01	3.54E-02	1968.7	2.08	0.0154	0.0037
4.25	1.1536	2.51E-01	1.17E-02	1942.0	2.05	0.0157	0.0036
5.25	1.6019	1.08E-01	6.90E-03	1920.6	2.55	0.0210	0.0027
6.25	1.9940	5.65E-02	5.79E-03	1904.8	3.61	0.0248	0.0023
7.25	2.3786	4.92E-02	5.07E-03	1887.7	5.50	0.0224	0.0025
8.25	2.7384	2.31E-02	3.77E-03	1869.6	7.28	0.0198	0.0028
9.5	3.2737	8.30E-03	2.66E-03	1849.0	9.82	0.0260	0.0022
11.5	3.9850	4.30E-03	2.57E-03	1826.6	19.11	0.0318	0.0018

Supported Activity: 4 Samples

A_b	A(0)	(Bq/g)	(±s.d.)
4.30E-03	1.28E+00	4.06E-02	9.87E-04

Core BH09-4MC CRS Calculation

Center of Interval	Cum. Dry Mass	Unsup. Activity	Error of Unsup. Act.	Date A.D.	Error of Age	Sediment Accum.	Error of Sed. Accum.
(cm)	(g/cm2)	(Bq/g)	(±s.d.)		(±s.d.)	(g/cm2 yr)	(±s.d.)
0.25	0.0735	1.55E+00	6.57E-02	2008.2	0.36	0.0274	0.0220
1.25	0.2428	1.33E+00	5.63E-02	2001.7	0.01	0.0262	0.0230
2.25	0.4898	8.71E-01	3.64E-02	1992.7	0.34	0.0274	0.0220
3.25	0.8900	2.54E-01	1.32E-02	1983.7	0.29	0.0448	0.0134
4.25	1.3808	1.49E-01	9.01E-03	1978.4	0.28	0.0911	0.0066
5.25	1.8767	1.80E-01	1.09E-02	1973.0	0.46	0.0925	0.0065
6.25	2.3462	3.61E-01	1.73E-02	1962.8	1.20	0.0459	0.0131
7.25	2.7941	2.88E-01	1.45E-02	1943.8	2.16	0.0237	0.0254
8.25	3.1655	1.57E-01	9.67E-03	1925.0	2.82	0.0197	0.0306
9.25	3.4363	1.08E-01	7.94E-03	1911.0	3.70	0.0193	0.0312
11.50	4.0908	3.50E-02	4.42E-03	1876.9	6.21	0.0192	0.0314
13.50	4.6017	1.14E-02	3.98E-03	1855.9	10.86	0.0243	0.0248
15.50	5.1048	3.50E-03	3.98E-03	1844.9	15.32	0.0459	0.0131
17.50	5.6227	5.90E-03	3.98E-03	1834.0	21.55	0.0476	0.0127

Supported Activity: 1 Sample

A_b	A(0)	(Bq/g)	(±s.d.)
5.90E-03	1.39E+00	5.13E-02	3.67E-03

Core BH09-5MC CRS Calculation

Center of Interval	Cum. Dry Mass	Unsup. Activity	Error of Unsup. Act.	Date A.D.	Error of Age	Sediment Accum.	Error of Sed. Accum.
(cm)	(g/cm2)	(Bq/g)	(±s.d.)		(±s.d.)	(g/cm2 yr)	(±s.d.)
0.3	0.1058	5.54E-01	2.59E-02	2008.9	0.03	0.0835	0.0098
1.3	0.3434	5.08E-01	2.20E-02	2006.0	0.03	0.0825	0.0099
2.3	0.6143	4.94E-01	2.14E-02	2002.6	0.16	0.0793	0.0103
3.3	0.9021	4.48E-01	2.00E-02	1998.8	0.29	0.0754	0.0108
4.3	1.2248	3.83E-01	1.73E-02	1994.5	0.43	0.0755	0.0108
5.3	1.5850	3.27E-01	1.52E-02	1989.8	0.56	0.0769	0.0106
6.3	1.9649	2.82E-01	1.35E-02	1984.9	0.69	0.0772	0.0106
7.3	2.3666	1.89E-01	9.79E-03	1980.3	0.80	0.0870	0.0094
8.3	2.7728	1.49E-01	8.03E-03	1976.4	0.90	0.1054	0.0077
9.3	3.1895	1.18E-01	7.07E-03	1972.9	0.96	0.1191	0.0068
11.5	4.3506	7.76E-02	4.84E-03	1964.4	1.02	0.1363	0.0060
13.5	5.2951	6.86E-02	4.78E-03	1957.7	1.13	0.1417	0.0058
15.5	6.1956	6.96E-02	4.83E-03	1950.2	1.20	0.1201	0.0068
17.5	7.1232	5.40E-02	4.20E-03	1941.4	1.26	0.1048	0.0078
18.5	7.6125	2.94E-02	3.25E-03	1937.6	1.32	0.1305	0.0062
19.5	8.0963	4.03E-02	4.02E-03	1934.1	1.34	0.1364	0.0060
24.5	10.4232	1.91E-02	3.28E-03	1914.2	1.36	0.1171	0.0070
29.5	12.7649	1.06E-02	2.95E-03	1895.7	1.42	0.1263	0.0065
34.5	15.1830	5.70E-03	2.95E-03	1877.0	1.46	0.1294	0.0063
39.5	17.5993	7.90E-03	2.95E-03	1841.0	1.47	0.0672	0.0121

Supported Activity: 1 Sample

A_b	A(0)	(Bq/g)	(±s.d.)
7.90E-03	1.50E+00	3.94E-02	2.22E-03

Appendix: B Bulk Elemental and Isotopic Analysis Data

Core Name	Depth (cm)	Age (yr)	C (%)	$\delta^{13}C$ (‰)	Suess Δ (‰)	Corr. $\delta^{13}C$ (‰)	N (%)	$\delta^{15}N$ (‰)	C/N Ratio
BH03-1MC	0.5	2002.8	1.82	-26.42	-8.13	-24.55	0.16	2.42	11.37
BH03-1MC	1.5	1998.8	1.78	-26.42	-7.98	-24.71	0.16	2.35	11.45
BH03-1MC	2.5	1994.7	1.81	-26.49	-7.84	-24.91	0.16	2.18	11.51
BH03-1MC	2.5	1994.7	1.82	-26.50	-7.84	-24.92	0.16	1.98	11.61
BH03-1MC	3.5	1990.5	1.69	-26.33	-7.71	-24.88	0.13	2.13	12.53
BH03-1MC	4.5	1986.4	1.82	-26.26	-7.59	-24.93	0.15	2.13	12.21
BH03-1MC	5.5	1982.2	1.93	-26.42	-7.48	-25.20	0.16	2.40	11.98
BH03-1MC	6.5	1977.9	2.06	-26.23	-7.38	-25.12	0.16	2.55	13.09
BH03-1MC	6.5	1977.9	2.08	-26.36	-7.38	-25.25	0.15	2.51	13.48
BH03-1MC	7.5	1973.6	2.19	-25.96	-7.29	-24.94	0.15	2.91	14.22
BH03-1MC	8.5	1969.2	2.17	-25.87	-7.20	-24.94	0.15	2.20	14.38
BH03-1MC	9.5	1964.8	2.38	-25.45	-7.12	-24.60	0.15	2.35	15.48
BH03-1MC	10.5	1960.4	2.38	-25.47	-7.05	-24.68	0.13	2.50	17.75
BH03-1MC	10.5	1960.4	2.50	-25.39	-7.05	-24.61	0.13	2.68	19.17
BH03-1MC	11.5	1955.9	2.30	-25.36	-6.99	-24.64	0.13	3.05	17.19
BH03-1MC	12.5	1951.4	2.39	-25.54	-6.93	-24.87	0.16	2.71	15.29
BH03-1MC	13.5	1946.8	2.36	-25.42	-6.87	-24.81	0.14	2.59	16.59
BH03-1MC	14.5	1942.2	2.48	-25.41	-6.83	-24.85	0.15	2.47	16.08
BH03-1MC	14.5	1942.2	2.62	-25.36	-6.83	-24.80	0.17	2.59	15.50
BH03-1MC	15.5	1937.6	2.69	-25.36	-6.79	-24.84	0.17	2.85	15.66
BH03-1MC	16.5	1932.9	2.79	-25.47	-6.75	-24.99	0.18	2.35	15.34
BH03-1MC	17.5	1928.1	2.59	-25.63	-6.72	-25.17	0.17	2.11	15.12
BH03-1MC	18.5	1923.3	2.44	-25.79	-6.69	-25.37	0.16	1.97	14.94
BH03-1MC	18.5	1923.3	2.48	-25.89	-6.69	-25.46	0.16	2.16	15.12
BH03-1MC	19.5	1918.5	2.48	-25.93	-6.66	-25.53	0.17	1.39	14.63
BH03-1MC	20.5	1913.6	2.34	-26.16	-6.64	-25.79	0.16	1.76	14.35
BH03-1MC	21.5	1908.7	2.13	-26.50	-6.62	-26.14	0.15	1.62	13.88
BH03-1MC	22.5	1903.7	2.17	-26.86	-6.60	-26.52	0.15	1.40	14.37
BH03-1MC	23.5	1898.7	1.89	-26.48	-6.59	-26.16	0.15	1.87	12.45
BH03-1MC	23.5	1898.7	1.87	-26.47	-6.59	-26.15	0.15	1.85	12.72
BH03-1MC	24.5	1893.6	1.80	-26.39	-6.57	-26.08	0.14	1.61	12.52
BH03-1MC	25.5	1888.5	1.69	-26.52	-6.56	-26.22	0.14	1.90	11.70
BH03-1MC	26.5	1883.4	1.77	-26.62	-6.55	-26.33	0.15	1.32	12.03
BH03-1MC	27.5	1878.2	1.61	-26.39	-6.54	-26.12	0.14	1.90	11.45
BH03-1MC	27.5	1878.2	1.59	-26.44	-6.54	-26.16	0.13	1.54	12.21
BH03-1MC	28.5	1873.0	1.46	-26.39	-6.53	-26.13	0.13	1.71	11.22
BH03-1MC	29.5	1867.7	1.47	-26.15	-6.52	-25.89	0.14	1.81	10.46
BH03-1MC	30.5	1862.4	1.36	-26.44	-6.51	-26.20	0.12	1.47	11.10
BH03-1MC	31.5	1857.0	1.31	-26.42	-6.50	-26.19	0.12	1.52	11.36
BH03-1MC	31.5	1857.0	1.30	-26.49	-6.50	-26.26	0.11	1.54	11.44

Core	Depth	Age	C	$\delta^{13}C$	Suess Δ	Corr. $\delta^{13}C$	N	$\delta^{15}N$	C/N
Name	(cm)	(yr)	(%)	(‰)	(‰)	(‰)	(%)	(‰)	Ratio
BH03-3MC	0.25	2002.1	3.01	-26.07	-8.10	-24.23	0.33	4.05	9.19
BH03-3MC	0.75	1998.1	3.02	-26.17	-7.96	-24.47	0.32	4.12	9.58
BH03-3MC	0.75	1998.1	2.99	-26.26	-7.96	-24.57	0.31	3.77	9.64
BH03-3MC	1.25	1992.5	2.90	-26.09	-7.77	-24.58	0.29	3.49	9.92
BH03-3MC	1.75	1985.5	2.94	-26.11	-7.57	-24.81	0.30	4.16	9.75
BH03-3MC	2.25	1977.2	3.10	-26.12	-7.36	-25.02	0.30	3.70	10.35
BH03-3MC	2.75	1967.8	2.85	-26.30	-7.17	-25.39	0.26	3.67	10.88
BH03-3MC	2.75	1967.8	2.81	-26.42	-7.17	-25.51	0.26	3.70	10.83
BH03-3MC	3.25	1957.5	2.74	-26.25	-7.01	-25.51	0.27	3.56	10.25
BH03-3MC	3.75	1946.4	2.54	-26.30	-6.87	-25.69	0.26	3.76	9.85
BH03-3MC	4.25	1934.8	2.46	-26.54	-6.76	-26.04	0.25	3.67	9.77
BH03-3MC	4.75	1922.7	2.50	-26.66	-6.68	-26.24	0.26	3.71	9.79
BH03-3MC	4.75	1922.7	2.26	-26.59	-6.68	-26.17	0.24	3.57	9.47
BH03-3MC	5.25	1910.3	2.26	-26.58	-6.63	-26.22	0.25	3.75	9.11
BH03-3MC	5.75	1897.8	2.29	-27.15	-6.58	-26.83	0.25	3.20	9.29
BH03-3MC	6.25	1885.4	2.30	-26.86	-6.55	-26.57	0.26	3.57	8.98
BH03-3MC	6.75	1873.2	2.25	-26.41	-6.53	-26.15	0.24	4.00	9.22
BH03-3MC	6.75	1873.2	2.23	-26.42	-6.53	-26.15	0.24	3.84	9.22
BH03-3MC	7.25	1861.4	2.31	-26.83	-6.51	-26.58	0.25	3.61	9.09
BH03-3MC	7.75	1850.2	2.37	-26.57	-6.49	-26.35	0.26	3.86	9.10
BH03-3MC	8.25	1839.7	2.39	-26.33	-6.47	-26.13	0.26	3.75	9.11
BH03-3MC	8.75	1830.0	2.67	-26.59	-6.45	-26.40	0.24	3.57	10.98
BH03-3MC	8.75	1830.0	2.35	-26.41	-6.45	-26.23	0.26	3.79	8.98
BH03-3MC	9.25	1821.4	2.26	-26.45	-6.43	-26.29	0.25	3.75	9.11

BH09-2MC	0.25	2008.6	3.68	-26.45	-8.37	-24.35	0.44	2.69	8.28
BH09-2MC	1.25	2004.4	3.51	-26.61	-8.19	-24.68	0.42	2.49	8.36
BH09-2MC	1.25	2004.4	3.51	-26.63	-8.19	-24.70	0.42	2.43	8.41
BH09-2MC	2.25	1999.4	3.40	-26.80	-8.00	-25.06	0.39	2.14	8.62
BH09-2MC	3.25	1993.3	3.18	-26.66	-7.80	-25.13	0.38	2.25	8.45
BH09-2MC	4.25	1985.9	3.07	-26.53	-7.58	-25.21	0.36	2.52	8.59
BH09-2MC	5.25	1977.9	2.92	-26.56	-7.38	-25.45	0.35	2.70	8.44
BH09-2MC	5.25	1977.9	2.93	-26.50	-7.38	-25.38	0.35	2.56	8.46
BH09-2MC	6.25	1969.4	2.83	-26.49	-7.20	-25.55	0.33	2.58	8.55
BH09-2MC	7.00	1960.1	2.81	-26.53	-7.04	-25.74	0.33	2.68	8.61
BH09-2MC	8.00	1949.8	2.68	-26.18	-6.91	-25.53	0.31	3.01	8.74
BH09-2MC	8.00	1949.8	2.69	-26.17	-6.91	-25.53	0.31	2.94	8.78
BH09-2MC	9.50	1933.5	2.66	-25.99	-6.75	-25.50	0.29	3.13	9.31
BH09-2MC	11.50	1909.0	2.67	-26.35	-6.62	-25.99	0.29	3.17	9.28
BH09-2MC	13.50	1881.9	2.71	-26.15	-6.55	-25.87	0.30	3.13	8.92
BH09-2MC	13.50	1881.9	2.70	-26.16	-6.55	-25.88	0.30	3.30	8.95
BH09-2MC	15.50	1850.9	2.89	-26.19	-6.49	-25.96	0.33	3.59	8.87
BH09-2MC	17.50	1822.7	2.82	-26.13	-6.43	-25.96	0.32	3.45	8.81
BH09-2MC	19.50		2.89	-26.13			0.33	3.38	8.70

Core	Depth	Age	C	$\delta^{13}C$	Suess Δ	Corr. $\delta^{13}C$	N	$\delta^{15}N$	C/N
Name	(cm)	(yr)	(%)	(‰)	(‰)	(‰)	(%)	(‰)	Ratio
BH09-3MC	0.25	2007.8	3.75	-26.99	-8.33	-24.92	0.44	2.96	8.45
BH09-3MC	1.25	1999.6	3.26	-26.90	-8.01	-25.16	0.37	2.99	8.72
BH09-3MC	1.25	1991.3	3.14	-26.93	-7.74	-25.46	0.36	2.90	8.69
BH09-3MC	2.25	1987.4	3.05	-26.74	-7.62	-25.39	0.34	3.37	9.05
BH09-3MC	3.25	1968.7	3.03	-26.49	-7.19	-25.56	0.31	3.28	9.85
BH09-3MC	4.25	1942.0	2.80	-26.25	-6.83	-25.69	0.27	3.88	10.43
BH09-3MC	4.25	1942.0	2.73	-26.27	-6.83	-25.71	0.26	3.75	10.51
BH09-3MC	5.25	1920.6	2.43	-26.45	-6.67	-26.04	0.25	3.82	9.80
BH09-3MC	6.25	1904.8	2.52	-26.62	-6.61	-26.27	0.25	3.66	10.02
BH09-3MC	7.25	1887.7	2.38	-26.96	-6.56	-26.67	0.26	3.73	9.28
BH09-3MC	8.25	1869.6	2.25	-26.78	-6.52	-26.52	0.24	3.33	9.23
BH09-3MC	8.25	1869.6	2.29	-26.81	-6.52	-26.55	0.25	3.27	9.23
BH09-3MC	9.5	1849.0	2.06	-26.86	-6.48	-26.64	0.22	3.27	9.18
BH09-3MC	11.5	1826.6	2.28	-26.66	-6.44	-26.48	0.25	3.29	9.19
BH09-3MC	13.5		2.20	-26.92			0.25	3.23	8.94
BH09-3MC	13.5		2.19	-26.90			0.25	3.04	8.74
BH09-3MC	15.5		2.17	-26.78			0.25	3.11	8.72
BH09-3MC	17.5		2.24	-26.68			0.26	3.65	8.72
BH09-3MC	19.5		2.23	-26.85			0.25	3.19	8.91

BH09-4MC	0.25	2008.2	3.10	-27.25	-8.35	-25.16	0.38	3.36	8.13
BH09-4MC	1.25	2001.7	2.74	-27.11	-8.09	-25.28	0.32	3.28	8.56
BH09-4MC	2.25	1992.7	1.97	-27.06	-7.78	-25.55	0.21	3.25	9.21
BH09-4MC	2.25	1992.7	1.96	-27.10	-7.78	-25.58	0.23	3.44	8.59
BH09-4MC	3.25	1983.8	0.96	-27.11	-7.52	-25.85	0.10	3.47	9.51
BH09-4MC	4.25	1978.4	1.02	-26.91	-7.39	-25.78	0.12	3.54	8.65
BH09-4MC	5.25	1973.1	1.97	-26.72	-7.28	-25.71	0.18	3.34	11.16
BH09-4MC	6.25	1962.8	2.98	-26.29	-7.09	-25.47	0.31	3.67	9.67
BH09-4MC	6.25	1962.8	3.02	-26.22	-7.09	-25.40	0.32	3.72	9.47
BH09-4MC	7.25	1943.9	3.91	-26.03	-6.84	-25.45	0.34	3.67	11.35
BH09-4MC	8.25	1925.0	2.92	-26.52	-6.70	-26.08	0.31	3.55	9.44
BH09-4MC	9.25	1910.9	3.13	-26.82	-6.63	-26.46	0.33	3.38	9.38
BH09-4MC	11.50	1876.8	2.70	-26.86	-6.54	-26.59	0.31	3.81	8.85
BH09-4MC	11.50	1876.8	2.70	-26.79	-6.54	-26.52	0.31	3.87	8.80
BH09-4MC	13.50	1855.8	2.74	-26.92	-6.50	-26.69	0.31	3.75	8.82
BH09-4MC	15.50	1844.8	2.97	-26.63	-6.48	-26.41	0.33	3.63	8.89
BH09-4MC	17.50	1833.9	2.78	-26.75	-6.45	-26.56	0.31	3.87	8.90
BH09-4MC	19.50		2.76	-26.50			0.31	3.90	8.77

Core	Depth	Age	C	$\delta^{13}C$	Suess Δ	Corr. $\delta^{13}C$	N	$\delta^{15}N$	C/N
Name	(cm)	(yr)	(%)	(‰)	(‰)	(‰)	(%)	(‰)	Ratio
BH09-5MC	0.25	2008.9	2.41	-26.40	-8.38	-24.29	0.25	2.15	9.55
BH09-5MC	1.25	2006.0	2.17	-26.39	-8.26	-24.40	0.22	2.27	9.80
BH09-5MC	2.25	2002.6	2.15	-26.52	-8.12	-24.66	0.21	1.93	10.07
BH09-5MC	3.25	1998.8	2.09	-26.81	-7.98	-25.09	0.21	1.76	10.16
BH09-5MC	3.25	1998.8	2.09	-26.77	-7.98	-25.06	0.20	1.43	10.65
BH09-5MC	4.25	1994.5	1.98	-26.78	-7.84	-25.21	0.18	1.83	11.04
BH09-5MC	5.25	1989.8	1.95	-26.60	-7.69	-25.18	0.16	1.62	12.21
BH09-5MC	6.25	1984.9	2.01	-26.57	-7.55	-25.29	0.16	1.95	12.40
BH09-5MC	6.25	1984.9	2.02	-26.54	-7.55	-25.25	0.17	1.88	12.17
BH09-5MC	7.25	1980.3	2.21	-26.39	-7.44	-25.22	0.16	1.94	13.51
BH09-5MC	8.25	1976.4	2.30	-26.23	-7.35	-25.15	0.17	2.25	13.65
BH09-5MC	9.25	1973.0	2.16	-26.14	-7.27	-25.13	0.15	2.22	14.30
BH09-5MC	11.50	1964.4	2.24	-25.66	-7.11	-24.81	0.14	2.32	15.57
BH09-5MC	11.50	1964.4	2.19	-25.76	-7.11	-24.91	0.14	2.19	15.32
BH09-5MC	13.50	1957.8	2.41	-25.59	-7.01	-24.84	0.16	2.46	15.42
BH09-5MC	15.50	1950.3	2.58	-25.63	-6.91	-24.98	0.18	2.44	14.61
BH09-5MC	17.50	1941.4	2.71	-25.86	-6.82	-25.30	0.17	2.06	15.70
BH09-5MC	18.50	1937.7	2.74	-26.18	-6.79	-25.66	0.18	2.08	15.20
BH09-5MC	19.50	1934.1	2.68	-25.88	-6.76	-25.38	0.17	1.91	16.05
BH09-5MC	19.50	1934.1	2.72	-25.93	-6.76	-25.43	0.17	1.98	16.23
BH09-5MC	24.5	1914.2	1.97	-26.53	-6.64	-26.15	0.16	2.07	12.61
BH09-5MC	29.5	1895.6	1.56	-26.53	-6.58	-26.21	0.15	2.21	10.66
BH09-5MC	34.5	1876.9	1.53	-26.57	-6.54	-26.29	0.14	2.17	11.03
BH09-5MC	39.5	1840.9	1.81	-26.31	-6.47	-26.11	0.17	1.98	10.81
BH09-5MC	44.5		1.67	-26.32			0.15	1.81	11.23

Appendix: C MAR of n-alkane Biomarkers

Core BH03-1MC

Center Depth (cm)	0.5	2.5	4.5	7.5	11.5
Date A.D.	2002.4	1994.3	1986.0	1973.2	1955.5
Sed. g / cm2 yr	0.0818	0.0777	0.0756	0.1038	0.1153
MAR C_{15}	0.000416	0.000470	0.000654	0.001392	0.001258
MAR C_{16}	0.001046	0.000883	0.001095	0.001723	0.002728
MAR C_{17}	0.050256	0.015146	0.019286	0.023620	0.066309
MAR C_{18}	0.073836	0.019856	0.032257	0.025130	0.089992
MAR C_{19}	0.103861	0.040788	0.042657	0.047054	0.132146
MAR C_{20}	0.067754	0.043584	0.039825	0.041111	0.109859
MAR C_{21}	0.099671	0.101428	0.084097	0.096219	0.189432
MAR C_{22}	0.069033	0.072601	0.063691	0.070050	0.128195
MAR C_{23}	0.171267	0.175374	0.150455	0.163053	0.277820
MAR C_{24}	0.057901	0.062412	0.060388	0.069294	0.123281
MAR C_{25}	0.193662	0.196748	0.184120	0.199398	0.354005
MAR C_{26}	0.062439	0.068303	0.072028	0.090475	0.139955
MAR C_{27}	0.351387	0.351784	0.354627	0.371059	0.582118
MAR C_{28}	0.063006	0.070242	0.075765	0.101375	0.148528
MAR C_{29}	0.314780	0.309529	0.302982	0.342321	0.584103
MAR C_{30}	0.065253	0.074112	0.082243	0.121673	0.157010
MAR C_{31}	0.247456	0.249523	0.235093	0.272787	0.461321
MAR C_{32}	0.047906	0.057052	0.055234	0.099908	0.118624
MAR C_{33}	0.081652	0.095694	0.094633	0.130879	0.195668
MAR C_{34}	0.020134	0.023388	0.039332	0.060253	0.072183
Center Depth (cm)	13.5	16.5	22.5	28.5	31.5
Date A.D.	1946.4	1932.5	1903.3	1872.6	1856.6
Sed. g / cm2 yr	0.1064	0.0891	0.1054	0.0891	0.0913
MAR C_{15}	0.002369	0.000857	0.000895	0.000242	0.000427
MAR C_{16}	0.004628	0.002154	0.001839	0.000656	0.001514
MAR C_{17}	0.054604	0.031724	0.040520	0.004668	0.013864
MAR C_{18}	0.054855	0.040630	0.051741	0.008486	0.015348
MAR C_{19}	0.079042	0.061282	0.098336	0.036487	0.039529
MAR C_{20}	0.071513	0.058448	0.074359	0.033955	0.035283
MAR C_{21}	0.154271	0.137945	0.153650	0.099043	0.101677
MAR C_{22}	0.118195	0.098251	0.099782	0.073519	0.065388
MAR C_{23}	0.285418	0.267598	0.285115	0.195409	0.185343

MAR C_{24}	0.128441	0.104685	0.086882	0.060951	0.060091
MAR C_{25}	0.373302	0.338666	0.308704	0.195472	0.201262
MAR C_{26}	0.147527	0.031679	0.089541	0.062152	0.059036
MAR C_{27}	0.646719	0.588115	0.495918	0.324479	0.334063
MAR C_{28}	0.149774	0.126670	0.086696	0.059307	0.052997
MAR C_{29}	0.651906	0.564576	0.518854	0.294780	0.299003
MAR C_{30}	0.145415	0.144571	0.087061	0.031354	0.034555
MAR C_{31}	0.504398	0.394512	0.373567	0.208074	0.203135
MAR C_{32}	0.066893	0.070146	0.082123	0.046298	0.038213
MAR C_{33}	0.203785	0.149895	0.119155	0.072834	0.064662
MAR C_{34}	0.068776	0.033784	0.019001	0.007759	0.008707

Core BH03-3MC

Center Depth (cm)	0.5	1.5	2.5	3.5	4.5	7.5
Date A.D.	2000.3	1990.5	1973.0	1951.2	1927.7	1857.0
Sed. g/cm2 yr	0.0177	0.0145	0.0982	0.0108	0.0128	0.0118
MAR C_{15}	0.000040	0.000097	0.000077	0.000025	0.000002	0.000034
MAR C_{16}	0.000877	0.000349	0.002942	0.000109	0.000025	0.000182
MAR C_{17}	0.027962	0.023001	0.259833	0.010538	0.001127	0.017262
MAR C_{18}	0.001036	0.001008	0.016549	0.000526	0.000343	0.001047
MAR C_{19}	0.035789	0.028903	0.240643	0.015490	0.002651	0.027726
MAR C_{20}	0.011848	0.008232	0.106279	0.006029	0.003513	0.007387
MAR C_{21}	0.030170	0.022992	0.223199	0.014972	0.010616	0.020606
MAR C_{22}	0.023861	0.020023	0.193911	0.011958	0.008094	0.014480
MAR C_{23}	0.064483	0.050859	0.435242	0.032355	0.018902	0.036226
MAR C_{24}	0.019410	0.016186	0.161139	0.010268	0.005923	0.013133
MAR C_{25}	0.063670	0.046819	0.412262	0.031855	0.015345	0.030431
MAR C_{26}	0.023592	0.019443	0.170230	0.012024	0.005921	0.009891
MAR C_{27}	0.181556	0.130738	0.949785	0.096673	0.028481	0.042936
MAR C_{28}	0.015970	0.012918	0.123663	0.009078	0.003966	0.005776
MAR C_{29}	0.112984	0.096604	0.672970	0.049774	0.030706	0.058512
MAR C_{30}	0.005873	0.006790	0.018662	0.003646	0.002633	0.000649
MAR C_{31}	0.069749	0.058336	0.469180	0.039321	0.017168	0.031996
MAR C_{32}	0.003405	0.002613	0.009868	0.002084	0.001651	0.004123
MAR C_{33}	0.025591	0.021428	0.154858	0.014792	0.007071	0.011686
MAR C_{34}	0.003521	0.003807	0.013450	0.001873	0.000767	0.002057

Core BH09-3MC

Depth (cm)	1.0	2.0	3.0	4.0	5.5	7.0	9.5
Date A.D.	2001.1	1986.5	1969.4	1950.3	1920.0	1889.9	1849.0
Sedg/cm2yr	0.0301	0.0180	0.0154	0.0157	0.0215	0.0230	0.0260
MAR C_{15}	0.000147	0.000102	0.000157	0.000096	0.000068	0.000000	0.000000
MAR C_{16}	0.000379	0.000338	0.000209	0.000265	0.000063	0.000149	0.000202
MAR C_{17}	0.029732	0.017483	0.007394	0.014764	0.036340	0.022656	0.034216
MAR C_{18}	0.001045	0.003142	0.000825	0.000605	0.000417	0.000319	0.002407
MAR C_{19}	0.058585	0.029688	0.018000	0.021083	0.056333	0.036984	0.065325
MAR C_{20}	0.019226	0.017691	0.007982	0.009613	0.011059	0.006018	0.023144
MAR C_{21}	0.063720	0.037837	0.024046	0.023333	0.027879	0.016428	0.042458
MAR C_{22}	0.053344	0.030186	0.020658	0.020985	0.022048	0.012211	0.027606
MAR C_{23}	0.166157	0.079665	0.061052	0.051635	0.051586	0.029469	0.053881
MAR C_{24}	0.031098	0.017646	0.018849	0.017225	0.015355	0.007959	0.018172
MAR C_{25}	0.116549	0.062141	0.059386	0.044680	0.039588	0.021364	0.039900
MAR C_{26}	0.040217	0.024674	0.024201	0.017778	0.014375	0.007996	0.015494
MAR C_{27}	0.337606	0.213540	0.205364	0.122852	0.074583	0.037574	0.055279
MAR C_{28}	0.027532	0.015601	0.015180	0.011345	0.010426	0.006785	0.010839
MAR C_{29}	0.160931	0.090124	0.078086	0.066816	0.079348	0.032217	0.047154
MAR C_{30}	0.014899	0.007313	0.014619	0.010525	0.008411	0.001935	0.001721
MAR C_{31}	0.129453	0.067062	0.065906	0.056862	0.050771	0.027332	0.048797
MAR C_{32}	0.005395	0.003209	0.006052	0.002525	0.004434	0.002745	0.007142
MAR C_{33}	0.047861	0.024493	0.024492	0.022647	0.018999	0.011997	0.020042
MAR C_{34}	0.009907	0.004647	0.005116	0.004958	0.004663	0.002285	0.004386

Core BH09-5MC

Center Depth (cm)	1.0	3.0	7.0	9.5	11.5
Date A.D.	2008.7	2005.3	1994.5	1989.7	1964.4
Sed. g / cm2 yr	0.1248	0.0768	0.0866	0.1203	0.1363
MAR C_{15}	0.000537	0.000459	0.000522	0.000949	0.002110
MAR C_{16}	0.001868	0.001122	0.000857	0.001852	0.004477
MAR C_{17}	0.030176	0.036199	0.018971	0.026897	0.037223
MAR C_{18}	0.013066	0.015166	0.010705	0.032926	0.023544
MAR C_{19}	0.055264	0.080095	0.031941	0.073137	0.053121
MAR C_{20}	0.032969	0.036743	0.022362	0.049454	0.045225
MAR C_{21}	0.092106	0.066926	0.062227	0.143789	0.113537
MAR C_{22}	0.069736	0.049008	0.043891	0.105870	0.074933
MAR C_{23}	0.220508	0.136025	0.128776	0.266128	0.195089

MAR C_{24}	0.066716	0.048189	0.048189	0.139020	0.087980
MAR C_{25}	0.240171	0.154595	0.150981	0.341410	0.248427
MAR C_{26}	0.067293	0.046335	0.053218	0.173124	0.102712
MAR C_{27}	0.423093	0.276231	0.288459	0.610030	0.484724
MAR C_{28}	0.065186	0.045380	0.054242	0.212871	0.120655
MAR C_{29}	0.389804	0.250642	0.231381	0.488102	0.455620
MAR C_{30}	0.044794	0.031818	0.037802	0.250075	0.106966
MAR C_{31}	0.314253	0.190623	0.165372	0.389065	0.338945
MAR C_{32}	0.058557	0.049432	0.038762	0.102983	0.090773
MAR C_{33}	0.122659	0.076105	0.076400	0.188518	0.163704
MAR C_{34}	0.029946	0.022516	0.024700	0.088180	0.055516
Center Depth (cm)	15.5	19.5	24.5	34.5	39.5
Date A.D.	1950.2	1934.1	1914.2	1877.0	1841.0
Sed. g/cm2 yr	0.1201	0.1364	0.1171	0.1294	0.0672
MAR C_{15}	0.000605	0.002528	0.000456	0.000279	0.000196
MAR C_{16}	0.001303	0.004156	0.001340	0.001747	0.000645
MAR C_{17}	0.039039	0.095459	0.010430	0.059204	0.007492
MAR C_{18}	0.039480	0.040070	0.013962	0.013003	0.010412
MAR C_{19}	0.075870	0.105006	0.036618	0.127616	0.031620
MAR C_{20}	0.059435	0.073993	0.029956	0.046204	0.024987
MAR C_{21}	0.139563	0.148983	0.082399	0.113005	0.070676
MAR C_{22}	0.090007	0.093485	0.053059	0.076328	0.047863
MAR C_{23}	0.229420	0.271198	0.163730	0.194032	0.128339
MAR C_{24}	0.100084	0.108728	0.050148	0.062450	0.042969
MAR C_{25}	0.282337	0.317901	0.179194	0.204296	0.132733
MAR C_{26}	0.107738	0.114086	0.053246	0.061288	0.042695
MAR C_{27}	0.472298	0.575175	0.291517	0.338014	0.213250
MAR C_{28}	0.108727	0.105056	0.051067	0.054662	0.041657
MAR C_{29}	0.472548	0.546850	0.297131	0.368329	0.203189
MAR C_{30}	0.107285	0.101951	0.043085	0.051116	0.021503
MAR C_{31}	0.365019	0.384171	0.208102	0.239370	0.141132
MAR C_{32}	0.126789	0.089331	0.075220	0.052107	0.045234
MAR C_{33}	0.145232	0.142948	0.066695	0.101687	0.045255
MAR C_{34}	0.044021	0.043822	0.006382	0.035776	0.005213

Appendix: D $\delta^{13}C$ of n-alkane Biomarkers

Core BH03-1MC

Depth (cm)	0.5	2.5	4.5	7.5	11.5	13.5	16.5	28.5	31.5
Date A.D.	2002.4	1994.3	1986.0	1973.2	1955.5	1946.4	1932.5	1872.6	1856.6
$\delta^{13}C_{17}$	-30.37	-31.42	-30.74	-31.12	-30.80	-30.68	-31.62	-37.55	-34.49
$\delta^{13}C_{18}$	-30.29	-31.27	-30.25	-31.24	-29.99	-29.26	-29.50	-32.78	-34.16
$\delta^{13}C_{19}$	-30.31	-30.89	-31.15	-32.02	-30.27	-29.23	-30.27	-34.28	-34.70
$\delta^{13}C_{20}$	-29.59	-29.55	-28.90	-28.07	-29.23	-28.28	-27.81	-31.71	-31.58
$\delta^{13}C_{21}$	-32.66	-33.70	-32.68	-31.81	-31.56	-31.74	-31.22	-34.55	-34.72
$\delta^{13}C_{22}$	-31.21	-34.02	-34.55	-35.18	-32.35	-32.75	-34.22	-35.50	-32.73
$\delta^{13}C_{23}$	-33.60	-34.08	-34.13	-33.02	-33.12	-32.91	-31.97	-34.23	-34.00
$\delta^{13}C_{24}$	-30.47	-31.73	-31.81	-30.62	-32.78	-30.85	-31.18	-32.45	-32.88
$\delta^{13}C_{25}$	-31.45	-31.78	-31.51	-31.06	-32.22	-31.72	-31.95	-31.66	-32.23
$\delta^{13}C_{26}$	-32.19	-32.68	-30.45	-31.44	-32.26	-28.50	-31.33	-31.99	-31.84
$\delta^{13}C_{27}$	-30.84	-32.12	-31.49	-32.43	-32.94	-31.32	-32.48	-31.72	-31.12
$\delta^{13}C_{28}$	-30.91	-30.32	-36.77	-29.81	-32.11	-34.20	-33.90	-32.60	-32.66
$\delta^{13}C_{29}$	-30.88	-31.27	-30.98	-30.86	-32.25	-31.41	-31.64	-31.90	-31.59
$\delta^{13}C_{30}$	-31.32	-31.35	-32.59	-36.51	-30.27	-35.60	-37.06	-32.35	-31.32
$\delta^{13}C_{31}$	-31.44	-31.61	-32.27	-31.38	-30.91	-32.46	-31.93	-32.05	-31.70
$\delta^{13}C_{32}$	-30.33	-31.56	-38.33	-30.51	-30.21	-31.62	-25.03	-34.69	-33.81
$\delta^{13}C_{33}$	-36.97	-31.60	-31.91	-32.78	-34.33	-33.54	-33.29	-34.45	-34.56
$\delta^{13}C_{34}$	-28.82	-29.82	-29.83	-33.08	-34.86	-31.64	-36.35	-38.39	-35.16

Core BH09-5MC

Depth (cm)	1	3	7	9.5	11.5	15.5	19.5	24.5
Date A.D.	2008.7	2005.3	1994.5	1989.7	1964.4	1950.2	1934.1	1914.2
$\delta^{13}C_{17}$	-32.01	-31.37	-34.54	-31.28	-30.43	-31.42	-32.86	-34.43
$\delta^{13}C_{18}$	-29.55	-29.46	-30.50	-30.97	-30.04	-30.24	-30.59	-32.17
$\delta^{13}C_{19}$	-30.09	-29.79	-28.70	-29.29	-29.31	-29.70	-31.13	-33.31
$\delta^{13}C_{20}$	-29.68	-27.50	-13.79	-27.05	-27.54	-28.72	-28.59	-28.85
$\delta^{13}C_{21}$	-33.42	-32.02	-31.96	-31.84	-30.61	-31.84	-32.71	-33.27
$\delta^{13}C_{22}$	-33.59	-35.33	-39.94	-32.30	-32.09	-34.39	-30.82	-33.44
$\delta^{13}C_{23}$	-33.89	-32.76	-32.93	-32.50	-31.80	-32.48	-32.64	-32.48
$\delta^{13}C_{24}$	-31.32	-29.58	-30.72	-31.99	-30.05	-28.72	-32.73	-32.39
$\delta^{13}C_{25}$	-30.74	-29.56	-29.82	-31.43	-30.41	-30.52	-31.30	-31.82
$\delta^{13}C_{26}$	-30.02	-28.92	-29.82	-30.76	-30.00	-30.58	-31.96	-31.83
$\delta^{13}C_{27}$	-31.87	-30.57	-31.68	-32.17	-30.98	-31.13	-32.26	-31.77
$\delta^{13}C_{28}$	-31.55	-28.30	-29.92	-31.48	-30.31	-32.43	-28.40	-33.35
$\delta^{13}C_{29}$	-30.56	-29.25	-30.85	-30.46	-30.88	-31.56	-32.82	-32.19
$\delta^{13}C_{30}$	-31.59	-28.57	-28.82	-35.42	-31.43	-27.52	-40.78	-31.93
$\delta^{13}C_{31}$	-30.78	-30.44	-29.83	-30.78	-30.95	-31.31	-31.87	-32.08
$\delta^{13}C_{32}$	-35.04	-32.09	-36.27	-31.86	-30.00	-31.08	-30.29	-28.81
$\delta^{13}C_{33}$	-32.19	-32.33	-30.66	-33.75	-35.88	-34.82	-36.72	-39.25
$\delta^{13}C_{34}$	-24.79	-32.92	-27.54	-30.12	-32.65	-29.81	-31.65	-38.18

Core BH09-5MC (cont.)

Depth (cm)	34.5	39.5
Date A.D.	1877.0	1841.0
$\delta^{13}C_{17}$	-41.64	-35.55
$\delta^{13}C_{18}$	-32.14	-32.46
$\delta^{13}C_{19}$	-33.01	-33.09
$\delta^{13}C_{20}$	-30.35	-31.02
$\delta^{13}C_{21}$	-33.49	-35.07
$\delta^{13}C_{22}$	-33.49	-34.05
$\delta^{13}C_{23}$	-32.25	-33.59
$\delta^{13}C_{24}$	-31.81	-32.10
$\delta^{13}C_{25}$	-30.53	-31.15
$\delta^{13}C_{26}$	-30.95	-31.25
$\delta^{13}C_{27}$	-30.46	-30.45
$\delta^{13}C_{28}$	-31.64	-30.97
$\delta^{13}C_{29}$	-30.95	-31.01
$\delta^{13}C_{30}$	-31.25	-31.61
$\delta^{13}C_{31}$	-30.87	-30.79
$\delta^{13}C_{32}$	-30.48	-21.94
$\delta^{13}C_{33}$	-37.90	-35.06
$\delta^{13}C_{34}$	-31.66	-33.78